CHAPTER 3

DEVELOPMENT OF POLE/CABLE BREAKAWAY SYSTEMS

3.1 INTRODUCTION

The experimental development of a workable scheme for modifying timber utility poles to breakaway on impact was conducted in two stages :

(i) A preliminary test series of seven impacts with poles modified by the crossed-hole scheme of Wolfe et al., (see Figure 1.1). These tests established the viability of the scale model test technique and revealed a number of areas in which detailed design development was required to improve the performance of the breakaway systems.

(ii) The main test series of 88 impacts was used to investigate the design changes made as a result of the preliminary test results, and to find the effects of different pole strengths and cable configurations and the speed and angle of approach of the impacting vehicle.

The total test program can be summarized in terms of pole/cable configuration and pole timber as follows :

Configuration	Material	Number of Tests
Two crossarms	Ironbark	59
One crossarm	Messmate	28
Luminaire	Messmate	6
Free-standing (pole only)	Ironbark	2

The details of experimental conditions and results for all tests are presented in Appendix D .

For the sake of brevity the following terminology will be adopted for the remainder of this report :

(i)	Two-crossarm pole	=	ironbark pole which supports a layer of high- and a layer of low-voltage conductors (Figure 2.1).
(ii)	Single-crossarm pole	=	messmate pole which supports a single layer of low voltage conductors (Figure 2.2).
(iii)	FSE	=	full scale equivalent ; i.e., derived from scale model results by applying the appropriate scale factor.

3.2 PRELIMINARY TEST SERIES

The preliminary series of seven tests involved impacts with ironbark, two-crossarm poles only. In five of the tests the poles were modified with crossed holes at the base and just below the lower crossarm. The holes were sized to maintain a FSE rated pole strength of about 6 kN (see Section 2.7). In the remaining tests impacts were made with an unmodified pole and a pole which had been sawn through at the base, these cases representing two extremes of base shear strength. In all tests the impact speed was nominally 75 km/h FSE and the vehicle approached the line of poles at an angle of 15°.

In the first few tests the modified pole base fractured successfully, but the upper zone failed to break because the standard strength cable ties (10 amp fuse wire - see Section 2.6.1) failed first. In order to establish whether or not the cables could develop enough tension to produce failure at the top modified zone of the pole, the cables were clamped to the crossarms for four of the remaining tests. These tests were successful in that the breakaway segment of the pole detached from the crossarms and upper-pole section. The cables withstood both the impact phase and the loads induced by bouncing of the remaining upper-pole/ crossarm section.

Figure 3.1 shows the accelerometer signal and the velocity change trace obtained in test No. 6, which involved a 7.63 m/s (75 km/h FSE) impact with a modified pole, the cables being clamped to the crossarms. It can be seen that the impact resulted in a peak vehicle deceleration of about 32 g, and a velocity change of 2.2 m/s (a full scale equivalent of 6.0 m/s or 21.5 km/h).

By way of comparison, the unmodified pole did not break on impact and brought the vehicle to rest (a FSE velocity change of 75 km/h), following a peak deceleration of 73 g.

The reduction in collision severity produced by modification of 6 kN poles may be assessed by the following comparison of the FSE results of test No. 3 (unmodified), the averaged data from tests Nos. 5 - 7 (modified), the TRB (1978) impulse criterion for no injury and Chi's (1976) serious injury threshold :

	Deceleration (G)		Velocity
	Peak	Average	Change (m/s)
Unmodified	73	26	21
Modified	30	16	7
No injury (TRB)	-	-	4
Serious Injury (Chi)	-	25	12

It is apparent that a worthwhile reduction in collision severity has resulted from the pole modification, but there is still a fair chance of some injury. Based on the data of Marsh (Figures C.4 and C.5, Appendix C), the chance of an occupant sustaining some injury (AIS 1 or higher) is greater than 50 percent, as shown in Table 3.1.

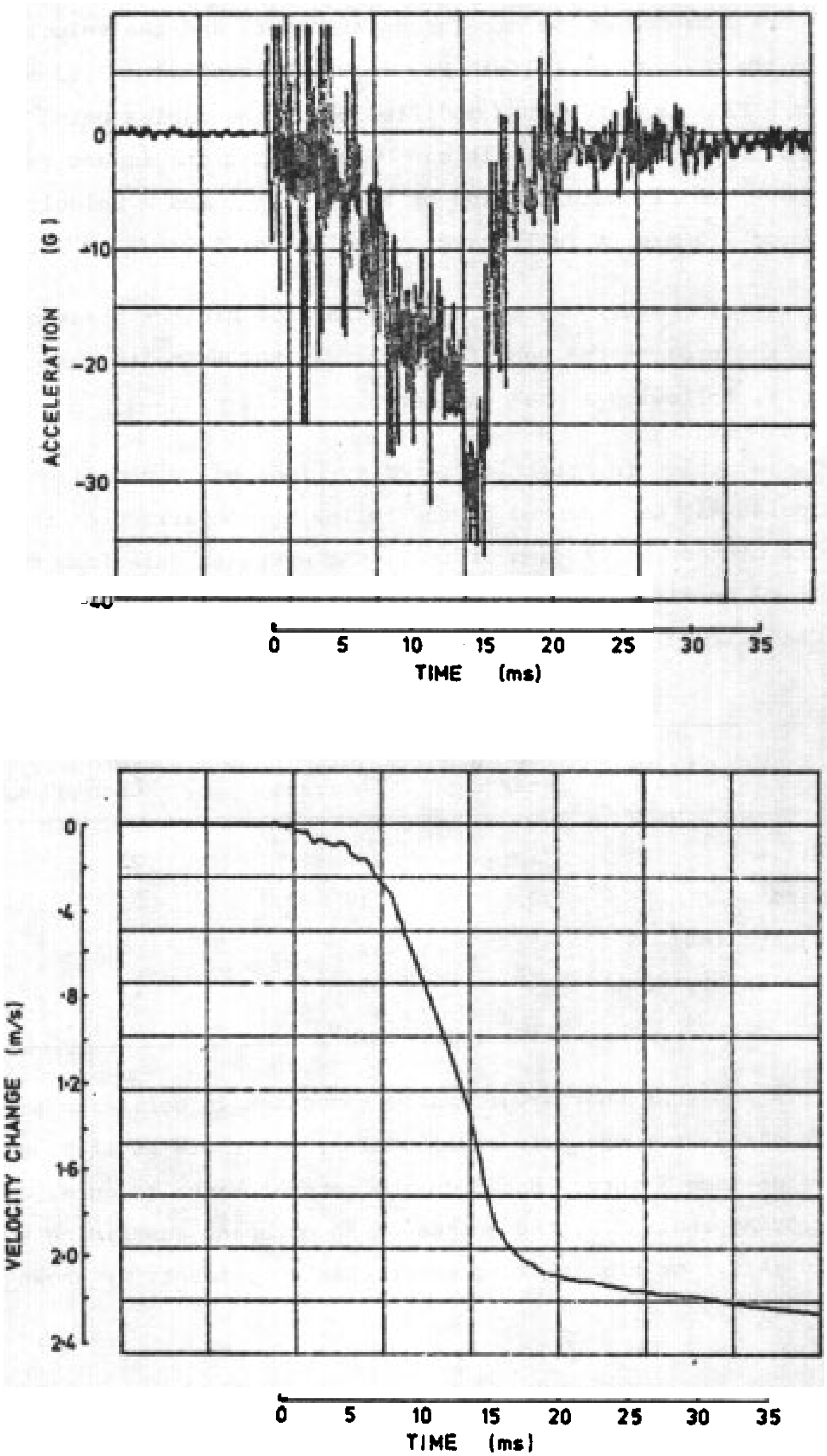

Figure 3.1.Scale model vehicle deceleration and velocity change traces for test #6

TABLE 3.1

PROBABILITY OF AN INJURY OF A GIVEN LEVEL OR HIGHER ACCORDING TO DATA OF MARSH *ET AL.*, (1977) FOR IMPACT AT 75 KM/H. (PRELIMINARY TEST SERIES).

INJURY LEVEL (1)	MODIFIED POLE (CROSSED HOLES)	UNMODIFIED POLE
AIS 1+	.54	.90
AIS 2+	.10	.55
AIS 3+	.01	.30

(1) AIS - Abbreviated Injury Scale (Committee on Medical Aspects of Automotive Safety, 1971).

These results were considered sufficiently encouraging to justify further development of the pole modification scheme. Aspects of the collision process which were identified as requiring further investigation included :

(a) The post-impact trajectory of the detached pole segment.

(b) Clashing of the overhead cables.

(c) Cable-tie strength requirements to ensure an upper pole section breakaway.

(d) The maximum loads induced in the cables.

(e) The effects of different impact speeds and angles.

(f) The effects of different pole/cable configurations.

(g) Alternative methods of modifying the pole to further reduce the impact severity.

3.3 MAIN TEST SERIES

3.3.1 Introduction

To meet the objectives of this series of tests, collisions were staged with poles modified at the base by Wolfe's crossed-holes, Labra's slot/shims and by a new slotted base developed in this project. Three impact velocities were used (40, 60 and 70 km/h FSE), three impact directions (15° , 30° and 50° from the pole line) and rated FSE pole strengths ranging from 2 kN to 8 kN . Both single- and two-crossarm pole/cable configurations were tested, as was a modified timber luminaire pole. Transducers were developed to monitor cable tensions and the problems of cable clash and cable/tie strength were resolved. A scheme for improving the post-impact trajectory of the breakaway pole was developed. The following sections describe the investigations made into these various aspects of the breakaway pole/cable system.

3.3.2 Effect of Moisture Content of Pole Timber

As the main test series was undertaken some twelve months after the preliminary tests, the first of the new tests were conducted in an attempt to replicate the earlier results. That is, two-crossarm ironbark poles modified by crossed-holes were impacted at a velocity of 70 km/h FSE and an angle of 15° to the cable line. The cables were clamped to the crossarms.

The preliminary test tesults were not reproduced precisely, in that the detached pole segment contacted the vehicle windshield and roof, a problem not encountered previously. This was found to be related to the moisture content of the poles used. The preliminary series poles were more moist than those in the later series and so the fractures tended to be less brittle. This meant that the upper failure zone acted as a hinge for a short time after the pole base was sheared, allowing the detached pole to swing up over the car. This effect was verified by testing a 'greener' pole : the breakaway pole segment then successfully cleared the vehicle.

The model poles were cut from full scale crossarms that had been weathered for a number of years. The model poles were then stored indoors for up to six months prior to testing. The condition of the poles at the time of testing was therefore 'air-dry'. This had implications also for the ultimate strength of the poles, because air-dry, unchecked poles can be up to 40% stronger than their 'green' counterparts. However, because the ultimate strength of the timber in each scale model pole was measured (Section 2.6.3), the effects of timber strength variations could be accounted for in interpreting the experimental results.

As was pointed out in Section 2.6.3, the in-service pole strength at the lower zone would probably approach the green timber value because of a high moisture content and decay of the sapwood. However, it would be reasonable to expect that the upper pole zone strength would be closer to the air-dry value.

3.3.3 Performance of Crossed-Hole Base Modification

Velocity change and deceleration data were obtained from a total (from both test series) of eight 70 km/h FSE impacts with two-crossarm poles modified at the base by crossed holes (Figure 1.1). The average impact severity for the various FSE pole strength ratings was as follows :

FSE Rated Pole Strength (kN)	Average Deceleration (G)	FSE Velocity Change (m/s)
0 (Sawn through)	2.8	2.3
4	11.8	5.5
6	15.5	7.0
8	13.5	7.9

Although the impact severity was less than Chi's (1976) serious injury threshold for all rated pole strengths, the TRB (1978) no-injury impulse criterion (which requires a velocity change of less than 3.6 m/s for the test vehicle) was never satisfied.

The phenomenon of vertical splitting of the pole timber during impact, which had been observed in the full-scale tests of Labra (1977), was also present in the scale model tests. Typically a piece of some 70 mm in length was torn from the impacted side of the pole. Failure on the other side of the pole usually occurred cleanly. This suggests that the crossed-hole modification may not take full advantage of the anisotropic nature of the pole material. It was decided therefore to investigate alternative base modification schemes which might reduce the impact severity.

3.3.4 Performance of Slot/Shim Base Modification

One 65 km/h impact test was conducted on a two-crossarm pole modified at the base by the slot/shim concept. The modification was carried out as detailed in Figure 1.3 (after Labra, 1977) with the untouched core width t being equal to 45 mm FSE so as to maintain a FSE rated pole strength of 8 kN. The shims were 7.5 mm thick (FSE) crossgrain ironbark. The base fractured satisfactorily, resulting in a less severe impact (ΔV = 5.1 m/s FSE, $\ddot{x}_{av}$ = 10.2 g) than for an 8 kN pole with crossed-holes. However, for the reasons outlined in Section 1.2.2, it was decided not to pursue this alternative further. Instead, a slotted-base modification scheme was developed, as described in the following section.

3.3.5 A New, Slotted-Base Modification Scheme

Figure 3.2 shows a pole base modified by drilling crossed-holes at two levels and joining these by vertical slots, thereby forming four columns. The rationale for this modification is that, while it uses crossed-holes to make efficient use of the outer pole fibres for resisting bending moments due to service loads applied at the top of the pole, the columns suffer high bending moments at their top and bottom when a shear load is applied just above the base modification. The longer the slot, the greater will these bending moments be for a given shear load. The idea is then, that the slots 'amplify' the effect of the shear load and cause failure of the columns in bending, rather than in shear. The same principle has previously been used in modifying timber sign supports, but with holes and slots in one direction only.

The derivation of a design equation to predict the shear load at car bumper height which will cause failure of the slotted base is given in Appendix F .

The severity of impacts with two-crossarm poles modified with the slotted base and with crossed holes is compared in Figures 3.3 and 3.4. In all these tests crossed-holes were used to provide the upper breakaway mechanism. In order to take account of the measured rupture stresses of the individual poles used in these tests, velocity change and deceleration are plotted in these figures against the 'ultimate' service strength of the pole - i.e.,

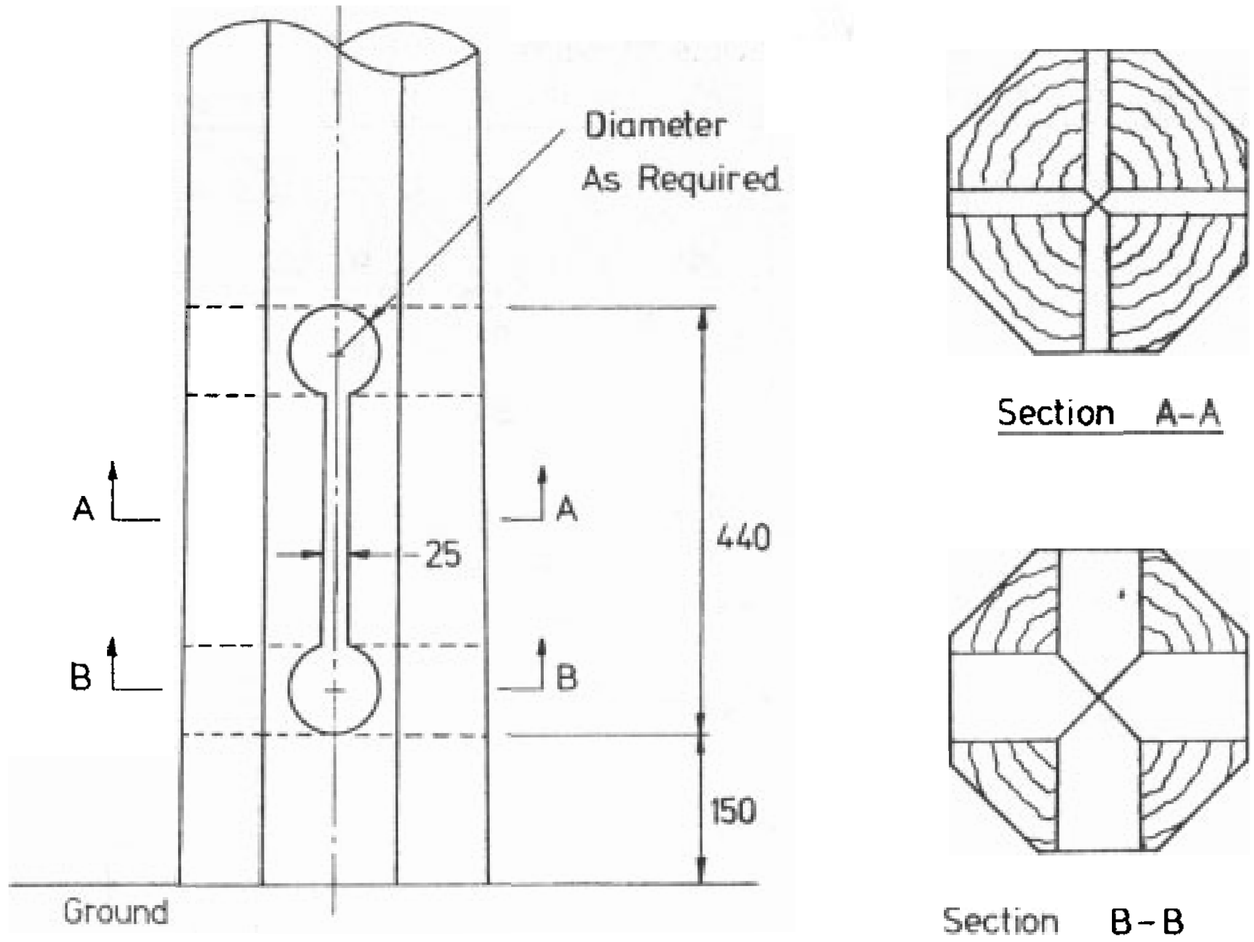

All dimensions in mm.

Figure 3.2. Slotted base modification scheme.

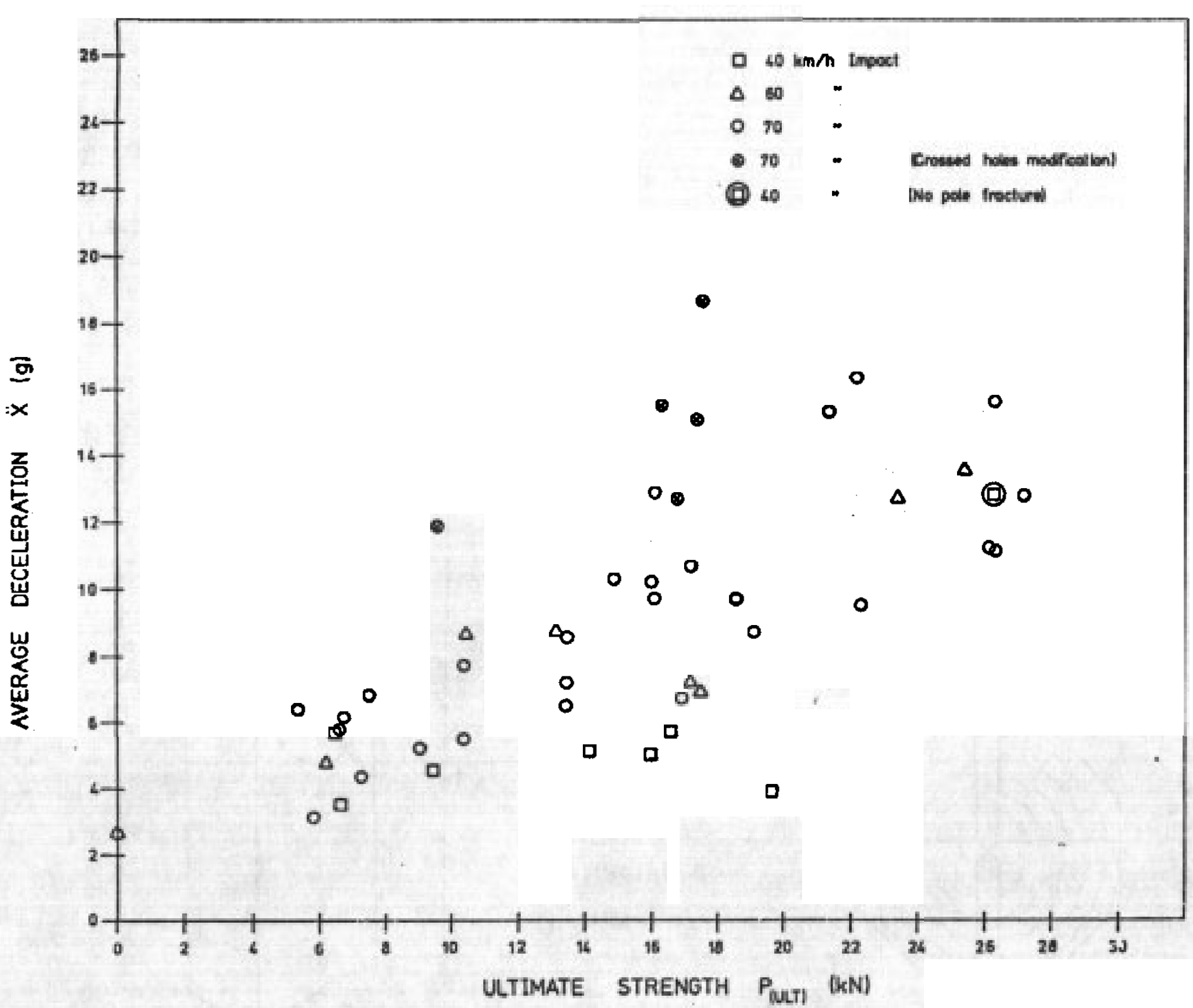

Figure 3.4. Vehicle average deceleration versus pole ultimate strength for impacts with two-crossarm ironbark poles modified by slots or crossed holes.

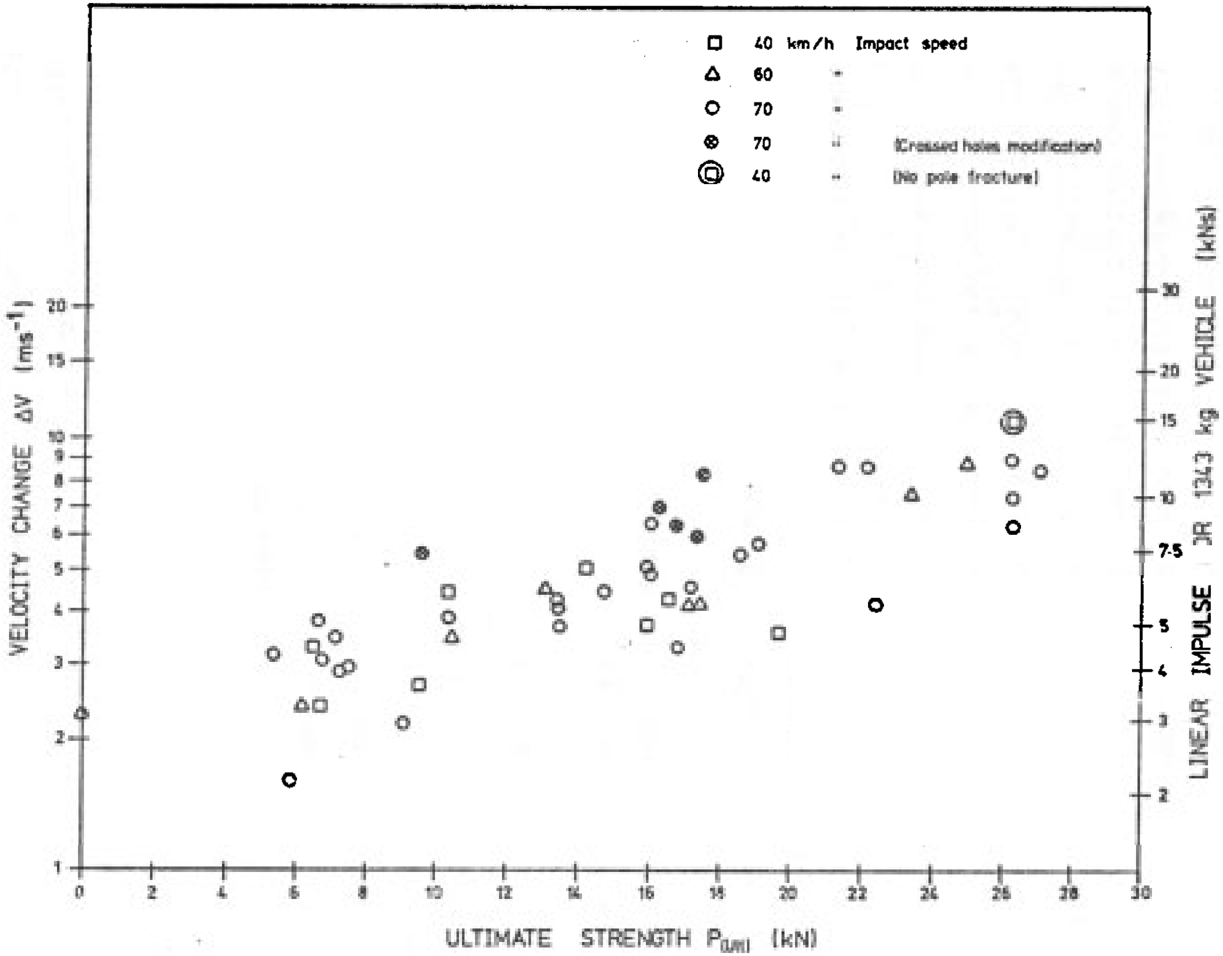

Figure 3.3. Vehicle velocity change versus pole ultimate strength for impacts with two-crossarm ironbark poles modified by slots or crossed holes.

the horizontal load applied at the top of the pole which conventional design calculations indicate will actually rupture the pole base. All the quantities shown in Figures 3.3 and 3.4 are full scale equivalent values obtained from the scale model results by applying the appropriate scale factors derived in Section 2.4 .

It can be seen that the crossed-hole modification for nominally the same pole bending strength results in a more severe impact than does the slotted base modification. The improved performance of the slotted base over the crossed-hole base is further demonstrated by comparing the deceleration trace of Figure 3.5 (slotted base) with that of Figure 3.1 (crossed hole base). The two poles have nominally the same rated bending strength and test conditions, yet the slotted base results in a substantially less severe impact.

Experimental results and analyses presented in the remainder of this chapter will therefore be confined to those tests in which the slotted-base modification was employed. In-service implementation of the slotted base would require some form of environmental protection for the pole core, perhaps through the use of expanding foam and external sealants.

3.3.6 Upper Pole Breakaway Mechanism

Crossed-holes were retained as the means of obtaining pole breakaway from the upper-pole/two-crossarm assembly. No attempt was made to model the crossarm release mechanism proposed by Labra (1977), as it was thought that it would prove prohibitively elaborate and expensive for in-service application. Further, the crossarm release mechanism may not be applicable to poles with two-crossarms (and hence two layers of cables) because of the possibility of the falling pole and crossarm segments snagging the conductors on the way down. Instead, the strength of the cable/tie connections required to produce failure of the upper crossed-hole modification was determined experimentally as described in Section 3.3.12.

No upper zone modification was employed for the single crossarm messmate pole tests. Instead, it was found that for all impact speeds and angles the crossarm stripped easily away from the conductors through failure of the tie wires. The tie wires used in

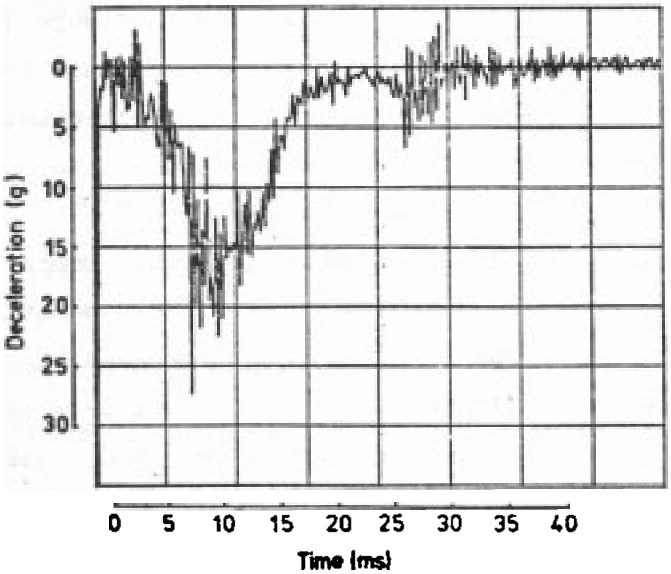

Figure 3.5. Deceleration record resulting from a 70.6km/h FSE impact with a 6kN ironbark pole (test # 41) modified at the base by vertical slots.

all the single crossarm tests were made from 10 amp fuse wire, which modelled the strength of the existing full scale installations (Section 2.6.1).

3.3.7 Post-Impact Trajectory of the Detached Pole Segment

For low rated pole strengths and high impact speeds the breakaway section of the pole did not contact the vehicle after the initial impact. Such a situation is illustrated in Figure 3.16 which shows post-impact positions of an unrestrained messmate luminaire pole and the vehicle. However, for most pole configurations and impact speeds, the pole struck the vehicle a second time on the windscreen, roof or trunk. Even the low shear strength luminaire pole landed on the vehicle roof after low speed impacts. Compared with conventional breakaway metal lighting columns, this behaviour is to be more expected with timber utility poles because of their greater mass and base shear strength. It was therefore decided to attach restraining cables between the target pole and adjacent poles. In the case of a run of modified poles, the restraining cables would be required between the modified poles, as well as between the outer modified poles and the adjacent unmodified poles.

A disadvantage of the restraining cables is that they cause additional wind loads to be applied to the pole and so a pole strength penalty is suffered. However, the effectiveness of the restraining cable in reducing the incidence and severity of the breakaway pole impacting the vehicle roof and windscreen is clearly demonstrated in Figures 3.6 through 3.18. Figures 3.6, 3.10, 3.14 and 3.15 are before- and after- test photographs for the three pole configurations investigated. It can be seen that in all after-test photographs, the top of the pole is suspended well clear of the ground. Figures 3.7, 3.8, 3.11, 3.12, 3.16 and 3.17 are time sequence plots taken from high-speed movies of tests with and without restraining cables for matched impact speeds and FSE rated pole strengths. These figures quite clearly demonstrate the benefit of the restraining cables. Figures 3.9, 3.10 and 3.13 are frames taken from high-speed movies of tests involving the three pole configurations with restraining cables. They also show the breakaway pole comfortably clearing the vehicle.

For the three pole configurations tested, the breakaway pole with restraining cables generally cleared the vehicle for impact speeds of 60 and 70 km/h FSE. For impact speeds around 40 km/h FSE, the secondary impact with the windscreen/roof was not prevented, but its severity was reduced.

The restraining cable also has the advantage that it prevents the detached pole segment from translating far from its starting point, thereby reducing the probability of secondary collisions with other vehicles.

The model restraining cable used was 1.5 mm diameter 19-strand stainless steel. The sag was set to 10 cm over a span of 4.74 m via turnbuckles which were strain-gauged to measure cable tension.

The restraining cable tension was recorded in the 'worst-case' situations for each pole configuration ; that is, an impact velocity of 70 km/h FSE , an impact angle of 50° and low pole base shear strength. For the ironbark, two-crossarm pole the peak restraining cable tension was found to be 890 N (FSE of 50.5 kN), and occurred about 200 ms after the base sheared. If this time is related to the time sequence plot of Figure 3.8, it can be seen that the peak tension corresponds to the first 'bounce' of the breakaway pole on the restraining cables. There was a second bounce of a lower magnitude some 400 ms later, after which the cable tension rapidly fell to its rest value of 50 N (2.8 kN FSE).

The messmate pole tests resulted in a peak restraining cable tension of 800 N (full scale equivalent of 45.5 kN) which also quickly decayed to the rest tension of around 50 N .

3.3.8 Influence of Impact on Adjacent Modified Poles

A number of tests were conducted to investigate the possibility of a 'domino effect' of successive failures occurring in a run of modified poles when one of their number was struck by a vehicle. Again, the 'worst case' situation was set up for each pole configuration. In the case of the single-crossarm and two-crossarm poles, the poles were modified to a FSE rated strength of 3.1 kN , while the luminaire poles were modified to a 2 kN FSE rating.

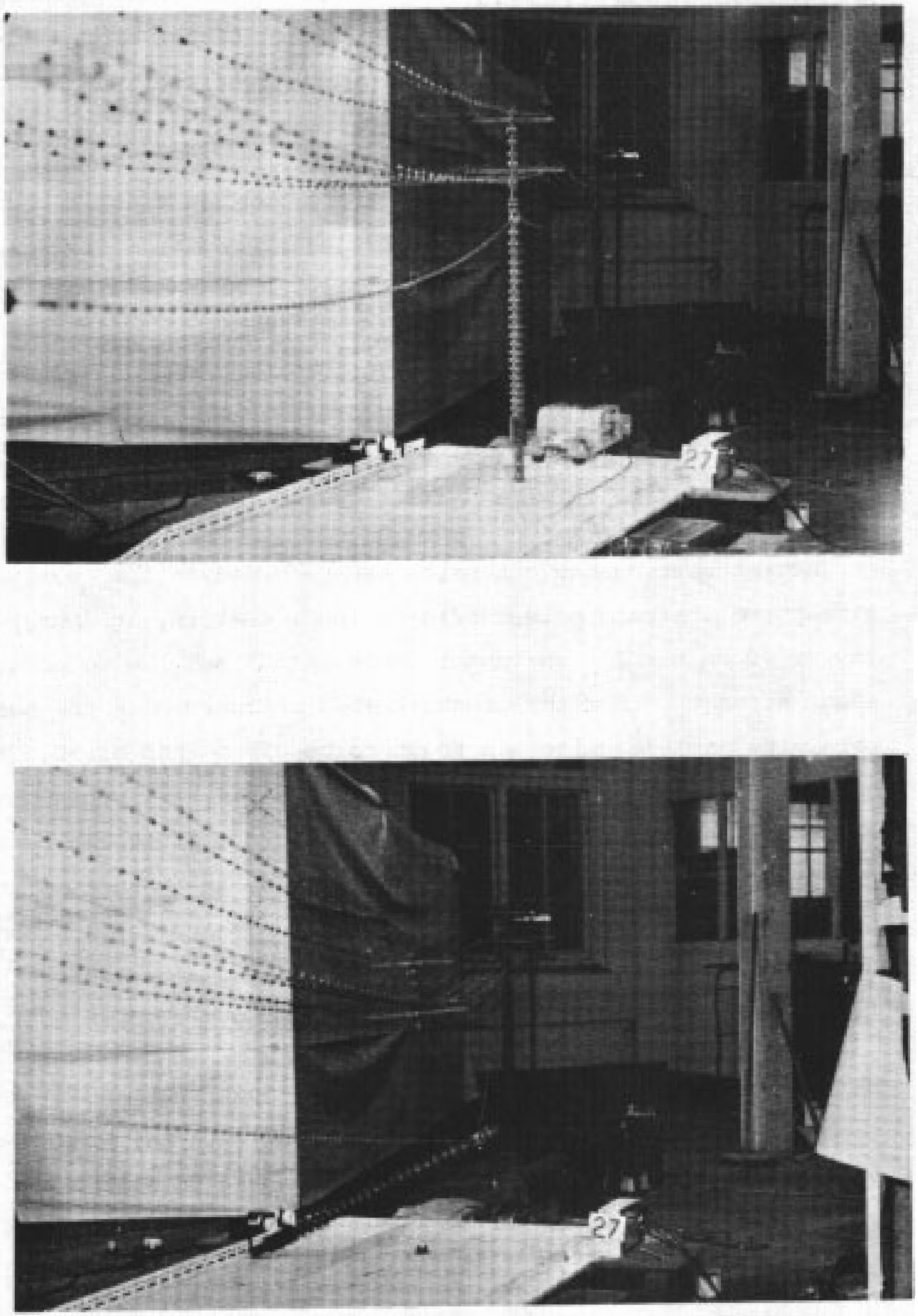

Figure 3.6. Before and after a 68.2km/h FSE velocity impact with a 3.1kN two-crossarm pole with restraining cable.

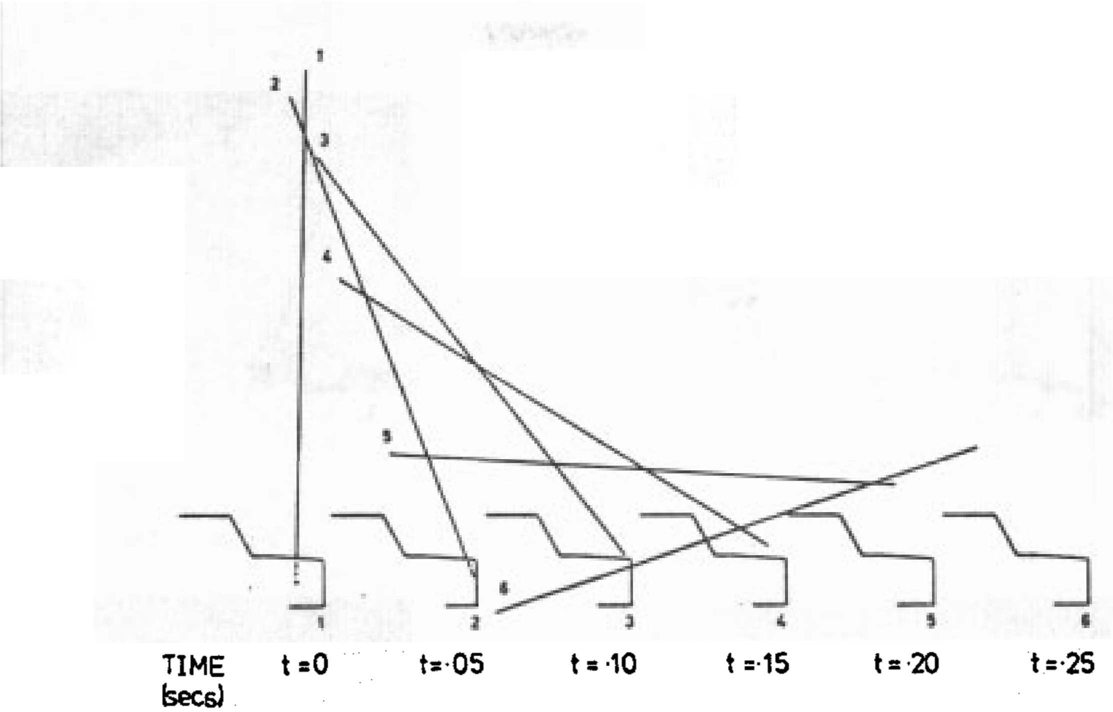

Figure 3.7. Scale model time sequence plot of a 3.1kN two-crossarm pole without restraining cable (test # 24) impacted at a FSE velocity of 68.0km/h.

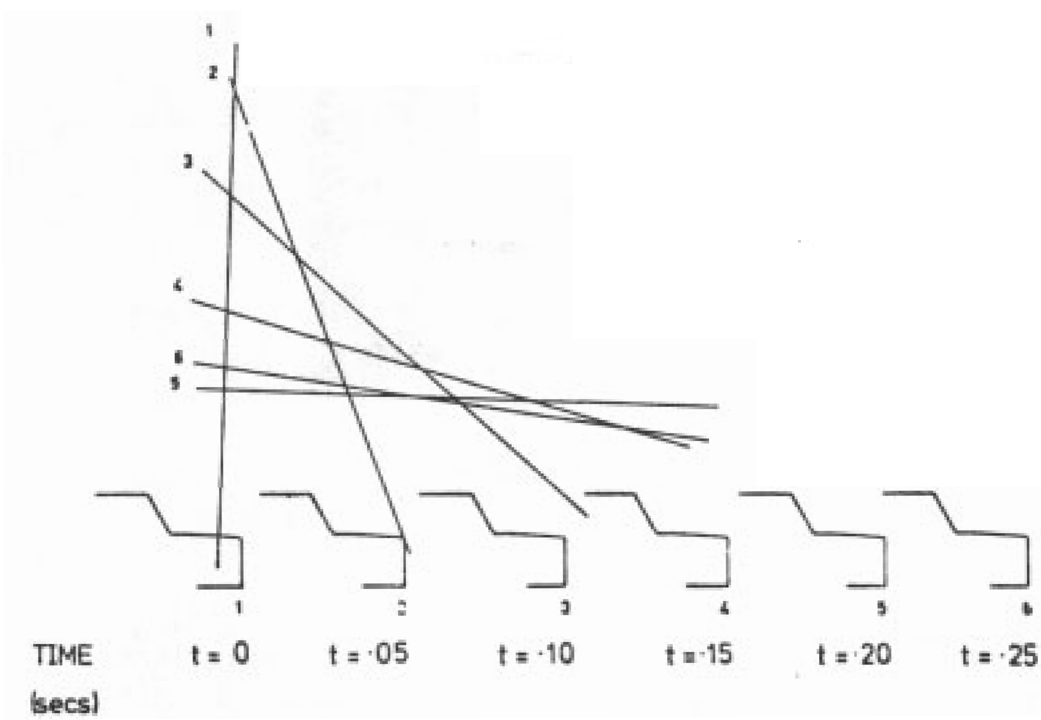

Figure 3.8. Scale model time sequence plot of a 3.4kN two-crossarm pole with restraining cable (test # 27) impacted at a FSE velocity of

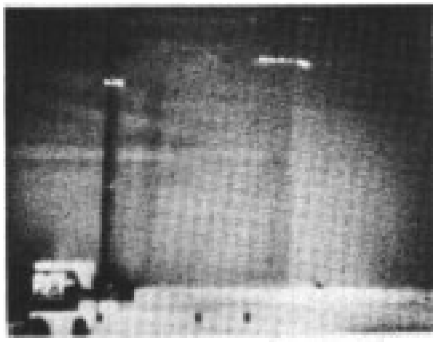

Base shear (Bs)

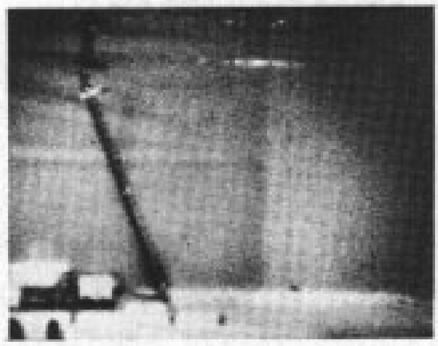

Bs + .05s

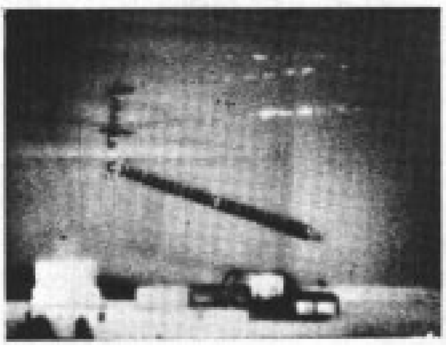

Bs + .10s

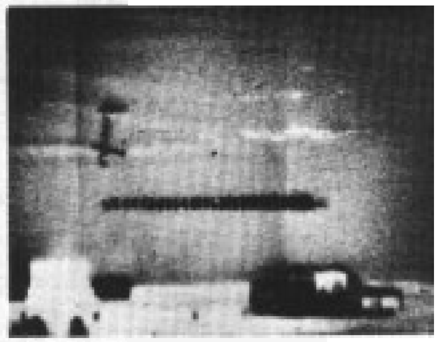

Bs + .15s

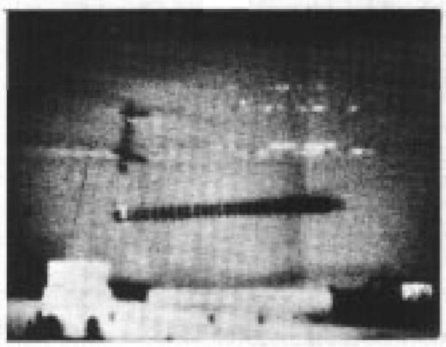

Bs + .20s

Figure 3.9. Frames taken from a high speed movie film of impact with 3.4kN two crossarm pole with restraining cable at a full scale equivalent velocity of 68.2km/h (test #28).

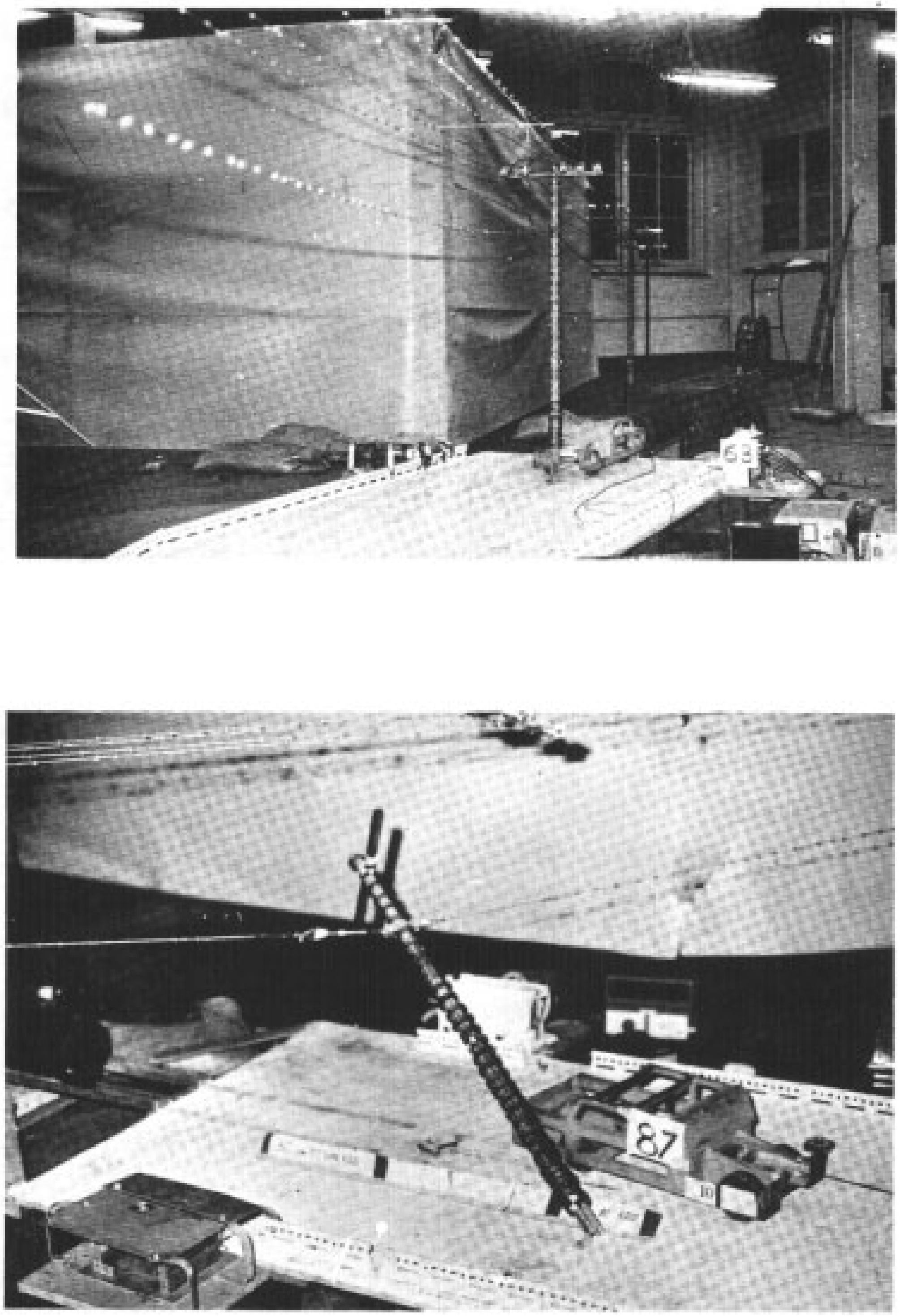

Figure 3.10. Before and after a 68.2km/h FSE velocity impact with a single crossarm messmate pole with restraining cable. (Not rest position of car).

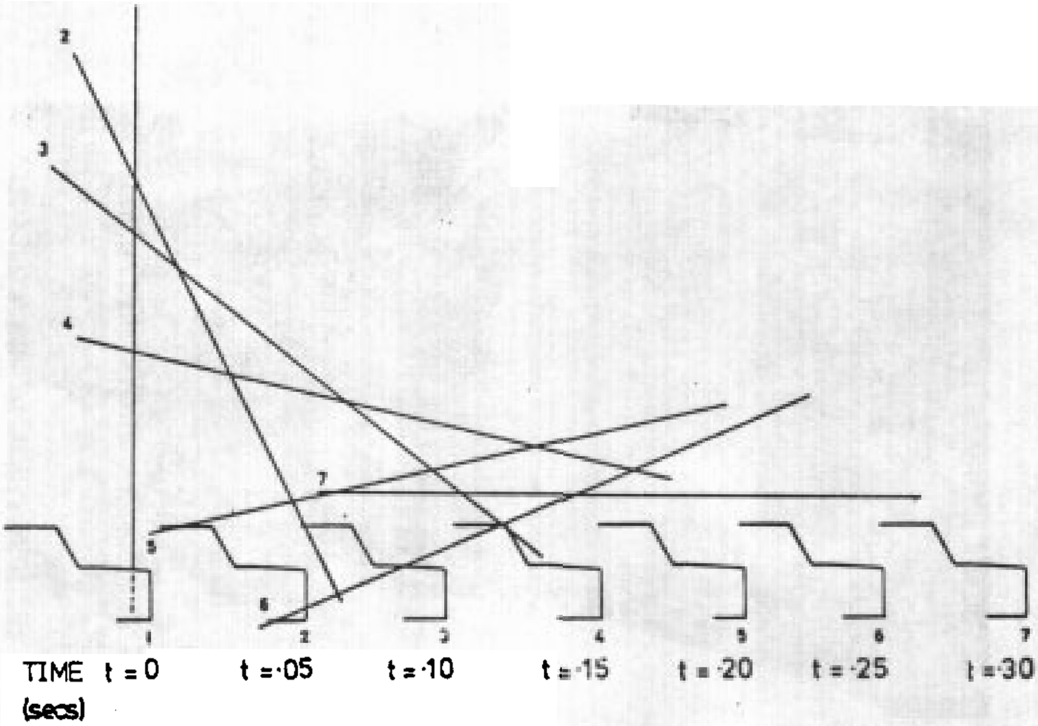

Figure 3.11. Scale model time sequence plot of a 3kN single crossarm pole without restraining cable (test # 61) impacted at a FSE velocity of 70.5km/h.

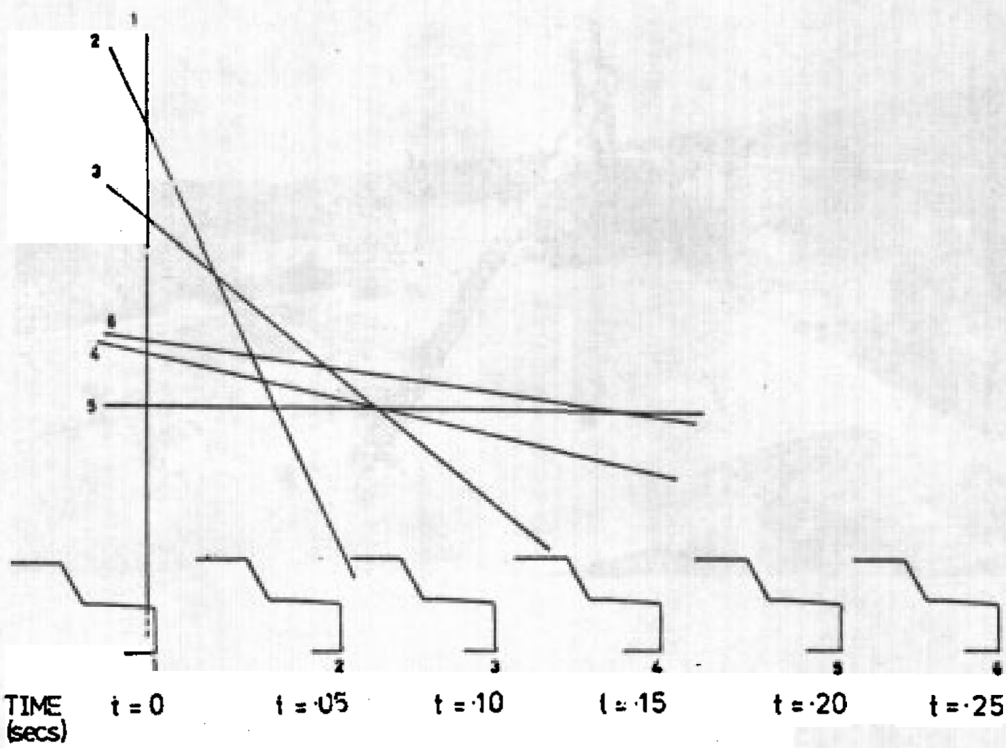

Figure 3.12. Scale model time sequence plot of a 3kN single crossarm pole with restraining cable (test # 62) impacted at a FSE velocity of

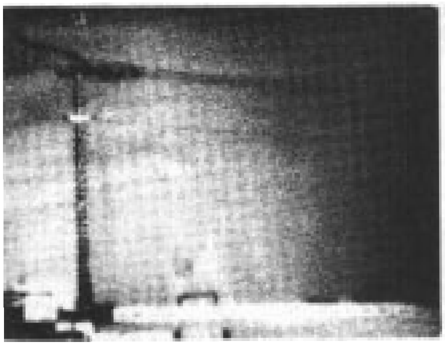

Base shear

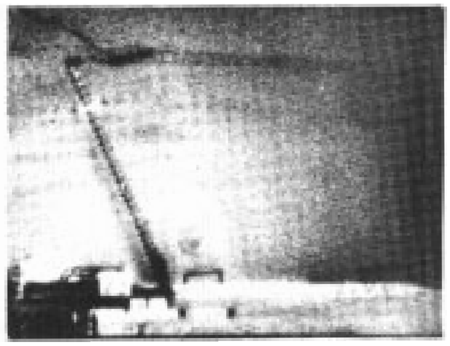

Bs + .05s

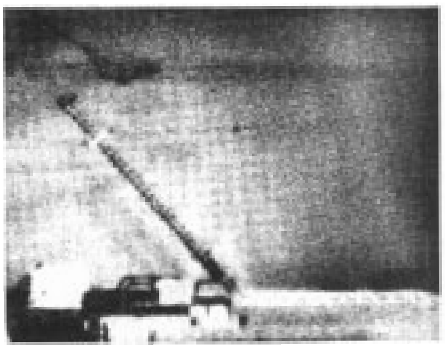

Bs + 0.10s

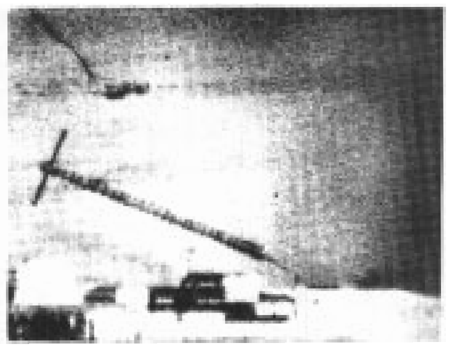

Bs + .15s

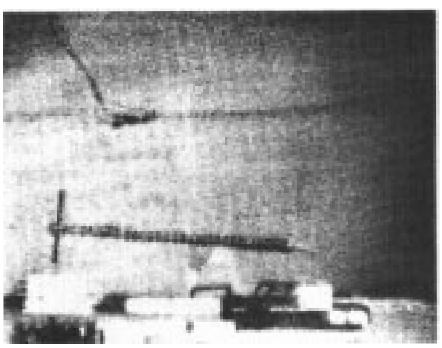

Bs + .20s

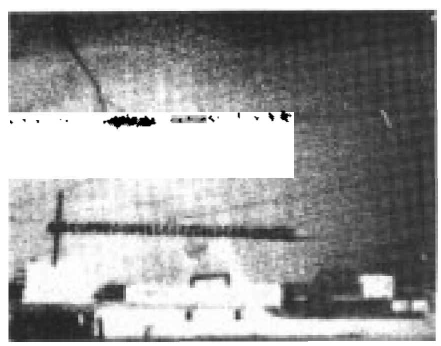

Bs + .25s

Figure 3.13. Frames taken from a high speed movie film of impact with 3kN single crossarm pole with restraining cable at a full scale equivalent velocity of 61.9km/h (test #73).

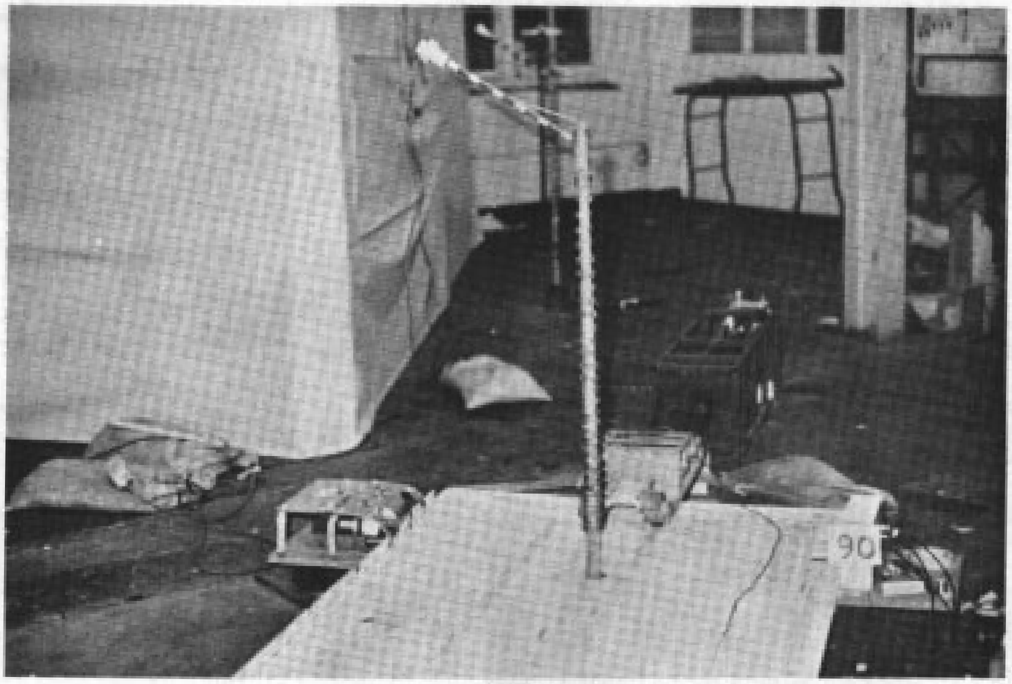

Figure 3.14. Photograph of the pre-test setup for a messmate luminaire pole without restraining cable.

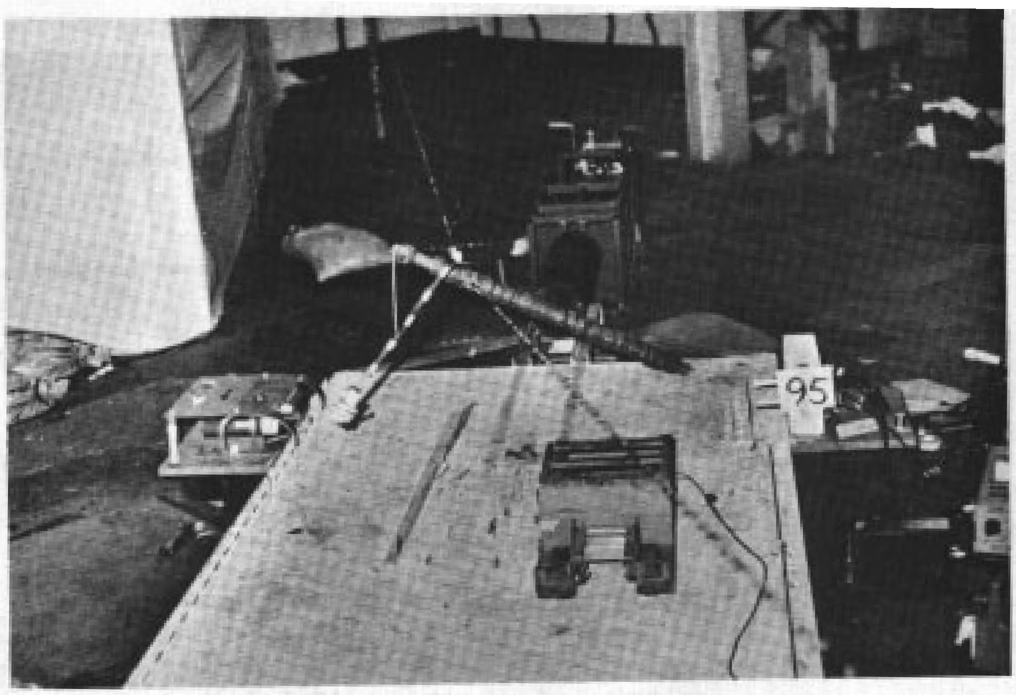

Figure 3.15. The results of a 70km/h FSE velocity impact with a 2kN messmate luminaire pole with restraining cable. (Not rest position of car).

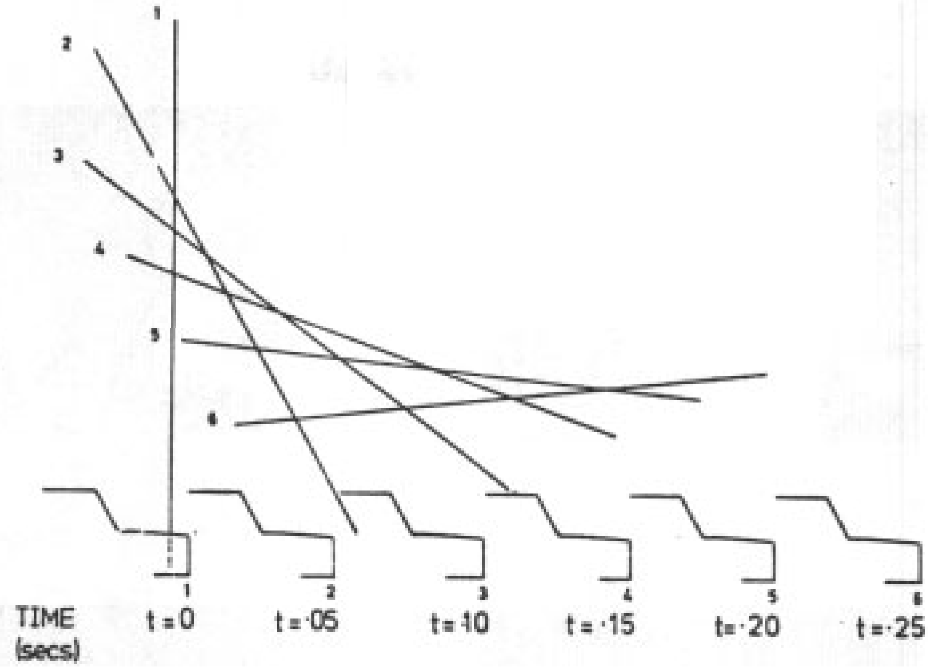

Figure 3.16. Scale model time sequence plot of a 2kN luminaire pole without restraining cable (test # 90) impacted at a FSE velocity of 70.3km/h.

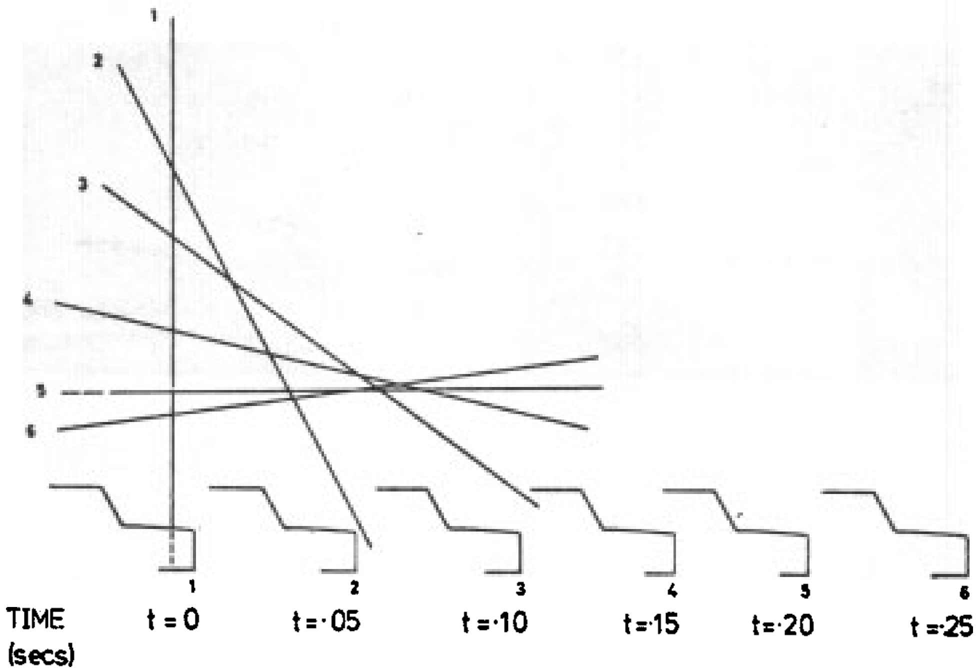

Figure 3.17. Scale model time sequence plot of a 2kN luminaire pole with restraining cable (test # 95) impacted at a FSE velocity of 70km/h.

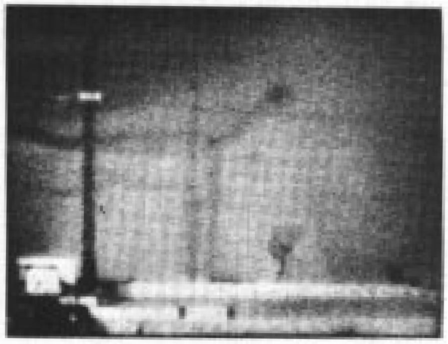

Base shear (Bs)

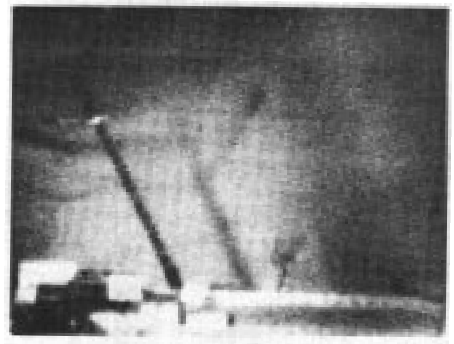

Bs + .05s

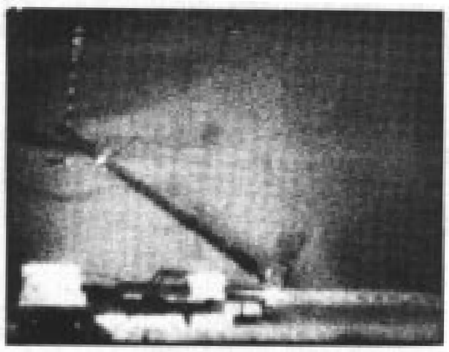

Bs + .10s

Bs + .15s

Bs + .20s

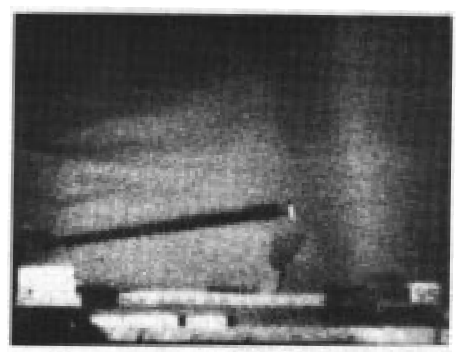

Bs + .25s

Figure 3.18. Frames taken from a high speed movie film of impact with 2kN luminaire pole with restraining cable at a full scale equivalent velocity of 70.0km/h (test #95).

For each pole configuration a line of three modified poles and two outer, termination poles were connected by restraining cables. The target pole was struck at a FSE velocity of 70 km/h and an impact angle of 50°. **While the target poles successfully broke** away, the adjacent modified poles remained intact in all cases.

3.3.9 Effect of Base Shear Strength, Pole Configuration and Impact Velocity on Crash Severity

Within the expected range of impact speeds on urban roads (40-80 km/h) the severity of the crash experienced by the vehicle and its occupants is mainly determined by the resistance to shearing of the pole base. **The inertia of the pole and the actual impact speed have a** smaller influence on the severity of the collision. For this reason the experimental measures of crash severity have been correlated with an estimate of the base shear strength, F_S, which takes into account both the measured rupture stress of the individual pole timbers and the geometry of the slotted base. **Presenting** the results in this way also allows comparison with the predictions of the mathematical model of the collision process described in Section 1.3, which uses **F_S as a pole parameter.**

It will be recalled from Section 2.7.3 that the amount of pole material that can be removed in the base modification is determined by the need to maintain a bending section modulus of Ph/σ_w **to** resist the pole rated load P, applied at a height h above the modification, without exceeding an allowable design stress σ_w. Because of the stress magnifying effect of the slotted base, the mechanism of failure when a shear load is applied just above the modification (as by an impacting vehicle) is different from that for the service load applied at the top of the pole. **For this** reason, and because of the different allowable working stresses for the various pole timber species, poles made to the same rated service strength of different materials may have quite different base shear strengths.

In Appendix F the following expression for the base shear strength is derived :

$$F_S = \frac{\sigma_{ult}}{\frac{h + \ell/2}{2Ad} + \frac{\ell}{8Z}} \qquad (3.1)$$

where

F_S = base shear strength

σ_{ult} = timber modulus of rupture

h = height of car bumper above the top of the slot

ℓ = slot length

A = cross-sectional area of each column

Z = section modulus of each column.

To check the accuracy of this calculation of the (static) shear strength of the slotted base, six ironbark poles modified at the base with the slot scheme were statically tested by applying a load to the pole at car bumper height, just above the top of the slot. Figure 3.19 shows the comparison between the measured and predicted shear strength of the poles. It can be seen that there is a good correlation between the measured and predicted values, but equation (3.1) consistently overestimates the shear strength by about 16 percent, possibly because of stress concentration effects not allowed for in the model. (It is noted that Pearson, Kloot and Boyd (1962) list a number of fairly substantial 'form factors' for modifying the calculated bending stresses in timber beams of different cross-sectional shapes.) It appears therefore that equation (3.1) provides a good parameter for ranking the base shear strengths of slotted base poles and gives a reasonably accurate estimate of their static strength.

Figure 3.20 shows vehicle average deceleration plotted against base shear strength calculated from equation (3.1). Both messmate and ironbark test results for the three impact velocities are plotted on the graph. On the basis of this plot there is little to distinguish between the three configurations (single-crossarm, two-crossarm or luminaire) and vehicle response appears to be independent of timber type or the mechanism of pole release from the overhead services. This is confirmed by the plots of maximum vehicle deceleration and velocity change against base shear strength presented in Figures 3.21 and 3.22 respectively. It is again noted that Figures 3.20 - 3.22 show full scale equivalent values derived from the scale model results by the application of the relevant scale factors presented in Section 2.4.

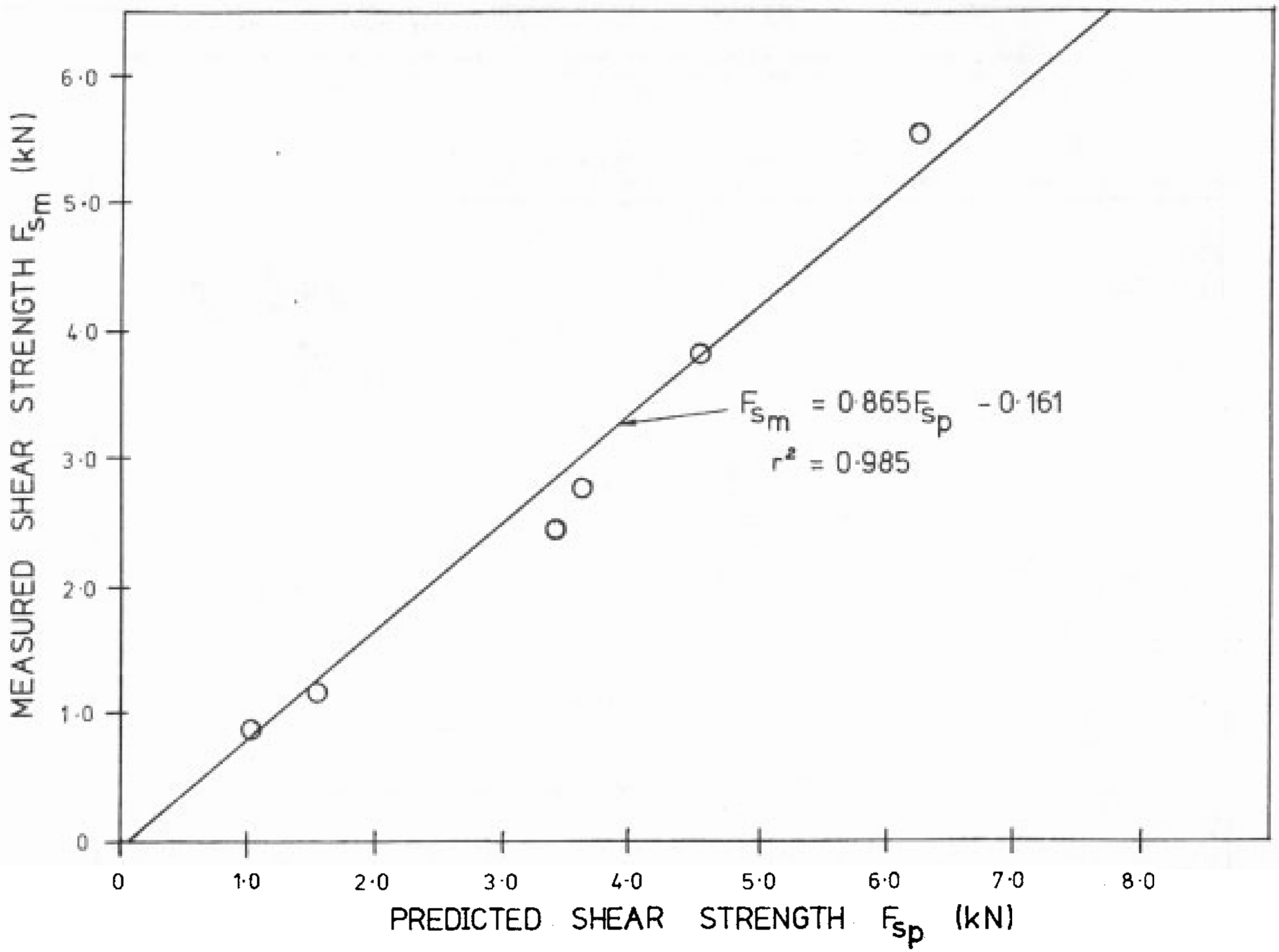

Figure 3.19. Measured static shear strength of slotted base scale model ironbark poles versus predicted shear strength.

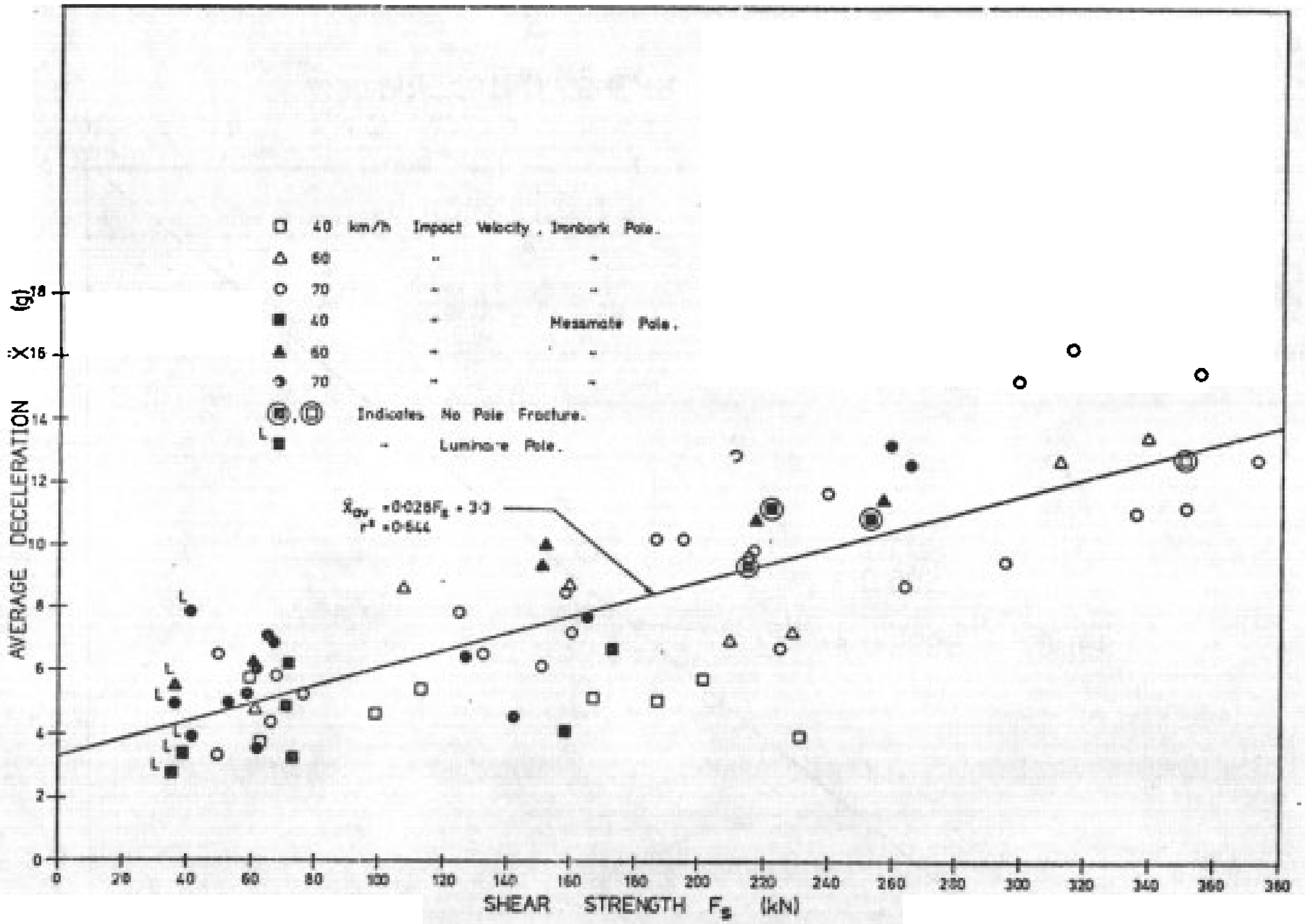

Figure 3.20. Average vehicle deceleration versus pole shear strength for all slotted base impact tests.

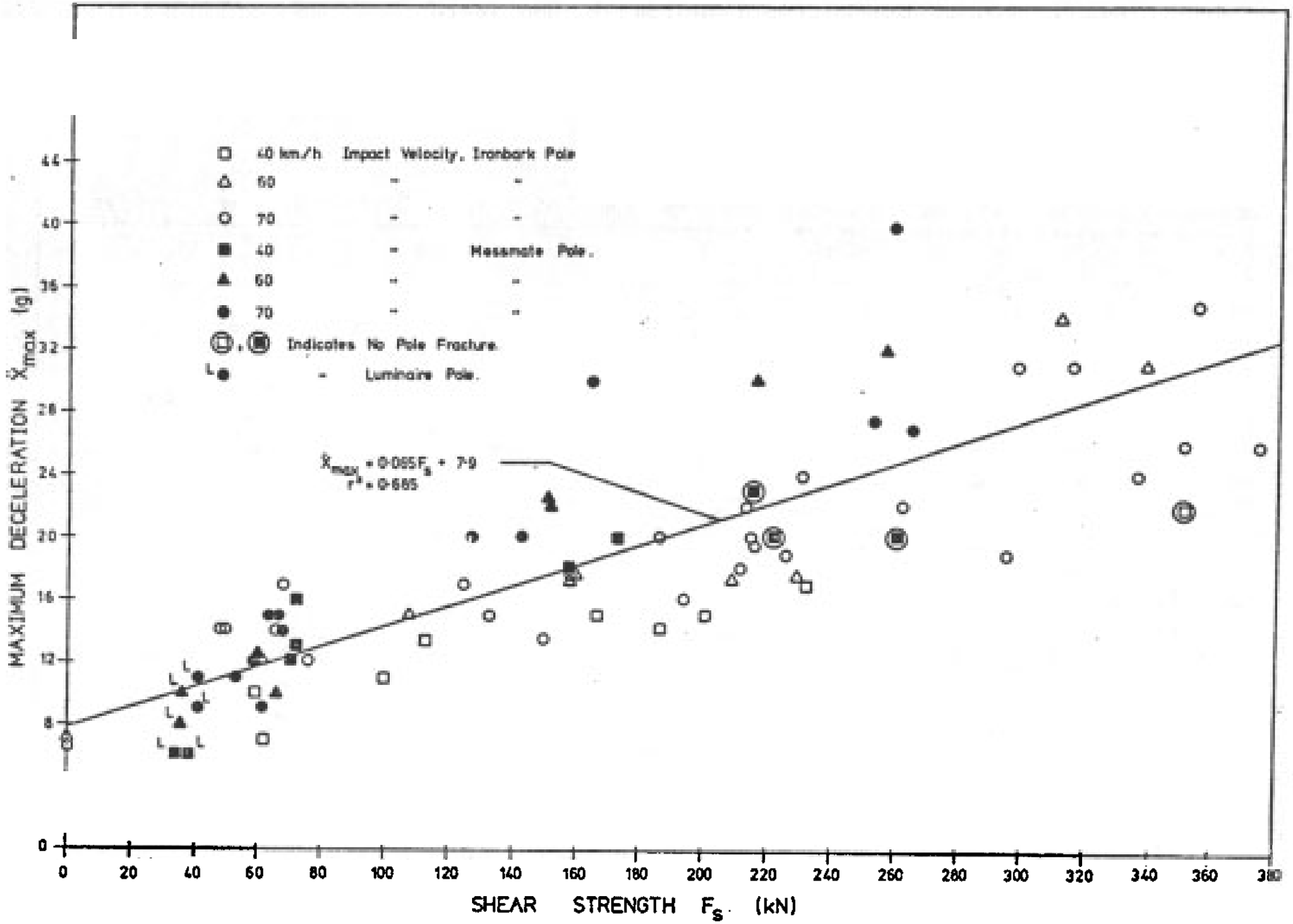

Figure 3.21. Maximum vehicle deceleration versus pole shear strength for all slotted base impact tests.

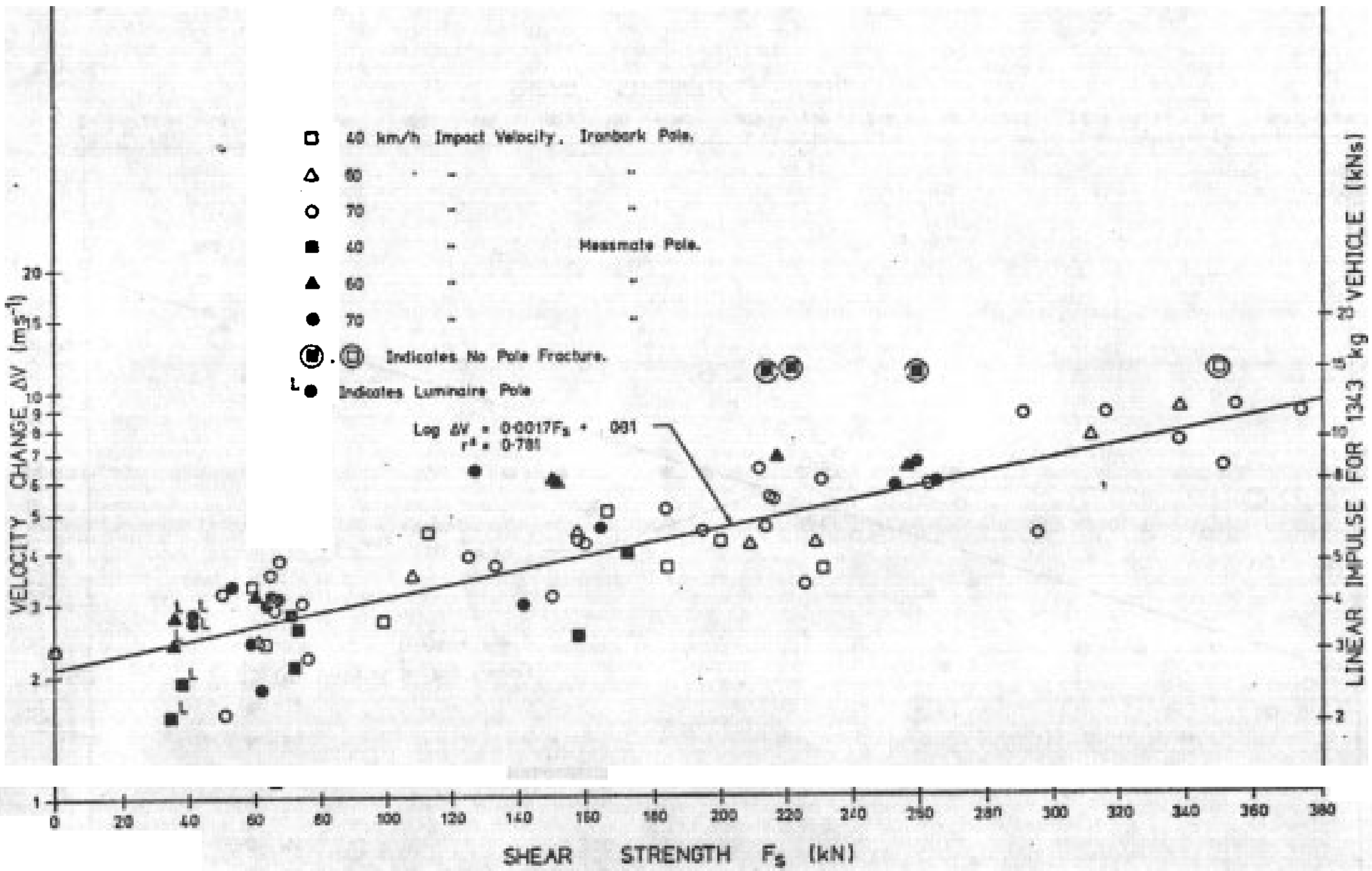

Figure 3.22. Full scale equivalent vehicle velocity change and impulse versus pole shear strength for all slotted base impact levels.

The plots in Figures 3.20 - 3.22 appear to provide a more consistent representation of the effects of pole strength on crash severity than do the plots in Figures 3.2 and 3.3, which are based on the ultimate strength for loads applied at the top of the pole. This is partly evidenced by the better correlation of the ironbark data on the F_S-based plot. Additionally, there is a clearly defined value of base shear strength F_S above which the messmate poles did not shear in 40 km/h FSE impacts. By comparison, there was no such clear ranking in terms of the ultimate strength P_{ult}.

Examining the plots in Figures 3.20 - 3.22 further, it can be seen that vehicle deceleration and the logarithm of vehicle velocity change increase approximately linearly with base shear strength. The regression lines shown on the plots are based only on those cases in which the pole broke away.

The scatter of data points about the regression lines could result from numerous sources of experimental variability, but the most important are likely to have been variations in timber strengths between the pole bases and the sample specimens used to measure rupture stress, defects in the timber, and manufacturing tolerances in machining the poles and the slot modifications.

It is difficult to detect consistent effects of impact velocity on crash severity, except for the 40 km/h FSE impacts with poles having a base shear strength of 200 kN or higher, for which the pole fails to breakaway and appears rigid to the vehicle. Further, collisions with FSE impact velocities of 40 km/h, on average, tend to result in lower vehicle deceleration and velocity change levels than those resulting from higher speed impacts.

Another measure of crash severity of interest is residual vehicle deformation. Table 3.2 shows vehicle deformation against rated pole strength for three impact velocities. As expected, vehicle deformation generally increases with increasing impact velocity and rated pole strength.

TABLE 3.2

MEAN FULL SCALE EQUIVALENT VEHICLE DEFORMATION (m)

FOR SLOTTED BASE-POLE IMPACTS

FSE Impact Velocity km/h	Rated Pole Strength 3	6	8	Unmodified
40	0.42	0.54	0.60	0.74
60	0.44	0.55	0.76	0.89
70	0.48	0.60	0.70	0.94

3.3.10 Comparison of Experimental Results with Mathematical Model.

A simplified mathematical model of the vehicle - pole impact was described in Section 1.3 (Appendix A contains the detailed derivation). This simplified model was used to generate the plots of vehicle velocity change and maximum deceleration against pole base shear strength F_S shown in Figures 3.23 and 3.24, respectively, for the experimental impact velocities of 40, 60 and 70 km/h FSE.

The form of the predicted plots is very similar to that of the experimental plots. The experimentally obtained regression lines correspond well with the model predictions, particularly for the velocity change plot, remembering that the experimental regressions excluded the non-breakaway results.

The relative insensitivity of crash severity to the range of impact speeds tested, which was noted for the experimental results, is confirmed by the simulation.

The mathematical model generally underestimates the peak vehicle deceleration, which is reasonable given the assumption of a linear vehicle crush stiffness element in the model. Figure 2.9 shows that the scale model crush stiffness was non-linear, particularly for high deformations where the crush forces rise sharply. The departure of the experimental peak deceleration results from the model predictions would therefore be expected to be greatest for high vehicle deformations, which in turn are associated with high base shear strengths. This is in fact the case. It is likely that if the mathematical model were further refined by the inclusion of a non-linear stiffness element, the experimental and

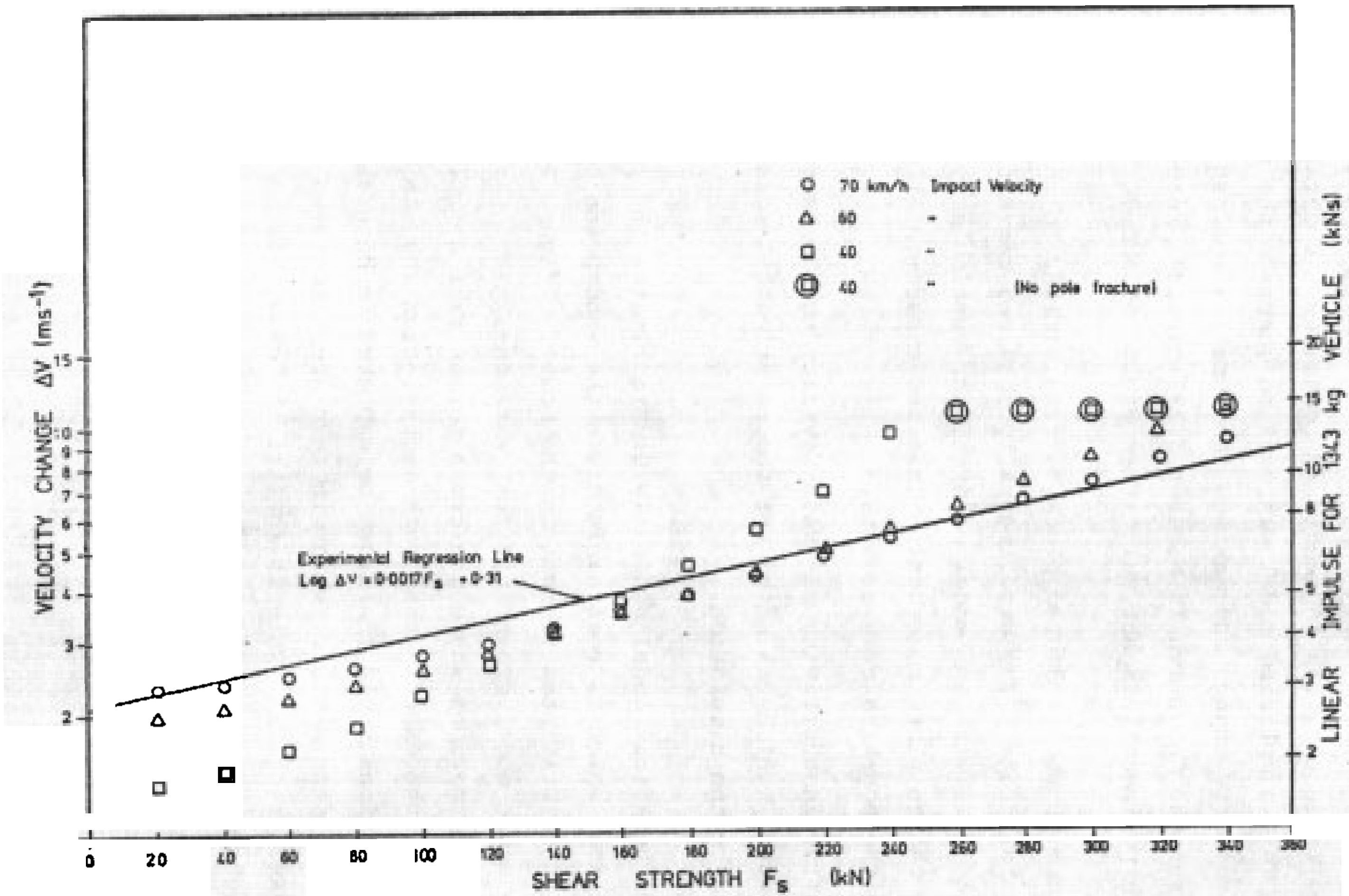

Figure 3.23 Vehicle velocity change and impulse predicted by the mathematical model versus pole shear strength for three impact velocities.

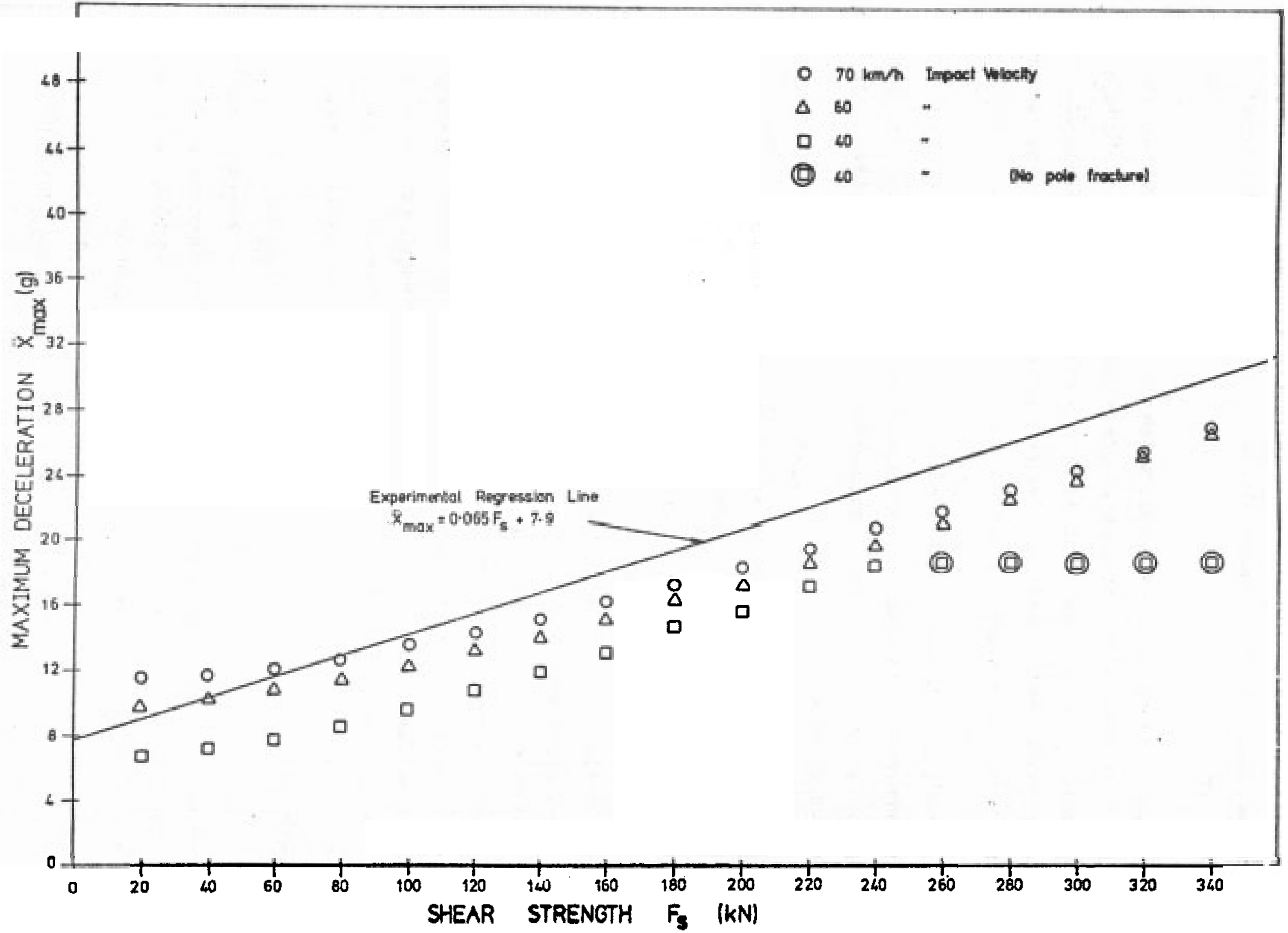

Figure 3.24. Maximum vehicle deceleration predicted by the mathematical model versus pole shear strength for three impact velocities.

predicted results would be in even better agreement. Appendix B details a model refinement which accounts for pole flexibility, but it was found that this made little difference to the predicted results.

One prediction of the model which was less successful was the level of base shear strength required for breakaway in a 40 km/h impact. This was well defined by the experiments at about 200 kN, whereas the model predicts a value just over 240 kN. The reason for this discrepancy has not been determined.

On the whole the simple model presented in Appendix A is remarkably successful in predicting the impact severity, and should prove a useful tool for investigating the effect of system parameter changes.

3.3.11 The Prediction of the Collision Performance of Modified In-Service Poles

The full scale equivalent results presented thus far have been related to the predicted base shear strength. It was established in Section 2.6.3 that the strength of the air-dry timber in the model poles was considerably greater than is likely to be encountered in full scale poles in service. Thus the FSE scale model impacts were more severe than would be expected for the majority of in-service poles with the same rated pole strength. However, because the calculation of the base shear strength took account of the measured modulus of rupture of each pole tested, the results can be simply related to full-scale poles of any given timber strength.

As a guide to the collision severity which can be expected from poles with the species mean modulus of rupture reported by Boyd (1961, 1968), the curves in Figures 3.25 and 3.26 have been derived for poles made of ironbark and messmate, respectively. These curves show the expected levels of vehicle deceleration and velocity change as a function of the rated (design) pole strength.

The predictions in Figures 3.25 and 3.26 are based on the regression lines shown in Figures 3.20, 3.21 and 3.22, and the timber properties detailed in Table 3.3. The calculation

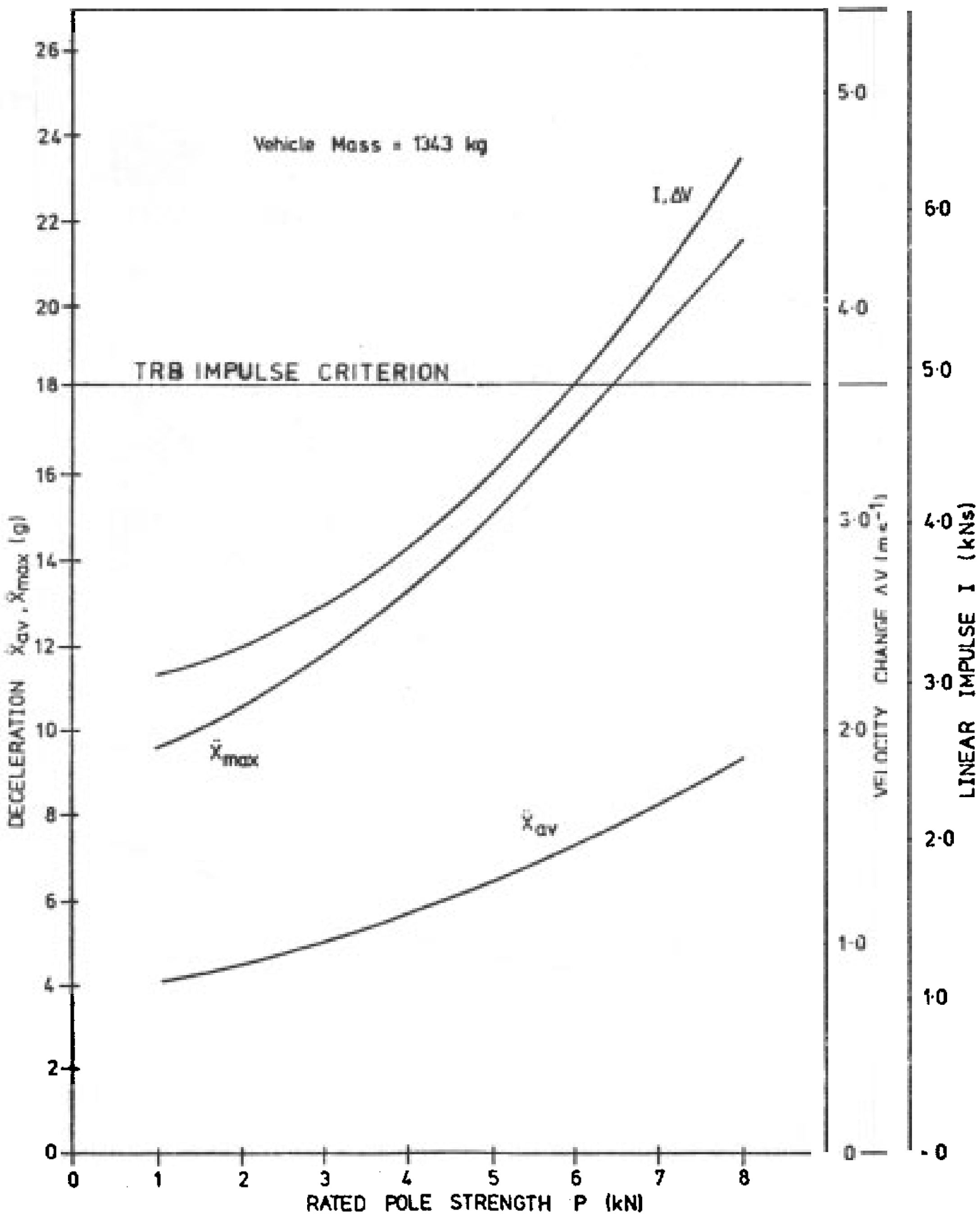

Figure 3.25. Expected crash severity versus rated pole strength based on species mean modulus of rupture for two-crossarm ironbark poles. **Impact speed 40-80km/h.**

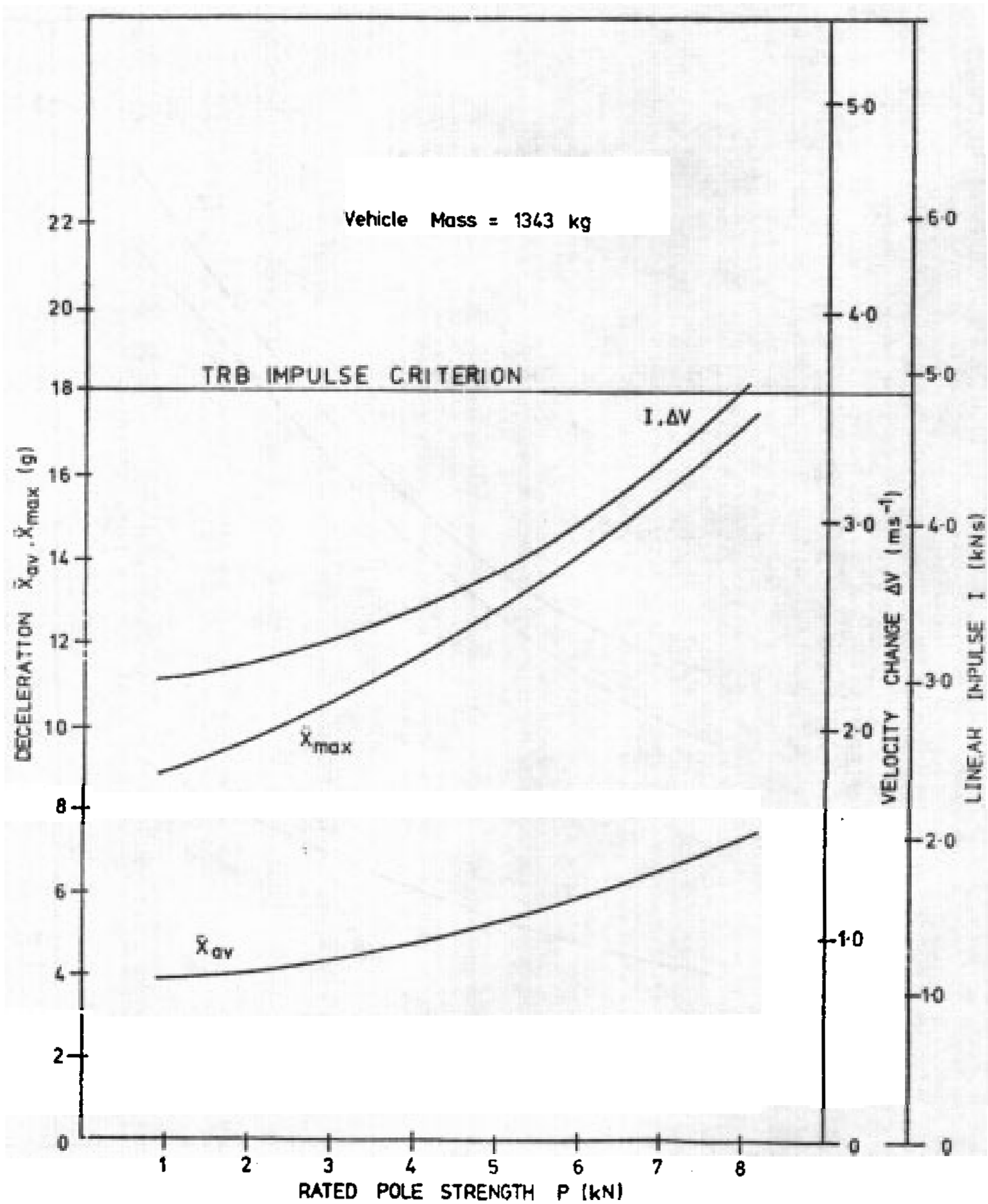

Figure 3.26. Expected crash severity versus rated pole strength based on species mean modulus of rupture for messmate single crossarm and luminaire poles. Impact speed 40-80km/h.

procedure was as follows :

(i) For a given pole rated or design strength and allowable working stress the slot modification dimensions were determined.

(ii) From the slot modification dimensions and the species mean modulus of rupture the base shear strength was calculated using equation (3.1).

(iii) Using the relevant regression equation and the calculated base shear strength, the value of the crash severity indices were calculated.

The curves of Figure 3.25 apply to 12 m (9.8 m above ground) ironbark poles with two-crossarms ; the curves of figure 3.26 relate to 11 m (8.6 m above ground) messmate single-crossarm or luminaire poles, as shown in Figures 2.1, 2.2 and 2.3 respectively.

The in-service species mean modulus of rupture adopted for each of the two timbers in Table 3.3 were the green timber values reported by Boyd, who found that ultimate strength of seasoned, desapped and resoaked poles (the likely in-service condition) did not vary greatly from the green timber value. It can be further noted that scale model results show that the crash severity is not related to the pole strength at the upper breakaway zone of two-crossarm poles.

TABLE 3.3

TIMBER PROPERTIES ADOPTED FOR THE PREDICTION OF COLLISION SEVERITY AS A FUNCTION OF RATED POLE STRENGTH

TIMBER SPECIES	WORKING STRESS σ_w (MPa)	MODULUS OF RUPTURE σ_{ult} (MPa)
Ironbark	60 (1)	129 (2)
Messmate	48 (1)	78 (3)

(1) From SECV (1978) Overhead Line Design Manual.

(2) From Boyd (1961).

(3) From Boyd (1968).

The use of the experimental regression lines in the derivation of the predicted crash severity curves neglects the effect of impact speed. However, as the mathematical model and the experimental data show, this effect is relatively small in the range of speeds tested. The curves should therefore provide reasonable estimates for impact speeds between 40 and 80 km/h, say.

The curves in Figures 3.25 and 3.26 are also only drawn for one vehicle mass, viz. 1343 kg. The mathematical model predicts that, for a given impact speed and base shear strength, the impulse suffered by the vehicle is relatively independent of vehicle mass. Hence the impulse curves apply approximately to other vehicle masses also. Velocity change can be predicted by dividing the impulse by the vehicle mass. The mathematical model results in Figure 1.8 show that the peak deceleration varies inversely with vehicle mass. Estimates of peak and average deceleration can therefore be derived by multiplying the values obtained from Figures 3.25 and 3.26 by 1343/M , where M is the vehicle mass in kg.

As has been pointed out in Chapter 1, and discussed at length in Appendix C, the prediction of likely injury severity from vehicle frame parameters is difficult in the present state of knowledge. However, for the purposes of design evaluation, the data of Chi (1976) and the Transportation Research Board (1978) were chosen as being representative of the fatal or serious injury, and no-injury limits, respectively. The limits reported by Chi for restrained occupants were an average vehicle deceleration of 25 g and a velocity change of 12 m/s.

The Transportation Research Board no-injury limit is an impulse of 4890 Ns for a vehicle with a mass of 1020 kg. However, as has just been pointed out, the impulse suffered in the collision appears to be insensitive to vehicle mass. Thus if the 4890 Ns limit is satisfied by poles impacted by the 1343 kg vehicle modelled in the present tests, it should also be satisfied for a 1020 kg vehicle.

It can be seen in Figures 3.25 and 3.26 that the TRB no-injury limit is met by modified ironbark poles with a rated strength of

6 kN or less, and by modified messmate poles with a rated strength of 8 kN or less. The severe injury limits are met by all modified poles with design or rated strengths in the range investigated. This is in sharp contrast to the likely outcome of an impact with an unmodified pole.

3.3.12 The Effect of Pole Breakaway on the Conductor Cables and Cable Ties

Cable tensions were measured for only eight of the two-crossarm ironbark pole tests. Seven of the eight tests involved poles with a FSE rated strength of 8 kN ; the remaining test was with a 6 kN FSE pole. Three impact velocities were used (40, 60 and 70 km/h) and the impact angle was 15° .

For this configuration, the pole is modified by crossed-holes just under the lower crossarm, as well as by vertical slots at the pole base. After the base of the pole has been sheared by the impacting vehicle, the breakaway pole section detaches from the upper-pole/crossarm section of the pole at the upper modified zone (see Figure 3.9). To achieve separation at the crossed-holes modification, the cables and cable ties must provide a reactive bending moment.

In the preliminary test series, it was found that conventional strength ties (10 amp fuse wire in the scale model) were not strong enough to achieve the upper breakaway, although the cables were found to be strong enough when clamped to the crossarms. In the main test series, 15 amp fuse wire cable ties performed successfully for FSE rated pole strengths up to and including 6 kN . For the 8 kN poles 20 amp fuse wire was required. Table 2.4 relates the size of the fuse wire to the full scale static strength of the cable tie - insulator connection required.

The positioning of the cable tension transducers for the two-crossarm and the single-crossarm configurations is shown in Figures 3.27 and 3.28 respectively. It can be seen that the tensions were only measured on the high tension side of the crossarms, due to limitations in the number of available recording channels. However, for one test, transducers were placed on both sides of the crossarm and it was found that, as the tension increased on one side of the

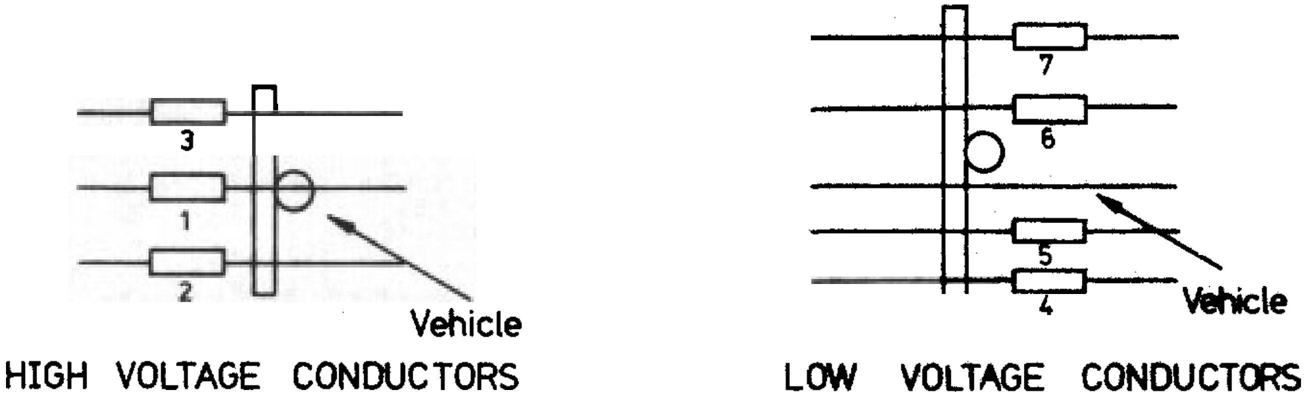

Figure 3.27. Placement of cable tensions transducers for the two crossarm configuration tests.

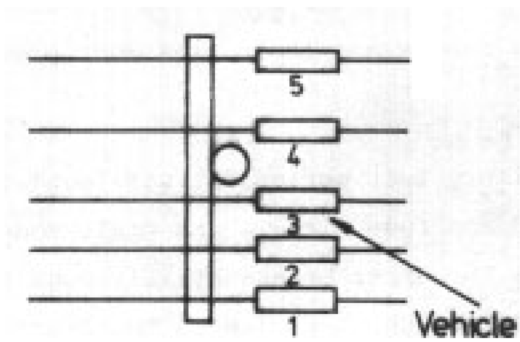

Figure 3.28. Placement of cable tension transducers for the single crossarm configuration tests.

crossarm following the impact, it quickly fell to zero on the other side.

Figure 3.29 shows two cable tension traces resulting from a 70 km/h FSE impact with 6 kN two-crossarm ironbark pole. Cable No. 1, which is the middle, upper cable, develops a peak tension of 215 N as the upper breakaway occurs. This may be compared with the model cable failure load of 440 N (which, it may be recalled from Section 2.6.2, scales perfectly with the full-scale conductor failure load). The pole breaks away at the upper modification as the peak tension is reached and the crossarms and top section of the pole then bounce up and down on the cables. The trace from cable No. 4 (a lower crossarm cable) in Figure 3.29 has a coarser time scale than the cable No. 1 trace. The initial tension peak which occurs at pole upper breakaway was consequently not registered in the plot because of lack of resolution in the digital storage CRO. If the initial segment of the signal is examined with a finer time scale the breakaway-induced tension peak appears, but has a magnitude less than the peaks due to the bouncing of the crossarms. The longer time scale for the cable No. 4 plot was used to show the decay of the bouncing mode, and the rest tension level which is about 50 N (FSE of 2840 N).

Cable No. 1 has the highest peak tension of all the cables, with the top three cables suffering generally higher tension peaks than those on the lower crossarm. The peak tension recorded for the 8 kN pole tests was marginally higher at 220 N. However, the tension peaks due to the bouncing crossarms were much the same for all tests. Of the lower crossarm cables, the roadside cables were subjected to the highest peak tensions.

There was no upper pole modification employed in the single-crossarm, messmate pole tests. Rather, the crossarm stripped away from the conductors through failure of the 10 amp fuse wire cable ties. The crossarm separated successfully for all impact velocities and angles, and the same set of model cables were able to be used throughout the tests. Figure 3.30 shows the tension traces for two wires resulting from a 70 km/h FSE impact with a 6 kN rated messmate pole. The initial tension spikes occur as the tie wire fails; the subsequent tension peaks result from cable bounce. The peak tension in the conductors is approximately 100 N (FSE of 5680 N).

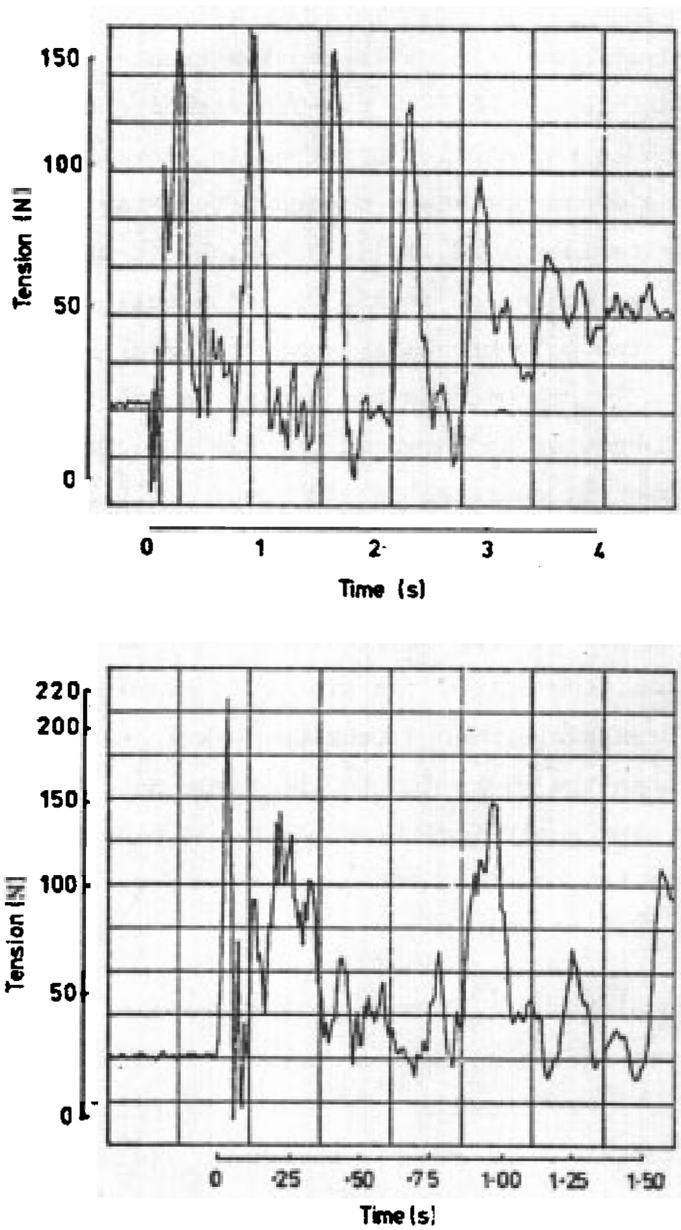

Figure 3.29 Scale model cable tension traces resulting from a 70km/h FSE velocity impact with a 6kN rated two-crossarm ironbark pole. The upper trace is from cable No.4 and the lower trace from cable No.1 (Figure 3.27).

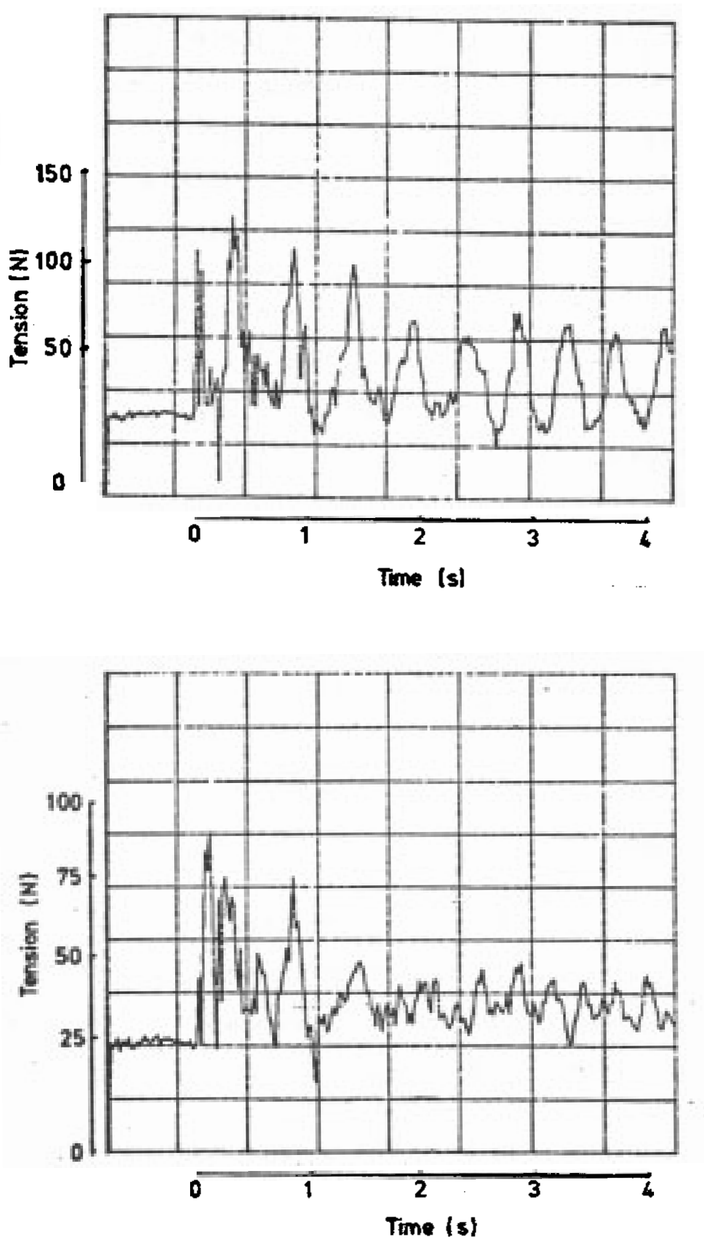

Figure 3.30 Scale model cable tension traces resulting from a 70km/h FSE velocity impact with a 6kN rated messmate single crossarm pole. The upper trace is from cable No.5 and the lower from cable No.1 (Figure 3.28).

The 10 amp fuse wire used for cable ties in the tests models the strength of the present in-service aluminium tie wire. Tables 2.3 and 2.4 provide details of the full scale equivalent strengths. Assuming that the ties were subjected to the peak cable tension recorded on one side, and effectively zero tension on the other side, traces such as those in Figure 3.30 suggest a dynamic failure load of about 100 N. This compares well with the static failure load of 94 N measured in oblique-pull tests (Table 2.4).

As was mentioned in the discussion of the preliminary results, high speed movies of the tests with conductor-supporting pole configurations revealed evidence of cable clash. This was completely eliminated for the single crossarm case by installing three cable spreaders in each span. For the two-crossarm case, spreaders were found to be necessary between the upper and lower cable layers as well as across the cable layers. In practice this means installing spreaders between high and low voltage conductors, which may pose some insulation problems.

3.4 SUMMARY

(i) The experimental program included 95 tests which investigated the collision performance of three modified pole configurations, for two species of timber, three impact velocities and three impact angles.

(ii) It was found that a pole modification system involving the cutting of two vertical slots between two layers of crossed-holes resulted in less severe collisions than a modification involving only a single layer of crossed-holes.

(iii) It was found necessary to install restraining cables between the target pole and adjacent poles to reduce the incidence of the breakaway pole crashing onto the vehicle roof and/or windscreen. This modification was successful in preventing such secondary collisions for all but the lowest speed impacts. Installation of the restraining cables has the added advantage of preventing the breakaway pole segment from travelling too far and becoming a hazard in itself.

(iv) Vehicle deceleration (peak and average), and the logarithm of vehicle velocity change were found to be approximately linearly related to the modified base shear strength.

(v) The experimental results agreed well with the predictions of the mathematical model described in Chapter 1.

(vi) Cable spreaders are required if the problem of post-impact cable clash is to be avoided.

(vii) Connections between cables and crossarms need to be stronger than those presently in service for the two-crossarm breakaway mechanism to perform satisfactorily.

(viii) Conductor cable tensions resulting from pole breakaway and subsequent cable bounce were well below the ultimate strength of the conductors.

(ix) All three modified pole configurations tested performed well, over a range of impact velocities and angles, in terms of reduced crash severity and maintenance of conductor integrity.

(x) Curves showing the peak vehicle deceleration, average deceleration and vehicle velocity change to be expected in collisions with in-service poles with rated strengths ranging from 1 kN to 8 kN were derived. Separate plots were presented for ironbark and messmate poles. The results show that impacts with slotted-base ironbark poles up to a rated strength of 6 kN, and messmate poles up to 8 kN, result in vehicle impulse levels below the TRB no-injury criterion. All modified poles in the rated strength range investigated (up to 8 kN) resulted in collision severities well below the severe or fatal injury limits of Chi (1976).

CHAPTER 4

SUMMARY AND RECOMMENDATIONS

4.1 BREAKAWAY CONCEPT FOR TIMBER UTILITY POLES

This study was motivated by the desirability of finding an economical and effective means of modifying existing timber utility poles so as to reduce the severity of vehicle collisions with them, while maintaining the integrity of the overhead conductors.

A review of the literature reveals two previous studies of breakaway timber utility poles. Wolfe et al., (1974) conducted a series of pendulum impact tests on poles modified at the base and near the crossarm by two crossed-holes. Wolfe's idea is that an impacting vehicle should cause the pole to break at the base and near the top, sustaining a tolerable deceleration level, and then continue on clear of the detached pole segment. Conductor damage should not occur because the cables are required to support only the relatively small mass of the crossarms and the very top section of the pole.

Labra (1977) carried out static and pendulum impact tests on a number of similar pole modification schemes. He recommended and crash tested a scheme involving a slot-shim modification at the pole base and a crossarm release mechanism to release the conductors from the pole.

The work of Wolfe et al., and Labra demonstrates the feasibility of the breakaway concept. However, direct extrapolation of the results to the heavier and stronger poles used in Australia is not considered valid. The present study was undertaken to develop a system suitable for local use.

4.2 MATHEMATICAL SIMULATION OF IMPACT WITH BREAKAWAY POLE

A simplified mathematical model of a vehicle-pole impact was developed to investigate the feasibility of a breakaway concept for Australian pole timbers and vehicles. The model was used in a parameter study of the vehicle/breakaway-pole system. The parameters which have most effect on collision severity were found to be the pole shear strength and vehicle mass, with vehicle impact speed having a somewhat smaller effect within the range most likely to be encountered on urban roads. The model results indicated that a significant reduction in collision severity could be achieved through the modification of utility poles, and further experimental study was justified.

4.3 INJURY TOLERANCE LEVELS

Published data on relationships between the level of vehicle occupant injury and vehicle motions during a collision do not lead to well-established injury tolerance limits. However, for the purposes of design evaluation in this project, the TRB (1978) impulse criterion of 4890 Ns (for a 1020 kg vehicle) was chosen as the no-injury limit ; the upper or serious injury limits were taken to be 12 m/s velocity change or 25 g average deceleration (Chi, 1976).

4.4 SCALE MODEL FACILITY FOR INVESTIGATION OF THE BREAKAWAY CONCEPT FOR CABLE-SUPPORTING POLES

A program of scale model tests was chosen in preference to full scale tests because :

(a) They should provide an accurate simulation of full scale tests, provided the laws of similitude revealed by dimensional analysis are adhered to.

(b) They allow the investigation of the feasibility of the idea, as well as the elimination of unimportant parameters, for a cost which is an order of magnitude less than for a comparable series of full scale tests.

(c) They have been used with great success in crash research previously.

Scale models were constructed from prototype materials, to a length scale factor of 1:7.38 , of the two most common pole/cable configurations found beside arterial roads in Melbourne. Timber luminaire poles were also made. Prototype materials were used because of the importance of the details of material behaviour to the performance of the system. The scale model vehicle was based on a standard six-cylinder sedan. It was provided with an easily replaceable, dynamically validated, crushable front structure.

Static tests were carried out on the model and prototype cable-tie/insulator systems, conductor cables and on the scale model pole timbers. The scale model timber was found to be, on average, 40% stronger than would be expected for in-service poles. This is because the timber in the scale models was drier, and had fewer defects, than that found in pole bases in service. However, this was taken into account in the prediction of full scale response from the scale model results.

The test set-up consisted of a line of five poles. The target pole was flanked by identical wooden poles and the conductor cables were terminated on adjustable turnbuckles mounted on two outer steel poles. The model vehicle was launched by a spring-actuated plunger at an angle to the pole line which was varied between 0° and 50° , at full-scale equivalent impact speeds of 40, 60 and 70 km/h.

Vehicle deceleration was recorded and processed by a digital processing oscilloscope system. A twin-light-beam timing gate allowed measurement of impact velocity, while specially-developed transducers monitored cable tensions during the tests. High-speed motion pictures were taken from two locations.

4.5 DEVELOPMENT OF POLE/CABLE BREAKAWAY SYSTEMS

4.5.1 Preliminary Test Series

A preliminary test series of seven impacts with poles modified by the crossed-hole scheme of Wolfe et al., was conducted. The tests established the viability of the scale model test technique and the substantial reduction in collision severity that can be achieved through pole modification. The tests also identified a number of areas requiring detailed design development in the main test series. These were :

(i) The post-impact trajectory of the detached pole segment.

(ii) Clashing of the overhead cables.

(iii) Cable tie and insulator strength requirements to ensure an upper pole breakaway.

(iv) The maximum load induced in the cables.

(v) The effect of varying impact speeds and angles.

(vi) The effect of different pole/cable configurations.

(vii) Alternative methods of modifying the pole to further reduce the impact severity.

4.5.2 Main Test Series

The main test series involved 88 impacts with poles modified at the base by Wolfe et al's. crossed-holes, Labra's slot/shims and by a new slotted base developed in this project. Three impact velocities were used (40, 60 and 70 km/h full scale equivalent) and three impact directions (15° , 30° and 50° from the pole line).

Poles are rated according to the transverse load which can be sustained at a point near the top of the pole without exceeding an allowable working stress in bending. In-line poles typically require a strength rating of about 3 kN to resist wind loads ; termination and deviation poles have higher rated strengths. Both single-crossarm messmate, and two-crossarm ironbark pole/cable configurations, modified to maintain full scale equivalent rated strengths from 3 kN to 8 kN, were tested. A 2 kN timber luminaire pole was also tested.

(a) Recommended modifications

Of the three pole base modifications tested, the slotted base illustrated in Figure 4.1 is recommended. Its impact performance is superior to the crossed-hole scheme and its potential for in-service degradation seems less than for the slot/shim modification.

The recommended upper pole breakaway mechanism for the two-crossarm pole configuration consists of two crossed-holes drilled through the pole just below the lower crossarm. On impact, the breakaway segment of the pole detaches at the slotted base and at

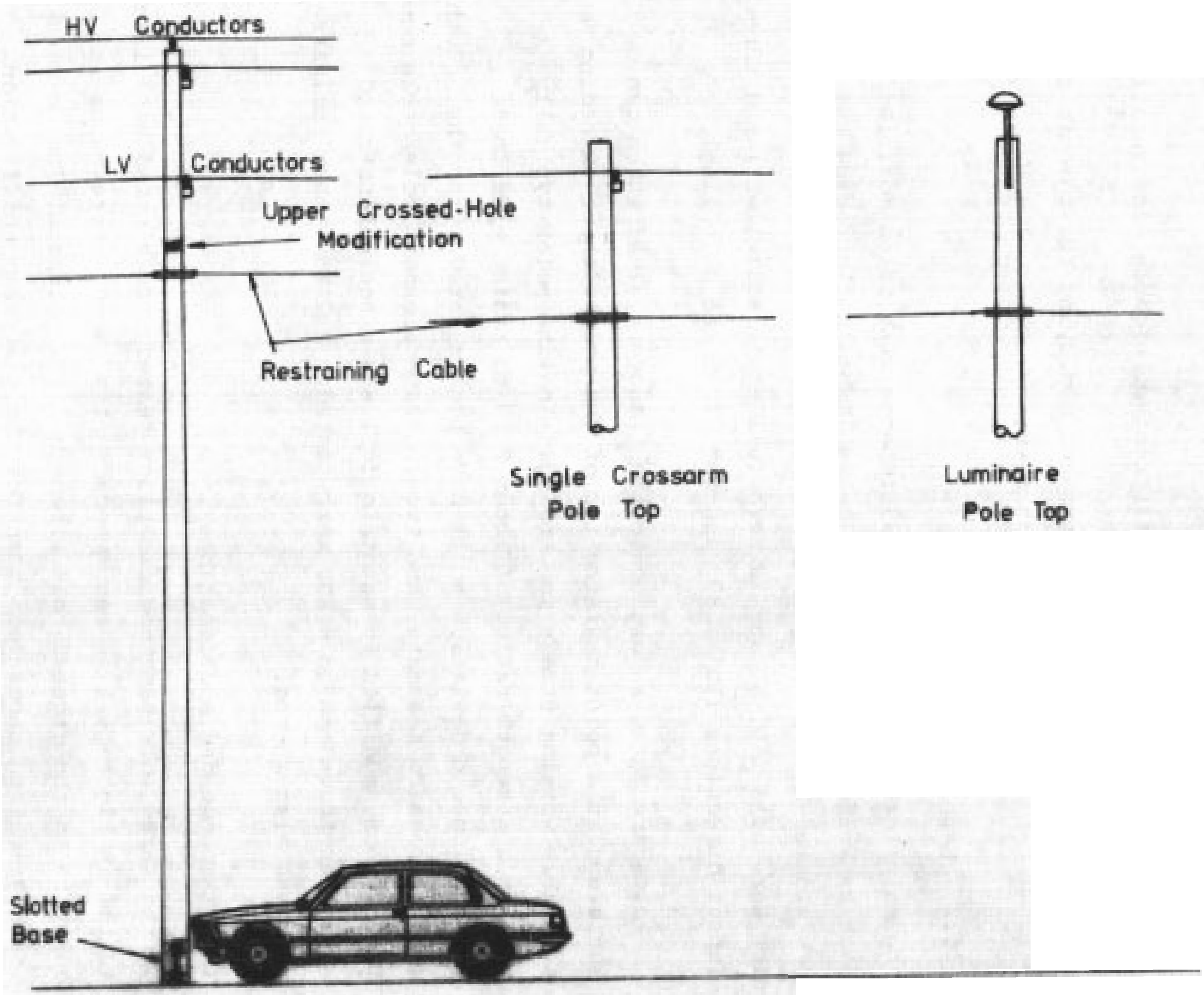

Figure 4.1 Recommended pole modification scheme

the upper crossed-holes, leaving the crossarms and pole top suspended on the conductors.

The maximum hole sizes allowable at both the base and upper modification can be determined from conventional pole design calculations. Environmental protection of the pole timber will be required. Filling the holes and slots with expanding foam and surface sealing is suggested.

Measured cable tensions indicate that the strength of the cable-tie/insulator system required for two-crossarm poles with rated strengths up to 6 kN is of the order of 9.5 kN. For poles with a rated strength of 8 kN, a cable-tie/insulator strength of 12.5 kN is required. By way of comparison, the aluminium tie wire system presently in service has a strength of 5 kN. Higher strength systems therefore need to be developed before a prototype modified pole can be tested.

The prototype conductor cables for this configuration were 19/3.25 AAC. The peak cable tension resulting from impact and subsequent pole breakaway was 12.5 kN. The ultimate strength of alternative conductors should be checked if they are to be used.

In the case of the single-crossarm pole, no upper pole modified zone is required. Instead, the pole and crossarm simply strip away from the conductors by breaking the standard strength cable ties. The peak cable tension resulting from impact and subsequent pole breakaway is 5.7 kN.

The installation of restraining cables between the target pole and the adjacent poles was found to be necessary to reduce the incidence and severity of the breakaway pole segment impacting the vehicle windscreen or roof. This has the additional advantage of preventing the detached pole segment from translating far from its starting point, thereby reducing the probability of secondary collisions with other vehicles. For ironbark poles the ultimate strength of the restraining cable should exceed 50 kN ; for messmate poles, 45 kN.

A number of tests were conducted to investigate the possibility of a 'domino effect' of successive failures occurring in a run of modified poles when one of their number was struck by a vehicle. No such effect was produced.

(b) Collision severity

The impact test results show that the vehicle deceleration (peak and average) and the logarithm of vehicle velocity change increase approximately linearly with base shear strength. For a given base shear strength, there is little to distinguish between the impact performance of different pole configurations or timber species. There is also little detectable effect of impact velocity on collision severity in the range of speeds tested.

The simple mathematical model predictions are generally in good agreement with the experimental results, and the model should prove a useful tool for investigating the effect of system parameter changes.

As a guide to the collision severity that can be expected from impacts with modified in-service poles, the curves in Figures 4.2 and 4.3 have been derived. These are for ironbark and messmate poles respectively, based on the species mean modulus of rupture reported by Boyd (1961, 1968). These curves show the expected levels of vehicle deceleration and velocity change as a function of rated pole strength.

The curves of Figure 4.2 apply to 12 m (9.8 m above ground) ironbark poles with two-crossarms ; the curves of Figure 4.3 relate to 11 m (8.6 m above ground) messmate single-crossarm or luminaire poles.

Although the curves have been derived for a vehicle mass of 1343 kg , the mathematical model results allow estimates of collision severity for vehicles of different mass to be made. Velocity change can be predicted by dividing the impulse by the vehicle mass, and estimates of peak and average deceleration can be derived by multiplying the values obtained from Figures 4.1 and 4.2 by 1343/M , where M is the vehicle mass in kg .

It can be seen in Figures 4.2 and 4.3 that the TRB no-injury impulse limit of 4890 Ns is met by modified ironbark poles with a rated strength of 6 kN or less, and by modified messmate poles with

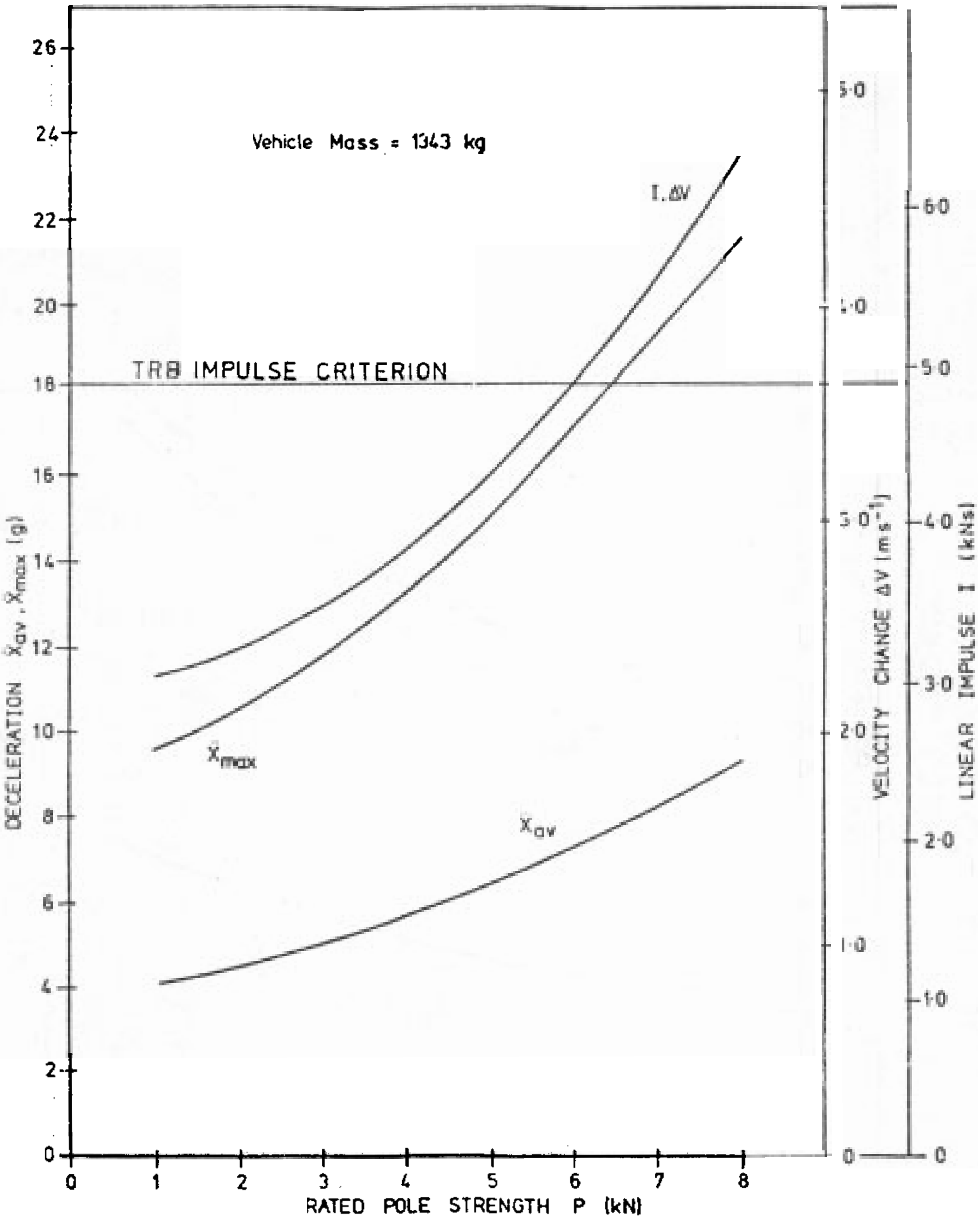

Figure 4.2. Expected crash severity versus rated pole strength based on species mean modulus of rupture for two-crossarm ironbark poles. **Impact speed 40-80km/h.**

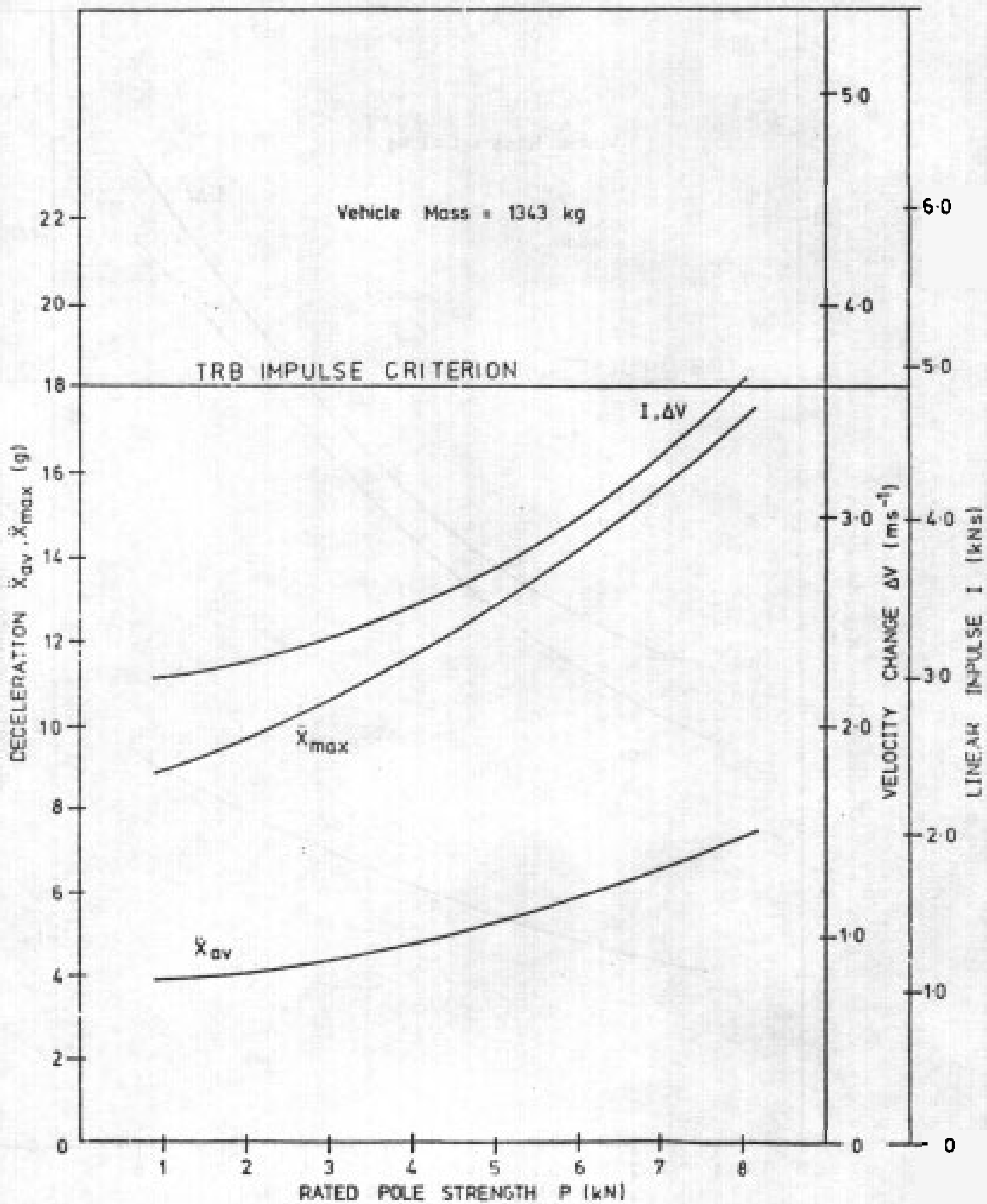

Figure 4.3. Expected crash severity versus rated pole strength based on species mean modulus of rupture for messmate single crossarm and luminaire poles. Impact speed 40-80km/h.

a rated strength of 8 kN or less. The severe or fatal injury limits of Chi (1976) (12 m/s velocity change or 25 g average deceleration) are met by all modified poles with design or rated strengths in the range investigated. This is in sharp contrast to the likely outcome of impacts with unmodified poles.

(c) Integrity of conductors

Conductor cable tensions resulting from pole breakaway and subsequent cable bounce are well below the ultimate strength of the conductors. The installation of cable spreaders was found to be necessary to avoid the problem of post-impact cable clash.

In general, all three modified pole configurations tested performed well, over a range of impact velocities and angles, in terms of reduced crash severity and maintenance of conductor integrity.

4.6 RECOMMENDATIONS FOR FURTHER WORK

It has been clearly demonstrated that a significant reduction in the severity of impacts with timber utility poles can be achieved through simple modifications to the pole. It is therefore recommended that a program of full scale tests be undertaken with the following objectives:

(a) Validation of the scale model test results. This would be achieved by replicating the test conditions and results of six tests involving the three modified pole configurations (Figures 2.1 - 2.3) being impacted by a 1350 kg vehicle at speeds of 40 and 70 km/h. Ideally, this would mean the replication of scale model test numbers 31, 33, 66, 68, 90 and 92. Given that the scale model response corresponds to that of the prototype for these test configurations, it is reasonable to assume that the remaining scale model results are valid simulations of full scale behaviour.

(b) Evaluation of the recommended in-situ utility pole modification schemes in terms of :

- (i) impact performance
- (ii) electrical integrity
- (iii) ease of installation
- (iv) service life

(c) Development of final prototype system specifications prior to in-service trials.

It is envisaged that the model validation tests would form the basis of a preliminary test series, the outcome of which would in turn determine the course of any subsequent test program.

It is also recommended that the scale model facility be maintained during the full scale tests so that any proposed design variations could be tested quickly and economically prior to full scale testing.

The utility authorities should be closely involved in the full-scale trials to ensure that all operational problems are defined and investigated. It is noted that before full-scale trials on two crossarm poles can be undertaken, the development of higher strength cable-tie/insulator systems is required.

Following successful full-scale trials, it is recommended that in-service trials of the in-situ modifications be undertaken at a number of sites where the accident risk justifies such action.

REFERENCES

AYRE, R.S., ABRAMS, J.F.(1954). Dynamics of Guardrail Systems. Proceedings, Highway Research Board, 33, 201-209

AYRE, R.S. (1955), Dynamics of Highway Guardrails; Laboratory Experiments I. Proceedings, Highway Research Board, 34, 162-172.

AYRE, R.S. (1956). Dynamics of Highway Guardrails ; Laboratory Experiments II. Proceedings, Highway Research Board, 35, 237-250..

BOYD, J.D. (1961). The Strength of Australian Pole Timbers I. Commonwealth Scientific and Industrial Research Organization, Division of Forest Products, Technological paper 15.

BOYD, J.D. (1962a). The Strength of Australian Pole Timbers II. Commonwealth Scientific and Industrial Research Organization, Division of Forest Products, Technological paper 22

BOYD, J.D. (1962b). The Strength of Australian Pole Timbers III. Commonwealth Scientific and Industrial Research Organization, Division of Forest Products, Technological paper 23

BOYD, J.D. (1964). The Strength of Australian Pole Timbers IV. Commonwealth Scientific and Industrial Research Organization, Division of Forestry Products, Technological paper 32.

BOYD, J.D. (1967). The Strength of Australian Pole Timbers V. Commonwealth Scientific and Industrial Research Organization, Division of Forestry Products, Technological paper 50.

BOYD, J.D. (1968). Strength of Australian Pole Timbers VI. Commonwealth Scientific and Industrial Research Organization; Division of Forestry Products, Technological paper 53.

BRONSTAD, M.E., MICHIE, J.D., WHITE, R.R. (1976). Pendulum Tests Using Rigid and Crushable Bumpers. Transp[illegible]ch Board, 566, 56-64.

CHI, M. (1976). Assessment of Injury Criteria in Roadside Barrier Tests. U.S. Department of Transportation, Federal Highway Administration Report No. FHWA-RD-75-74.

CHISHOLM, D.B., VINER, J.G. (1973). Dynamic Testing of Luminaire Supports. FHWA, U.S. Department of Transportation, Report No, FHWA-RD-73-55.

COMMITTEE ON MEDICAL ASPECTS OF AUTOMOTIVE SAFETY. (1971). Rating the Severity of Tissue Damage, I. the abbreviated scale. Journal of the American Medical Association, 212, (2), 277-280.

COWLEY, J.E., CAMERON, M.H. (1976). Prediction of Motor Vehicle Occupant Fatality Trends Following Seat Belt Wearing Legislation. Proceedings Australian Road Research Board, 8, 20-29

DEN HARTOG, J.P. (1956). Mechanical Vibrations (4th ed.) New York: McGraw-Hill.

EDWARDS, T.C. MARTINEZ, J.F. McFARLAND, W.F., ROSS, H.E. (1969) Development of Design Criteria for Safer Luminaire Supports. Highway Research Board National Co-operative Highway Research Program, report No. 77

EMORI, R.I. (1973). Scale Models of Automobile Collisions with Breakaway Obstacles. Experimental Mechanics, 13, (2), 64-69.

FAY, R.J., WITTROCK, E.P. (1971). Scale Model Testing of an Energy Absorbing Barrier. Highway Research Board, (343), 75-82.

FEDERAL HIGHWAY ADMINISTRATION (1970). Application of Highway Safety Measures - Breakaway Luminaire Supports. FHWA, U.S. Department of Transportation, Notice T.O.-20.

FOX, J.C., GOOD, M.C., JOUBERT, P.N. (1979). Collisions with Utility Poles. Commonwealth Department of Transport, Office of Road Safety, report No. CR1.

GRAHAM, M.D., BURNETT, W.C., GIBSON, J.S. (1967). New Highway Barriers : the Practical Application of Theoretical Design. Highway Research Record, (174) 88-189.

GRIME, G. (1976). Probabilities of Injury in Road Accidents. Accident Analysis and Prevention,9, 125-142.

HELM, B.R., FREE, J.C., WARNER, C.Y., FRANSDEN, G.B. (1976). Scale Model Evaluation of Frictional Effects and Redirection Mechanism for Angle Barrier Impacts. Transportation Research Board, (566) 23-30.

HOLMES, B.S., COLTON, J.D. (1974). Scale Model Experiments for Safety Car Development. S.A.E. Transactions, 82, (1) 239-247.

HOLMES, B.S., SLITER, G. (1974). Scale Modelling of Vehicle Crashes - Techniques, Applicability, and Accuracy : Cost Effectiveness. Proceedings 3rd International Conference on Occupant Protection, Michigan, July 10-12, 1974, S.A.E. Paper No. 740586.

JOHNSON, J.H., MESSER, C.J. (Eds.) (1970). Roadside Safety Design-Course Notes. Texas Transportation Institute, Texas A & M University.

JURKAT, R.M., STARRET, J.A. (1967). Automobile Barrier Impact Studies Using Scale Model Vehicles. Highway Research Record, (174), 30-41.

LABRA, J.J. (1977). Development of Safer Utility Poles, Interim Report. Southwest Research Institute, report No. 03-4502-1.

MARSH, J.C., CAMPBELL, K.L., KINGHAM, B.C. (1977). An Assessment of the Relationship Between Frontal Impact Severity and Injury Level. S.A.E. Paper No. 770156.

McHENRY, R.R., SEGAL, D.J., DELEYS, N.J. (1967). Computer Simulation of Single Vehicle Accidents. S.A.E. Paper No. 670904 11th STAPP Car Crash Conference, 8-56.

McHENRY, R.R., BAUM, A.S., NEFF, D.D. (1977). Yielding Barrier Test Data Base - A Study of Side Impact Cases in the Multi-disciplinary Accident Investigation (MAI) File. Calspan Corporation. Report No. ZR-5954-V-2.

MELVIN, J.W., MOHAN, D., STAWAKER, R.L. (1975). Occupant Injury Assessment Criteria. S.A.E. Paper No. 750914.

MICHIE, J.D., CALCOTE, L.R., BRONSTAD, M.E. (1971). Guardrail Performance and Design. Highway Research Board, National Co-operative Highway Research Program, Report 115.

OLSON, R.M., POST, E.R., McFARLAND, R.F. (1970). Tentative Service Requirements for Bridge Rail System. Highway Research Board, National Co-operative Highway Research Program, Report No. 86.

OLSON, R.M., IVEY, D.L., POST, E.R., GUNDERSON, R.H., CENTINER, A., (1974). Bridge Rail Design Factors, Trends and Guidelines. Highway Research Board National Co-operative Highway Research Program, Report No. 149.

OWINGS, R.P., CANTOR, C.C. (1976). Simplified Analysis of Change in Vehicle Momentum During Impact with a Breakaway Support. Transportation Research Record, 594, 39-44.

PEARSON, R.G., KLOOT, N.H., BOYD, J.D. (1962). Timber Engineering Design Handbook. The Jacanadra Press, 2nd. Ed., 1962.

SLECHTER, A. (1971). The United States 4000 lb Experimental Safety Vehicle - Performance Specification. Proceedings of the 1st International Conference on Experimental Safety Vehicles, Paris.

STATE ELECTRICITY COMMISSION OF VICTORIA (SECV) (1978). Overhead Line Design Manual.

STATE ELECTRICITY COMMISSION OF VICTORIA (SECV) (1971). Overhead Line Manual, 1-3.

TRANSPORTATION RESEARCH BOARD, (1978). Recommended Procedures for Vehicle Crash Testing of Highway Appurtenances. Transportation Research Circular, (191).

VAUGHAN, R.G., WOOD, R., CROFT, P.G. (1974). Some Aspects of Compulsory Seat Belt Wearing. Proceedings [illegible]ad Research Board, 7, (5), 103-127.

WOLFE, G.K., BRONSTAD, M.E., MICHIE, J.D., WONG, J. (1974). A Breakaway Concept for Timber Utility Poles. Transportation Research Record, (486), 64-77.

APPENDIX A

MATHEMATICAL MODEL OF IMPACT WITH BREAKAWAY RIGID UTILITY POLE

The model proposed is illustrated in Figure A.1. A vehicle of mass M, with velocity V and crush stiffness k, impacts a pole of length ℓ, shear strength F_s and a moment of inertia about its top of I.

There are two phases in the collision sequence modelled. The results of phase I provide the initial conditions for the equations describing phase II.

At the moment of impact, the vehicle is assumed to be in contact with an immovable pole. This continues until the vehicle crush has developed to the extent that the force between the pole and the vehicle is equal to F_s. This is phase I. As soon as the impact force reaches F_s, the pole is assumed to shear and is then free to rotate about O. Discussion of this assumption is contained in the main text.

The assumptions contained in the model are:

(a) Once the impact force reaches F_s, shearing of the pole is instantaneous.

(b) The vehicle has a linear crush characteristic with zero coefficient of restitution.

(c) The pole is rigid.

(d) After shearing, the pole rotates about O.

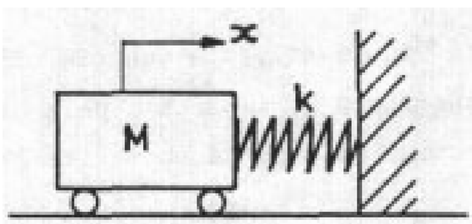

Phase I - Vehicle crush with no pole displacement.

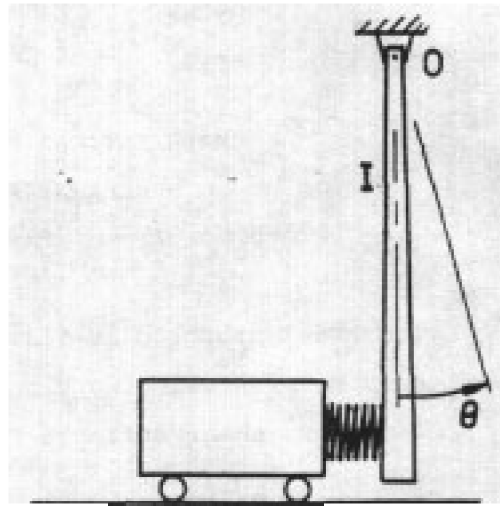

Phase II - Pole free to rotate about O.

where:

- F_s - Pole shear strength
- I - Moment of inertia of pole about O
- k - Vehicle crush spring stiffness
- ℓ - Pole length
- M - Mass of vehicle
- V - Impact velocity
- x,θ - Generalized co-ordinates
- t - Time

Figure A.1. Mathematical Model.

Until the force between the vehicle and the pole reaches F_s, the equation of motion for the vehicle is (with no pole motion during this phase):

$$M\ddot{x} + kx = 0 \tag{A-1}$$

That is,

$$\ddot{x} + \omega_o^2 x = 0, \qquad \omega_o = \sqrt{\frac{k}{M}} \tag{A-2}$$

The solution to this equation, with initial conditions, $x(0) = 0$, $\dot{x}(0) = V$ is,

$$x = V\sqrt{(M/k)}\ \sin\omega_o t \tag{A-3}$$

Thus the velocity is

$$\dot{x} = V\omega_o\sqrt{(M/k)}\ \cos\omega_o t \tag{A-4}$$

The force between the vehicle and the pole is

$$F = kx$$

Hence

$$F = V\sqrt{kM}\ \sin\omega_o t \tag{A-5}$$

The pole shears when $F = F_s$. That is, when

$$\sin\omega_o t = \frac{F_s}{V\sqrt{kM}}$$

Thus, at the end of phase I

$$x_I = \frac{F_s}{k}$$

$$\dot{x}_I = V\sqrt{1 - F_s^2/kMV^2}$$

These form the initial conditions for the post-shear phase, or phase II.

The equations of motion for phase II are:

$$M\ddot{x} + kx - k\ell\theta = 0 \tag{A-6}$$

$$I\ddot{\theta} - k\ell x + k\ell^2\theta = 0$$

Assuming a solution of the form

$$\{q\} = \{\phi\} e^{i\omega t}$$

results in

$$\begin{bmatrix} -M\omega^2 + k & -k\ell \\ -k\ell & -I\omega^2 + k\ell^2 \end{bmatrix} \begin{Bmatrix} x \\ \theta \end{Bmatrix} = \begin{Bmatrix} 0 \end{Bmatrix} \qquad \text{(A-8)}$$

ie

$$[f]\{\phi\} = \{0\}$$

where $[f]$ is the characteristic matrix

and $\{\phi\}$ is a modal vector.

The characteristic equation is obtained as

$$|f| = (-M\omega^2 + k)(-I\omega^2 + k\ell^2) - k\ell^2 = 0$$

ie $$MI\omega^4 - (Mk\ell^2 + kI)\omega^2 = 0$$

The roots of the characteristic equation yield the system natural frequencies:

$$\omega_1 = 0 \quad \text{(rigid body mode)}$$

and

$$\omega_2 = \sqrt{(1 + M\ell^2/I)(k/M)}$$

Solving (A-8) for each of the modes in turn yields the modal matrix

$$[\phi] = \lfloor \{\phi^{(1)}\}\ \{\phi^{(2)}\} \rfloor = \begin{bmatrix} \ell & -\frac{I}{m\ell} \\ 1 & 1 \end{bmatrix}$$

Hence the general solution of the equations of motion is

$$\begin{Bmatrix} x\ (t) \\ \phi\ (t) \end{Bmatrix} = \begin{vmatrix} \ell & -\frac{I}{M\ell} \\ 1 & 1 \end{vmatrix} \begin{Bmatrix} C_1 t + C_2 \\ C_3 \sin\ (\omega_2 t + \psi) \end{Bmatrix}$$

where C_1, C_2, C_3 and ψ are constants of integration. That is,

$$x\ (t) = \ell(C_1 t + C_2) - \frac{I}{M\ell} C_3 \sin\ (\omega_2 t + \psi) \qquad \text{(A-9)}$$

$$\theta\ (t) = C_1 t + C_2 + C_3 \sin\ (\omega_2 t + \psi) \qquad \text{(A-10)}$$

$$x\ (t) = \ell C_1 - \frac{I}{M\ell} C_3\ \omega_2 \cos\ (\omega_2 t + \psi) \qquad \text{(A-11)}$$

$$\dot{\theta}\ (t) = C_1 + C_3 \omega_2 \cos\ (\omega_2 t + \psi) \qquad \text{(A-12)}$$

The initial conditions for phase II are,

vehicle: $x\ (o) = \frac{F_S}{k}$, $\dot{x}(o) = V\sqrt{1 - F_s{}^2/kMV^2}$

pole: $\theta\ (o) = 0$, $\dot{\theta}(o) = 0$

Inserting these initial conditions in equations (A-9) - (A-12) and solving for ψ, C_1, C_2 and C_3 gives:

$$C_1 = \frac{V\ \sqrt{1 - F_S{}^2/kMV^2}}{\ell\ (1 + I/M\ell^2)} \qquad \text{(A-13)}$$

$$C_2 = F_s/(k\ell)(1 + I/M\ell^2) \qquad \text{(A-14)}$$

$$C_3 = - \frac{C_2}{\sin \psi} \tag{A-15}$$

$$\tan \psi = \frac{C_2 \omega_2}{C_1} \tag{A-16}$$

The vehicle crush δ, is given by

$$\delta = x - \ell\theta$$

Thus $$\delta = -C_3 \left(\frac{I}{M\ell^2} + 1 \right) \ell \sin (\omega_2 t + \psi)$$

and $$\dot{\delta} = - C_3 \ell \omega_2 \left(\frac{I}{M\ell^2} + 1 \right) \cos (\omega_2 t + \psi)$$

The maximum crush is

$$\delta_{MAX} = - C_3 \ell \left(\frac{I}{M\ell^2} + 1 \right)$$

and occurs at

$$t_{MAX} = \frac{\Pi - 2\psi}{2\omega_2}$$

Since

$$F_{MAX} = k\delta_{MAX} = -M \ddot{x}_{MAX}$$

Then

$$\ddot{x}_{MAX} = \frac{C_3 \ell k}{M} \left(\frac{I}{M\ell^2} + 1 \right)$$

As zero restitution is assumed, the pole and vehicle separate at t_{MAX} when δ_{MAX} has been reached.

Thus, from equation (A-11), the total velocity change is given by

$$\Delta V = V - \ell C_1$$

APPENDIX B

MATHEMATICAL MODEL OF IMPACT WITH A FLEXIBLE BREAKAWAY UTILITY POLE

The model described here is an extension of the model derived in Appendix A, to account, approximately, for the effects of pole flexibility. The assumptions concerning the vehicle crush stiffness, the shearing of the pole, and the top pin joint remain. In order to simplify the calculations, however, the pole has been assumed to be cylindrical with a uniform mass distribution.

Phase I of the motion proceeds as in the rigid pole model.

For phase II, generalized coordinates x(car displacement), θ(rigid body pole rotation) and η(elastic deflection of pole) are employed.

The elastic deflection of the pole at a distance y from the top is taken as

$$\upsilon(y) = \eta\phi(y) \tag{B-1}$$

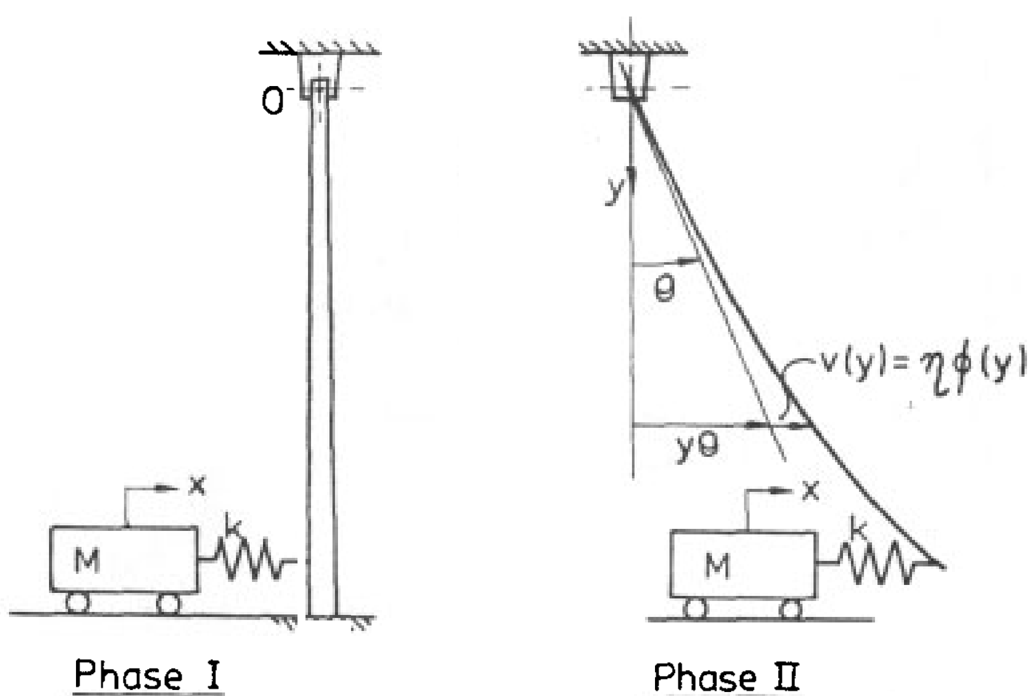

Figure B.1. Flexible pole model

where the deflection pattern of the beam is assumed to be that of the fundamental elastic mode of a pinned-free uniform beam. This mode shape may be approximated by (Den Hartog, 1956):

$$\phi(y) = \sin\pi y/\ell - 3y/\pi\ell \tag{B-2}$$

The kinetic energy T of the system may be written:

$$T = \tfrac{1}{2}M\dot{x}^2 + \int_0^\ell \tfrac{1}{2}\mu(y\dot{\theta} + \dot{\upsilon})^2 dy \tag{B-3}$$

where M is the vehicle mass and μ is the mass per unit length of the pole, which is of length ℓ.

Equation (B-3) may be written

$$T = \tfrac{1}{2}M\dot{x}^2 + \tfrac{1}{2}I\dot{\theta}^2 + \tfrac{1}{2}\dot{\eta}^2 \int_0^\ell \mu\phi(y)^2 dy + \dot{\theta}\dot{\eta}\int_0^\ell \mu y\phi(y)dy \tag{B-4}$$

where

$$I = \int_0^\ell \mu y^2 dy$$

is the moment of inertia of the pole about the pin joint O.

Substituting the assumed deflection pattern (B-2) into (B-4) results in

$$T = \tfrac{1}{2}M\dot{x}^2 + \tfrac{1}{2}I_O\dot{\theta}^2 + \tfrac{1}{2}\dot{\eta}^2(.1960)\mu\ell \tag{B-5}$$

The potential energy V of the system may be written

$$V = \tfrac{1}{2}k[x - \ell\theta - \upsilon(\ell)]^2 + \tfrac{1}{2}EI\int_0^\ell \left(\frac{\partial^2\upsilon}{\partial y^2}\right)^2 dy$$

where k is the vehicle crush stiffness and EI is the bending stiffness of the pole.

Using (B-2),

$$V = \tfrac{1}{2}k[x^2 - 2\ell x\theta + \ell^2\theta^2 - 2\phi(\ell)x\eta + 2\ell\phi(\ell)\theta\eta + \phi(\ell)^2\eta^2] + \frac{\tfrac{1}{2}\pi^4 EI\,\eta^2}{2\ell^3} \tag{B-6}$$

From the general quadratic forms for T and V in equations (B-5) and (B-6) the system mass and stiffness matrices may be deduced. The equations of motion are then:

$$\begin{bmatrix} M & 0 & 0 \\ 0 & I & 0 \\ 0 & 0 & .196\mu\ell \end{bmatrix} \begin{Bmatrix} \ddot{x} \\ \ddot{\theta} \\ \ddot{\eta} \end{Bmatrix} + \begin{bmatrix} k & -k\ell & -k\phi(\ell) \\ -k\ell & k\ell^2 & k\ell\phi(\ell) \\ -k\phi(\ell) & k\ell\phi(\ell) & k\ell\phi(\ell)^2 + \frac{\pi^4 EI}{2\ell^3} \end{bmatrix} \begin{Bmatrix} x \\ \theta \\ \eta \end{Bmatrix} = \{0\}$$

The characteristic equation,

$$\begin{vmatrix} -\omega^2 M + k & -k\ell & -k\phi(\ell) \\ -k\ell & -\omega^2 I + k\ell^2 & k\ell\phi(\ell) \\ -k\phi(\ell) & k\ell\phi(\ell) & -\omega^2 .196\mu\ell + k\phi(\ell)^2 + \frac{\pi^4 EI}{2\ell^3} \end{vmatrix} = 0$$

can be written

$$\omega^2[\omega^4 - \omega^2(\omega_0^{\ 2} + \omega_{20}^{\ 2} + \omega_{30}^{\ 2}) + \omega_{20}^{\ 2}\omega_{30}^{\ 2}] = 0$$

where $\omega_{20}^{\ 2} = \frac{k}{M}(1 + \frac{M\ell^2}{I})$

$\omega_{30}^{\ 2} = \frac{\pi^4 EI}{0.392\mu\ell^4}$

and $\omega_0^{\ 2} = \frac{k\phi^2(\ell)}{0.196\mu\ell}$

The natural frequencies are thus given by

$$\omega_1^{\ 2} = 0$$

$$\omega_{\substack{2\\3}}^{\ 2} = \tfrac{1}{2}\{\omega_0^{\ 2} + \omega_{20}^{\ 2} + \omega_{30}^{\ 2} \pm \sqrt{[\omega_0^{\ 2} + (\omega_{30} - \omega_{20})^2][\omega_0^{\ 2} + (\omega_{30} + \omega_{20})^2]}\}$$

The corresponding mode shapes, assembled into a modal matrix $[\phi]$, are

$$[\phi] = \begin{bmatrix} \ell & \frac{-I}{M\ell} & \frac{-I}{M\ell} \\ 1 & 1 & 1 \\ 0 & \frac{I}{k\ell\phi(\ell)}(\omega_2^2 - \omega_{20}^2) & \frac{I}{k\ell\phi(\ell)}(\omega_3^2 - \omega_{30}^{\ 2}) \end{bmatrix}$$

The general solution of the equation of motion is therefore

$$\begin{Bmatrix} x(t) \\ \theta(t) \\ \eta(t) \end{Bmatrix} = [\phi] \begin{Bmatrix} C_o t + C_1 \\ C_2 \sin(\omega_2 t + \psi_2) \\ C_3 \sin(\omega_3 t + \psi_3) \end{Bmatrix}$$

where C_o, C_i and ψ_i $(i = 1, 2, 3)$ are constants of integration. That is,

$$x(t) = \ell C_o t + \ell C_1 - \frac{I}{M\ell} C_2 \sin(\omega_2 t + \psi_2) - \frac{I}{M\ell} C_3 \sin(\omega_3 t + \psi_3) \quad \text{(B-7)}$$

$$\theta(t) = C_o t + C_1 + C_2 \sin(\omega_2 t + \psi_2) + C_3 \sin(\omega_3 t + \psi_3) \quad \text{(B-8)}$$

$$\eta(t) = \frac{I}{k\ell\phi(\ell)} (\omega_2{}^2 - \omega_{20}{}^2) C_2 \sin(\omega_2 t + \psi_2) + \frac{I}{k\ell\phi(\ell)} (\omega_3{}^2 - \omega_{20}{}^2) \cdot C_3 \sin(\omega_3 t + \psi_3) \quad \text{(B-9)}$$

The initial conditions for phase II, as derived for the termination of phase I in Appendix A, are

$$\theta(o) = \eta(o) = 0$$

$$\dot{\theta}(o) = \dot{\eta}(o) = 0$$

$$x(o) = \frac{F_s}{k}$$

$$\dot{x}(o) = V\sqrt{1 - F_s{}^2/kMV^2}$$

where F_s = shear strength of pole

V = impact velocity

M = vehicle mass

k = Vehicle crush stiffness

Inserting the initial conditions into equations (B-7) - (B-9) and their derivatives, results in

$$C_o = \frac{VM\ell\sqrt{1 - F_s{}^2/kMV^2}}{I\,(1 + M\ell^2/I)} \quad \text{(B-10)}$$

$$C_1 = \frac{F_s M\ell}{kI(1 + \frac{M\ell^2}{I})} \tag{B-11}$$

$$C_2 = \frac{-C_1 + C_3\sin\psi_3}{\sin\psi_2} \tag{B-12}$$

$$C_3 = \frac{C_o\sin\psi_2 - C_1\cos\psi 2}{\sin\psi_3\cos\psi_2 - \omega_3\sin\psi_2\cos\psi_3} \tag{B-13}$$

$$\tan(\psi_2) = \frac{\omega_2 C_1}{C_o} \tag{B-14}$$

$$\tan(\psi_3) = \frac{\omega_3 C_1}{C_o} \tag{B-15}$$

Vehicle deformation, δ, is given by

$$\delta = x - \ell\theta$$

From equations B-7 and B-8.

$$\delta = -\ell(I/M\ell^2 + 1)\{C_2\sin(\omega_2 t + \psi_2) + C_3\sin(\omega_3 t + \psi_3)\} \tag{B-16}$$

Maximum vehicle deceleration occurs when the crush is a maximum,

$$\ddot{x}_{MAX} = -\frac{k}{M}\delta_{MAX}, \tag{B-17}$$

at time $t = t_{MAX}$

The total vehicle velocity change is given by

$$\Delta V = V - \dot{x}(t_{MAX}),$$

assuming that the pole and vehicle separate at the moment of maximum vehicle deformation. Hence

$$\Delta V = V - \ell C_o - \frac{I}{M\ell}\left[C_2\omega_2\cos(\omega_2 t_{MAX} + \psi_2) + C_3\omega_3\cos(\omega_3 t_{MAX} + \psi_3)\right] \tag{B-18}$$

Upon substitution of numerical values, equation (B-16) may be evaluated as a function of time until the maximum crush is reached at t_{MAX}. Equations (B-17) and (B-18) then yield the maximum deceleration and overall velocity change for the impact.

APPENDIX C

INJURY TOLERANCE LEVELS

The evaluation of crash severity during an impact attenuation test program requires the prediction of probable occupant injury levels. Typically, such predictions are based on vehicle deceleration and velocity change resulting from the impact. This assumes a relationship between vehicle dynamics and occupant injury, and ignores large sources of variability such as occupant size, health, restraint and vehicle interior geometry.

Considerable effort has been put into relating injury severity to vehicle frame velocity change and deceleration levels. However, the present state-of-the-art is such that reported tolerance levels can at best be interpreted as lower-bound estimates. Work is currently underway in the USA to review and refine the evaluation criteria for impact severity (Transportation Research Board, 1978).

The bulk of tolerance data reported relates to vehicle-vehicle or vehicle-barrier collisions. Thus they do not encompass the special problems created by pole collisions such as massive penetration of the occupant space as a result of the narrow, concentrated impact. Conditions grossly affecting the tolerance figures reported, such as pulse shape and restraint type, vary widely from study to study, further complicating the selection of appropriate levels.

TABLE C.1.

LIMITS OF TOLERABLE DECELERATION (G), GRAHAM ET AL (1967)

Occupant Restraint	Lateral	Longitudinal	Total
Unrestrained	3	5	6
Lap belt	5	10	12
Lap belt and shoulder harness	15	25	25

Consequently a comparison of reported tolerance figures must take into consideration experimental conditions, particularly the occupant restraint system and the time profile of the parameter under study. Figure C.1 from Michie and Bronstad (1971) demonstrates the effect of acceleration duration on tolerance levels, while Table C.1 from Graham et al (1967) shows the effect of occupant restraint type. The figures reported by Graham are assumed to be low injufy probability levels, although this is not specified.

Chi (1976), in his review of barrier-crash injury criteria also outlines the effect of restraint type, exposure time and onset rate on proposed injury tolerance levels.

Head and chest injuries are the most critical injuries and trauma in these regions has been the subject of considerable study. Tolerance figures are typically reported for a number of body regions in terms of the deceleration, impulse, velocity change etc., experienced by a particular region (eg. 80g for 3ms at the head).

Melvin, Mohan and Stalnaker (1975) present a comprehensive review of available data on these 'localized' tolerance figures, and point out that the data are largely incomplete. This is particularly so in the area of head injury where the roles of linear and angular motions and their interactions in the injury producing mechanism are not well understood or modelled. Application of 'localized' tolerance figures requires the use of occupant simulators during a crash test program to establish the various exposure levels for different body zones.

A simplification of the test program would be achieved if tolerance figures could be set for vehicle-frame parameters.

One source of information in this area is the Experimental Safety Vehicle (ESV) program, in which a number of worldwide vehicle manufacturers attempted to produce a prototype vehicle which would meet specifications for crashworthiness, accident avoidence, post crash behaviour and pedestrian safety. The ESV

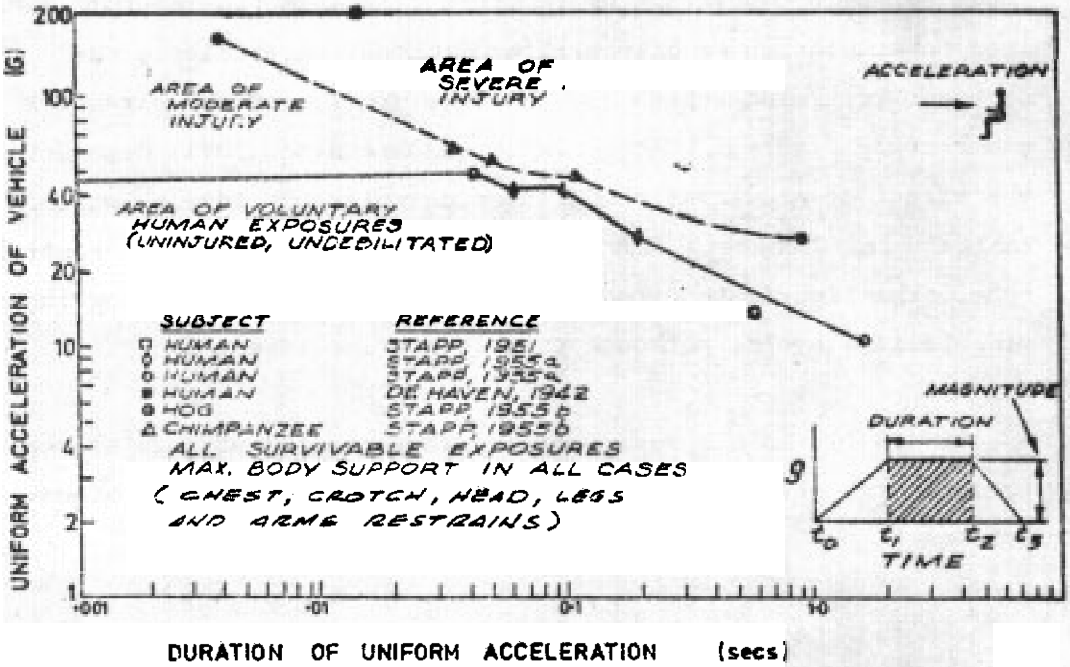

Figure C.1. Tolerance limits to longitudinal acceleration (sternum-ward G) (Michie et al, 1971)

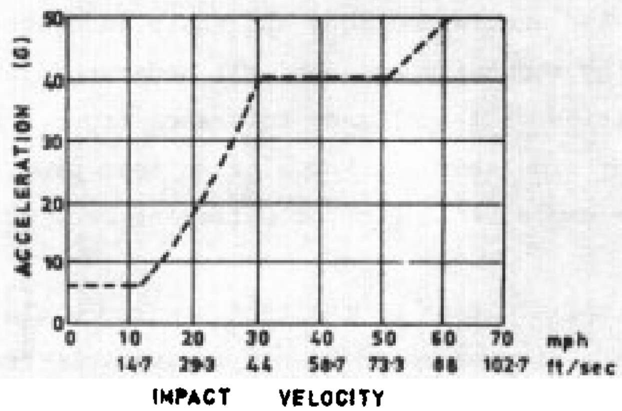

Figure C.2. Maximum permissable acceleration vs impact velocity Slechter, 1971) program criterion for maximum permissible deceleration as a function of impact velocity, is shown in Figure C.2.

The ESV crash test specifications (Slechter, 1971) included requirements for a 50 mph (80 km/h) frontal pole impact, as well as a 15 mph (24 km/h) pole side impact. Test specifications allowed a maximum of three inches of occupant space penetration. The frontal impact response had to satisfy occupant space integrity requirements as well as achieve deceleration levels below those set out in Figure C.2.

Table C.1 specifies tolerable vehicle frame acceleration levels for different occupant restraint systems. This table was subsequently reported by Olson, Ivey, Post, Gunderson, and Centiner (1974) and Michie, Calcote and Bronstad (1971). The levels are for an exposure duration of 200 ms, and a maximum onset rate of 500 g/s.

Much of the acceleration tolerance level data resulted from sled tests and laboratory experiments using both volunteer and animal subjects.

Another approach adopted by a number of authors has been to attempt to correlate vehicle damage levels with occupant injury severity, using accident data files and photographs of the damaged vehicles. Accident-vehicle damage was in turn compared with vehicle damage resulting from controlled barrier crash tests, to allow estimates of accident-vehicle deceleration and velocity-change levels.

Olson et al (1970) used this method to derive the following formula:

$$G = 13.7 P$$

where G = average longitudinal deceleration

P = probability of injury due to longitudinal acceleration.

This equation gives tolerance levels below those reported in Table C.1.

The applicability of barrier test results to high velocity change pole collisions is doubtful because of the larger occupant space penetrations in pole collisions. Figures derived from barrier tests in this range of ΔV, can at best be considered as upper bounds for tolerance levels in pole collisions.

Tolerance figures in terms of vehicle velocity change have also been reported. Johnson amd Messer (1970) considered a velocity change of 11mph (17.7 km/h) to be the injury threshold for unrestrained occupants.

Grime (1976) and Marsh, Campbell and Kingham (1977) used the effective-barrier-speed (EBS) approach as the basis of their work. Effective barrier speeds are estimated by comparing the level of vehicle damage resulting from a controlled barrier collision test with the level of damage to the accident vehicle. Grime derived plots of cumulative percentage of injured occupants against EBS (as a measure of collision severity) for slight injury, serious injury and fatalities. The data base was vehicle-to-vehicle frontal impacts. Although not clearly stated, it appears that the data are for unrestrained occupants. Grime's results, for collisions between vehicles of equal mass, are shown in Figure C.3.

Figure C.3 is interpreted as "Y% of slight/serious/fatal injuries occur at velocity changes of X or less".

Marsh et al (1977) transformed recorded accident vehicle crush (CRUSH inches)into effective barrier speed (EBS mph) using the following equation:

$$EBS = 7.5 + 0.9 \times CRUSH$$

The EBS calculation assumes a distributed crush zone and thus its use is invalid for damage resulting from pole accidents.

The plots derived by Marsh et al and by Grime could perhaps be used for pole impacts which result in low velocity changes (say $\Delta V < 35$ km/h). In such impacts, pole penetration would be low. The vehicle velocity change and deceleration would then be the predominant factors in injury causation. Breakaway pole impacts would fall into this category for successful pole designs.

Marsh et al employed the abbreviated injury scale (AIS) (Committee on Medical Aspects of Automotive Safety, 1971) as a measure of injury severity. They plotted the cumulative percentage of injured occupants against EBS for AIS levels 0 through 4 (Figure C.4).

Marsh et al also plotted the probability of a given level of injury or greater against EBS (Figure C.5). For example, Figure C.5 shows that for an EBS of 30 mph (48 km/h) the probability of an AIS of 3 or greater is 4 percent. It is unfortunate that both Marsh et al, and Grime both conclude their discussions by stating that the data base used to derive the crash severity and injury level distributions were scant.

In addition it is likely that both data bases were for unrestrained occupants. They therefore form a lower bound for Australian conditions, where compulsory seatbelt wearing legislation has lead to a seatbelt wearing rate ranging from 65 to 85% (Vaughn, Wood and Croft, 1974); Cowley and Cameron, 1976). It is thought however, that the seatbelt wearing rate may be lower amongst accident victims.

In their study of vehicle-to-vehicle side impacts, McHenry, Baum and Neff (1977) estimated the velocity change for both the striking and and struck vehicle using the CRASH 2 accident-reconstruction for cases from the Multi-Disciplinary Accident Investigation File (National Highway

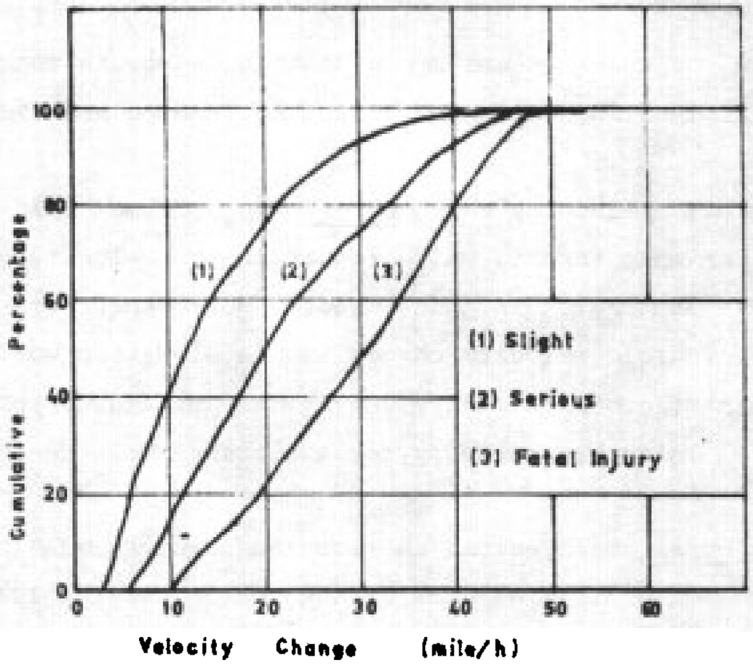

Figure C.3 Cumulative percentage of injured occupants vs velocity change (Grime, 1976)

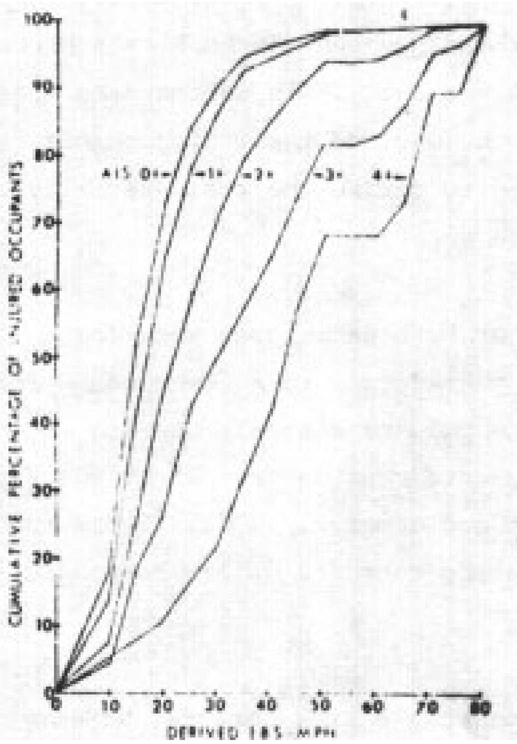

Figure C.4. Cumulative EBS by occupant injury level (Marsh et al, 1977)

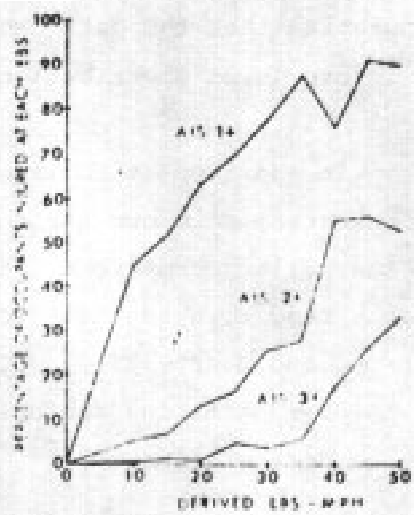

Figure C.5. Probability of occupant injury by derived EBS (Marsh et al, 1977)

TABLE C.2.

INJURY VS ΔV FOR STRIKING VEHICLE (ALL SIZES)
(McHENRY, BAUM AND NEFF, 1976)

ΔV MPH	INJURY RATING (AIS) 0	1	2	3	4	5	6	Total
0 - 5	1	2						3
0 - 10	7	12	4			1		24
11 - 15	7*	22*	14	6			1	50
16 - 20	3	13	15*	4*				35*
21 - 25	1	10	11	3	1			26
26 - 30	1	5	5					11
31 - 35		2	1	3				6
36 - 40		1		1				2
41 - 45		1		1			1	3
46 - 50						1		1
51 - 55							1	1
56 - 60							1	1
< 60								
Total	20	68	50	18	1	2	4	163

* Indicates the 50th percentile ΔV category for eath injury severity.

TABLE C.3.

RECOMMENDED MAXIMUM DECELERATION (G) LIMITS FOR FATAL OR IRREVERSIBLY DISABLING INJURIES (CHI, 1976)

Occupant Restraint	Longitudinal		Lateral		Vertical	
	ΔV	a	ΔV	a	Δa	a
Lap and shoulder belts	12	25	12	25	3	12
Lap belts only	12	20	6	20	3	12
Unrestrained	6	20	6	20	3	12

where ΔV = Velocity change due to the occupant impacting the vehicle interior in meters/sec (usually the terminal velocity before impact).

a = Average deceleration in G - units over the duration of impact.

Traffic Safety Administration). These velocity changes were tabulated against injury severity (AIS) and the results for the striking vehicle are shown in Table C.2. As in the majority of published information in this area, no firm tolerance figures can be derived from the results because of the small case numbers involved in each category, and data shortcomings.

Chi (1976) adopted the approach of calculating the average deceleration in a crash test as the vehicle velocity change divided by the impact duration. The velocity change was obtained by integrating the deceleration record. This value along with the average deceleration, forms the basis of Table C.3, which specifies tolerance limits for fatal or irreversibly disabling injuries.

Chi defined "tolerance limits" as the maximum acceleration or velocity change which will not cause fatal or irreversible damage.

For conservative designs, Chi recommends the application of a factor of safety of two or three to the tabulated figures, although lower values may be argued on the basis of cost-benefit studies for a particular design.

The only known source of tolerance data for pole collisions (apart from the ESV specifications comes from the testing of breakaway luminaire and sign supports. Edwards, Martinez, McFarland and Ross (1968) report a velocity change of 6 mph (9.6 km/h) as the injury threshold for unrestrained occupants. The FHWA (1970) sets an impulse limit of 4943 Ns for full scale crash testing of breakaway luminaire supports. This is equivalent to 6 mph (9.65 km/h) for a 4000 lb (1810 kg) vehicle, and 11 mph (17.7 km/h) for a 3000 lb (1357 kg) vehicle.

The latest procedure guide for the vehicle crash testing of highway apurtenances (Transportation Research Board, 1978) has maintained the impulse criterion of 4890 Ns as the principal measure of impact severity.

It would be perhaps more rational to replace the impulse criterion with a velocity change criterion as the latter does not vary with vehicle mass.

The impulse criterion has to be satisfied at two impact velocities 8.9 m/s (20 mph) and 26.8 m/s (60 mph) with the vehicle mass being 1020 kg.

For the purposes of design evaluation and comparison it was decided to use the TRB impulse criterion (4890 Ns) as the lower bound (no-injury level) and the average deceleration (25 g) and velocity change (12 m/s) figures reported by Chi (1976) as the upper bound (serious injury tolerance limit). Crude estimations of the likely reduction in occupant injury obtained for a particular design will be obtained from the results of McHenry et al (1977) and Grime (1976).

APPENDIX D

SUMMARY OF TEST RESULTS

This Appendix details the set-up and results of each test conducted. Some of the information is presented in shorthand form, the numbers in the brackets corresponding to those in the explanation of the codes which follows. It is noted that the results presented here are the scale model results. Full scale equivalents must be derived using the appropriate scale factors.

1. Pole material :

   I - ironbark

   M - messmate.

2. Test mode - details pole configuration, impact angle, and presence of restraining cable. The code consists of both letters and numbers, the numbers referring to the angle of impact (vehicle path relative to pole line) and the letters as follows :

   DL - double layer of conductors supported by two cross-arms (Figure 2.1) ;

   DLR - as for DL, with a restraining cable ;

   SL - single layer of conductors supported by single cross-arm (Figure 2.2) ;

   SLR - as for SL, with a restraining cable ;

   LP - luminaire pole (Figure 2.3) ;

   LPR - luminaire pole with restraining cable.

   T - free standing pole.

3. Lower modification type :

   X-holes - crossed holes (Figure 1.1) ;

   Slot - two layers of crossed holes connected by slots (Figure 3.2)

   Slt/Shm - slot/shim method (Figure 1.3) ;

   ST - sawn through.

4. Lower hole diameter :

   In the case of the two layers of crossed holes joined by slots, both sets of holes were the same size.

5. Velocity change :

   The full scale equivalent in km/h is given in the brackets.

6. Roof/windscreen impact :

   This notes whether or not the pole end strikes the vehicle windscreen and/or roof as the vehicle passes underneath. The first letter refers to the severity of impact (L - light , M - moderate , S - severe) and the remaining letters to impact zone (R - roof , W - windscreen).

7. Tie wire :

   The tie wire used to attach the conductors to the insulator pins in the scale model was fuse wire. This item records the amp rating of fuse wire used which can be related to a static strength (refer Section 2.5.1). The category clamps refers to the set-ups where the conductors were clamped to the cross-arms.

8. Upper fracture occurred :

   Notes whether or not the pole successfully detached from the upper modified zone.

9. Lower fracture occurred :

   Notes whether or not the pole successfully detached from the lower modified zone.

Test Parameter	Test Number 1	2	3	4
Pole material (1)	I	I	I	I
Test mode (2)	DL15	DL15	DL15	DL15
Lower modif. (3)	X-holes	X-holes	Unmod.	S.T.
Lower hole dia. (cm)	1.27	1.43	-	-
Section modulus remaining-lower zone (cm^3)	2.11	1.39	4.88	0
Pole design strength (kN)	6.00	3.94	13.85	0
Impact vel. (m/s)	7.17	7.63	7.63	7.63
Velocity change (m/s) (5)	2.35 (23)	2.02 (19.8)	7.63 (74.6)	0.84 (8.2)
Peak decel. (g)	32	31	73	6.5
Average decel. (g)	12.8	11.8	26.2	2.7
Vehicle nose def. (cm)	10.2	10.0	12.8	2.5
Roof/windscreen impact (6)	NO	NO	NO	NO
Tie wire (7)	10	Clamps	10	Clamps
Conductor failure	NO	NO	NO	NO
Upper fracture occurred (8)	NO	YES	NO	YES
Lower fracture occurred (9)	YES	YES	NO	-
Rupture stress (MPa)	177.8	153.4	180.8	-

Test Parameter	Test Number 5	6	7	8
Pole material (1)	I	I	I	I
Test mode (2)	DL15	DL15	DL15	DL15
Lower modif. (3)	X-holes	X-holes	X-holes	X-holes
Lower hole dia. (cm)	1.31	1.31	1.31	N.A.
Section modulus remaining-lower zone * (cm^3)	2.15	2.23	2.09	2.90
Pole design strength (kN)	6.09	6.32	5.93	8.24
Impact vel. (m/s)	7.63	7.63	7.63	6.58
Velocity change (m/s) (5)	3.08 (30.1)	2.20 (21.52)	2.56 (25.02)	N.A.
Peak decel. (g)	37	32	33	N.A.
Average decel. (g)	18.6	15	15.5	N.A.
Vehicle nose def. (cm)	10.0	10.2	11.4	11.7
Roof/windscreen impact (6)	NO	NO	NO	N.A.
Tie wire (7)	Clamps	Clamps	15	Clamps
Conductor failure	NO	NO	NO	NO
Upper fracture occurred (8)	YES	YES	NO	NO
Lower fracture occurred (9)	YES	YES	YES	YES
Rupture stress (MPa)	182.7	174.8	174.6	-

Test Parameter	Test Number 9	10	11	12
Pole material (1)	I	I	I	I
Test mode (2)	DL15	DL15	DL15	DL15
Lower modif. (3)	X-holes	Slot	Slt/shm.	S.T.
Lower hole dia. (cm)	1.03	1.11	-	-
Section modulus remaining-lower zone (cm^3)	2.90	2.76	N.A.	0
Pole design strength (kN)	8.24	8.08	8.0	0
Impact vel. (m/s)	6.88	6.51	6.56	6.49
Velocity change (m/s) (5)	3.42 (33.4)	1.54 (15.1)	1.87 (18.3)	0.84 (8.2)
Peak decel. (g)	34	17.5	26	7.0
Average decel. (g)	15.5	7.2	10.2	2.76
Vehicle nose def. (cm)	N.A.	9.0	10.0	6.0
Roof/windscreen impact (6)	SR, SW	SR, SW	SR, SW	SR
Tie wire (7)	Clamps	Clamps	Clamps	Clamps
Conductor failure	NO	NO	NO	NO
Upper fracture occurred (8)	YES	YES	YES	YES
Lower fracture occurred (9)	YES	YES	YES	-
Rupture stress (MPa)	-	134.6	110.0	149.7

Test Parameter	Test Number 13	14	15	16
Pole material (1)	I	I	I	I
Test mode (2)	DL15	DL15	DL15	T15
Lower modif. (3)	X-holes	X-holes	Slot	Slot
Lower hole dia. (cm)	1.31	1.31	1.19	1.11
Section modulus remaining-lower zone (cm^3)	2.9	2.9	2.76	2.76
Pole design strength (kN)	8.24	8.24	8.08	8.08
Impact vel. (m/s)	6.99	6.97	6.97	6.94
Velocity change (m/s) (5)	2.63 (25.7)	2.70 (26.4)	2.37 (23.2)	1.23 (12.1)
Peak decel. (g)	35	35	18	19
Average decel. (g)	12.6	12.5	12.9	6.7
Vehicle nose def. (cm)	10.2	11.1	8.0	8.0
Roof/windscreen impact (6)	MW, MR	LW	MR	NO
Tie wire (7)	Clamps	Clamps	Clamps	N.A.
Conductor failure	NO	NO	NO	-
Upper fracture occurred (8)	YES	YES	YES	-
Lower fracture occurred (9)	YES	YES	YES	YES
Rupture stress (MPa)	-	-	126.6	132.9

Test Parameter	Test Number 17	18	19	20
Pole material (1)	I	I	I	I
Test mode (2)	DL15	T15	DL15	DL15
Lower modif. (3)	Slot	Slot	Slot	Slot
Lower hole dia.(cm)	1.19	1.07	1.19	0.99
Section modulus remaining-lower zone (cm^3)	2.76	2.76	2.76	2.76
Pole design strength (kN)	8.08	8.08	8.08	8.08
Impact vel. (m/s)	7.03	6.93	7.00	6.95
Velocity change (m/s) (5)	2.22 (21.8)	1.80 (17.6)	1.68 (16.4)	2.14 (20.9)
Peak decel. (g)	24	17.5	22	22
Average decel. (g)	10.7	9.8	N.A.	8.7
Vehicle nose def. (cm)	10.2	7.9	8.0	10.0
Roof/windscreen impact (6)	SR	SR	SB	LW
Tie wire (7)	Clamps	N.A.	Clamps	Clamps
Conductor failure	NO	-	NO	ALL
Upper fracture occurred (8)	YES	-	YES	NO
Lower fracture occurred (9)	YES	YES	YES	YES
Rupture stress (MPa)	134.6	126.4	134.6	149.7

Test Parameter	Test Number 21	22	23	24
Pole material (1)	I	I	I	I
Test mode (2)	DL15	DL15	DL15	DL15
Lower modif. (3)	Slot	D.Slot	Slot	Slot
Lower hole dia.(cm)	0.99	1.19	1.39	1.71
Section modulus remaining-lower zone (cm^3)	2.76	2.76	1.06	1.06
Pole design strength (kN)	8.08	8.08	3.1	3.1
Impact vel. (m/s)	6.94	7.21	6.96	6.95
Velocity change (m/s) (5)	1.56 (15.3)	1.65 (16.1)	1.12 (11.0)	1.06 (10.4)
Peak decel. (g)	26	16	13.5	14
Average decel. (g)		10.3	6.1	4.3
Vehicle nose def. (cm)	10.0	8.0	6.0	7.2
Roof/windscreen impact (6)	SB	NO	SR	SW, SR
Tie wire (7)	Clamps	15	15	15
Conductor failure	NO	3	NO	NO
Upper fracture occurred (8)	YES	NO	YES	YES
Lower fracture occurred (9)	YES	YES	YES	YES
Rupture stress (MPa)	218.1	115.9	140.2	149.7

Test Parameter	Test Number 25	26	27	28
Pole material (1)	I	I	I	I
Test mode (2)	DLR15	DLR15	DLR15	DLR15
Lower modif. (3)	Slot	Slot	Slot	Slot
Lower hole dia.(cm)	1.75	1.71	1.23	1.75
Section modulus remaining-lower zone (cm^3)	1.06	1.06	1.06	1.16
Pole design strength (kN)	3.1	3.1	3.1	3.4
Impact vel. (m/s)	6.98	6.99	6.97	6.98
Velocity change (m/s) (5)	0.58 (5.7)	1.09 (10.7)	1.18 (11.6)	1.29 (12.6)
Peak decel. (g)	14	16	14	N.A.
Average decel. (g)	3.2	6.8	6.4	N.A.
Vehicle nose def. (cm)	6.5	6.9	6.8	6.0
Roof/windscreen impact (6)	NO	NO	NO	NO
Tie wire (7)	15	15	15	15
Conductor failure	NO	NO	NO	NO
Upper fracture occurred (8)	YES	YES	YES	YES
Lower fracture occurred (9)	YES	YES	YES	YES
Rupture stress (MPa)	121.1	156.3	110.0	152.9

Test Parameter	Test Number 29	30	31	32
Pole material (1)	I	I	I	I
Test mode (2)	DLR15	DLR15	DLR15	DLR15
Lower modif. (3)	Slot	Slot	Slot	Slot
Lower hole dia.(cm)	1.75	1.71	1.43	1.43
Section modulus remaining-lower zone (cm^3)	1.16	1.16	2.04	2.04
Pole design strength (kN)	3.4	3.4	6.0	6.0
Impact vel. (m/s)	5.97	3.92	6.93	5.92
Velocity change (m/s) (5)	0.87 (8.5)	0.87 (8.5)	1.43 (14.0)	1.65 (16.1)
Peak decel. (g)	12	7.0	17.0	17.5
Average decel. (g)	4.7	3.55	7.8	8.7
Vehicle nose def. (cm)	6.0	5.5	7.3	7.5
Roof/windscreen impact (6)	NO	LW	NO	NO
Tie wire (7)	15	15	15	15
Conductor failure	NO	NO	NO	NO
Upper fracture occurred (8)	YES	YES	YES	YES
Lower fracture occurred (9)	YES	YES	YES	YES
Rupture stress (MPa)	115.9	126.4	110.0	140.2

Test Parameter	Test Number 33	34	35	36
Pole material (1)	I	I	I	I
Test mode (2)	DLR15	DLR30	DLR30	DLR30
Lower modif. (3)	Slot	Slot	Slot	Slot
Lower hole dia. (cm)	1.43	1.67	1.59	1.75
Section modulus remaining-lower zone (cm^3)	2.04	1.16	1.16	1.16
Pole design strength (kN)	6	3.4	3.4	3.4
Impact vel. (m/s)	3.88	7.31	6.26	4.12
Velocity change (m/s) (5)	1.65 (16.1)	1.42 (13.9)	1.28 (12.5)	1.23 (12.0)
Peak decel. (g)	13.5	17.0	15.0	10.0
Average decel. (g)	5.4	5.8	8.6	5.7
Vehicle nose def. (cm)	6.9	7.0	6.5	5.3
Roof/windscreen impact (6)	NO	NO	LW	SW
Tie wire (7)	15	15	15	15
Conductor failure	NO	NO	NO	NO
Upper fracture occurred (8)	NO	YES	YES	YES
Lower fracture occurred (9)	YES	YES	YES	YES
Rupture stress (MPa)	110.0	126.4	196.9	121.1

Test Parameter	Test Number 37	38	39	40
Pole material (1)	I	I	I	I
Test mode (2)	DLR30	DLR30	DLR30	DLR50
Lower modif. (3)	Slot	Slot	Slot	Slot
Lower hole dia. (cm)	1.27	1.31	1.35	1.75
Section modulus remaining-lower zone (cm^3)	2.04	2.04	2.04	1.16
Pole design strength (kN)	6	6	6	3.4
Impact vel. (m/s)	7.20	6.35	4.21	7.25
Velocity change (m/s) (5)	1.87 (18.3)	1.53 (15.0)	1.56 (15.3)	0.80 (7.9)
Peak decel. (g)	20.0	17.5	15.0	12.0
Average decel. (g)	10.2	6.2	5.7	5.2
Vehicle nose def. (cm)	7.8	7.3	7.0	6.0
Roof/windscreen impact (6)	NO	LW	SW	NO
Tie wire (7)	15	15	15	15
Conductor failure	NO	NO	NO	NO
Upper fracture occurred (8)	YES	YES	YES	YES
Lower fracture occurred (9)	YES	YES	YES	YES
Rupture stress (MPa)	170.1	186.0	176.6	170.1

Test Parameter	Test Number 41	42	43	44
Pole material (1)	I	I	I	I
Test mode (2)	DLR50	DLR50	DLR50	DLR50
Lower modif. (3)	Slot	Slot	Slot	Slot
Lower hole dia. (cm)	1.35	1.59	1.31	1.23
Section modulus remaining-lower zone (cm^3)	2.04	1.16	2.04	2.04
Pole design strength (kN)	6	3.4	6	6
Impact vel. (m/s)	7.21	4.18	4.17	7.21
Velocity change (m/s) (5)	1.57 (15.3)	0.99 (9.7)	1.32 (12.9)	2.02 (19.7)
Peak decel. (g)	17.5	11.0	17.0	20.0
Average decel. (g)	8.5	4.6	3.9	5.7
Vehicle nose def. (cm)	8.0	6.0	7.5	7.0
Roof/windscreen impact (6)	LW	SR	SR	LW
Tie wire (7)	15	15	15	15
Conductor failure	NO	NO	NO	NO
Upper fracture occurred (8)	YES	YES	YES	YES
Lower fracture occurred (9)	YES	YES	YES	YES
Rupture stress (MPa)	143.6	177.9	208.9	196.9

Test Parameter	Test Number 45	46	47	48
Pole material (1)	I	I	I	I
Test mode (2)	DLR 50	DLR 50	DLR 50	DLR 15
Lower modif. (3)	Slot	Slot	Slot	Slot
Lower hole dia.(cm)	1.27	1.27	1.23	1.03
Section modulus remaining-lower zone (cm^3)	2.04	2.04	2.04	2.90
Pole design strength (kN)	6	6	6	8
Impact vel. (m/s)	7.22	7.22	3.48	7.40
Velocity change (m/s) (5)	1.54 (15.1)	1.35 (13.2)	1.89 (18.5)	2.73 (26.7)
Peak decel. (g)	17.5	14.0	15.0	24.0
Average decel. (g)	7.2	5.0	>5.1	11.1
Vehicle nose def. (cm)	7.3	7.0	7.0	9.5
Roof/windscreen impact (6)	NO	SW, SR	NO	NO
Tie wire (7)	15	15	15	15
Conductor failure	NO	NO	NO	NO
Upper fracture occurred (8)	YES	YES	YES	YES
Lower fracture occurred (9)	YES	YES	YES	YES
Rupture stress (MPa)	143.6	170.1	150.5	208.9

Test Parameter	Test Number 49	50	51	52
Pole material (1)	I	I	I	I
Test mode (2)	DLR15	DLR15	DLR15	DLR15
Lower modif. (3)	Slot	Slot	Slot	Slot
Lower hole dia. (cm)	1.27	0.71	0.91	0.95
Section modulus remaining-lower zone (cm^3)	2.04	2.90	2.90	2.90
Pole design strength (kN)	6	8	8	8
Impact vel. (m/s)	7.37	7.37	7.26	7.26
Velocity change (m/s) (5)	1.36 (13.3)	3.19 (31.2)	1.62 (15.9)	3.3 (32.2)
Peak decel. (g)	15.0	33	19.0	31.0
Average decel. (g)	6.5	16.3	9.5	13.5
Vehicle nose def. (cm)	7.0	10.5	8.3	10.3
Roof/windscreen impact (6)	NO	SW, SR	SW	MW
Tie wire (7)	15	20	20	20
Conductor failure	NO	NO	NO	NO
Upper fracture occurred (8)	YES	YES	YES	YES
Lower fracture occurred (9)	YES	YES	YES	YES
Rupture stress (MPa)	143.6	176.6	177.9	201.7

Test Parameter	Test Number 53	54	55	56
Pole material (1)	I	I	I	I
Test mode (2)	DLR15	DLR15	DLR15	DLR15
Lower modif. (3)	Slot	Unmod.	Unmod.	Unmod.
Lower hole dia. (cm)	0.91	-	-	-
Section modulus remaining-lower zone (cm^3)	2.90	4.59	4.59	4.59
Pole design strength (kN)	8	12.7	12.7	12.7
Impact vel. (m/s)	6.43	6.34	4.39	7.19
Velocity change (m/s) (5)	2.81 (27.5)	6.34 (62)	4.39 (43.0)	7.19 (70.3)
Peak decel. (g)	34.0	47.5	34.0	73.0
Average decel. (g)	12.7	21.6	13.1	30.5
Vehicle nose def. (cm)	11.0	12.0	10.0	13.0
Roof/windscreen impact (6)	MW	NO	NO	NO
Tie wire (7)	20	20	20	20
Conductor failure	NO	NO	NO	NO
Upper fracture occurred (8)	YES	NO	NO	NO
Lower fracture occurred (9)	YES	NO	NO	NO
Rupture stress (MPa)	186.0	170.1	170.1	170.1

Test Parameter	Test Number 57	58	59	60
Pole material (1)	I	I	I	I
Test mode (2)	DLR15	DLR15	DLR15	DLR15
Lower modif. (3)	Slot	Slot	Slot	Slot
Lower hole dia. (cm)	0.91	0.95	0.95	0.83
Section modulus remaining-lower zone (cm^3)	2.90	2.90	2.90	2.90
Pole design strength (kN)	8	8	8	8
Impact vel. (m/s)	7.21	4.1	7.11	7.17
Velocity change (m/s) (5)	3.35 (32.8)	4.1 (41.0)	2.34 (22.9)	3.19 (31.2)
Peak decel. (g)	35	22.0	36.0	33.0
Average decel. (g)	15.6	12.8	11.2	15.3
Vehicle nose def. (cm)	10.8	8.0	8.5	9.8
Roof/windscreen impact (6)	MR, LR	NO	SW	MW, LR
Tie wire (7)	20	20	20	20
Conductor failure	NO	NO	NO	NO
Upper fracture occurred (8)	YES	NO	YES	YES
Lower fracture occurred (9)	YES	NO	YES	YES
Rupture stress (MPa)	208.9	208.9	208.9	170.0

Test Parameter	Test Number 61	62	63	64
Pole material (1)	M	M	M	M
Test mode (2)	SL15	SLR15	SLR15	SLR15
Lower modif. (3)	Slot	Slot	Slot	Slot
Lower hole dia. (cm)	1.59	1.55	1.51	1.51
Section modulus remaining-lower zone (cm^3)	1.35	1.35	1.35	1.35
Pole design strength (kN)	3.0	3.0	3.0	3.0
Impact vel. (m/s)	7.21	7.21	7.07	4.01
Velocity change (m/s) (5)	0.87 (8.7)	1.10 (10.8)	1.16 (11.3)	1.03 (10.1)
Peak decel. (g)	12.0	15.0	15.0	12.0
Average decel. (g)	5.2	6.0	7.0	4.8
Vehicle nose def. (cm)	6.3	6.0	6.0	6.0
Roof/windscreen impact (6)	SR	NO	NO	SW
Tie wire (7)	10	10	10	10
Conductor failure	NO	NO	NO	NO
Upper fracture occurred (8)	-	-	-	-
Lower fracture occurred (9)	YES	YES	YES	YES
Rupture stress (MPa)	104.4	104.4	104.4	104.4

Test Parameter	Test Number 65	66	67	68
Pole material (1)	M	M	M	M
Test mode (2)	SLR15	SLR15	SLR15	SLR15
Lower modif. (3)	Slot	Slot	Slot	Slot
Lower hole dia. (cm)	1.51	0.91	0.95	0.91
Section modulus remaining-lower zone (cm^3)	1.35	2.70	2.70	2.70
Pole design strength (kN)	3.0	6.0	6.0	6.0
Impact vel. (m/s)	6.12	7.07	5.98	4.06
Velocity change (m/s) (5)	1.14 (11.11)	1.70 (16.6)	2.19 (21.5)	4.06 (39.7)
Peak decel. (g)	12.0	30.0	22.0	N.A.
Average decel. (g)	6.2	7.7	10.0	N.A.
Vehicle nose def. (cm)	6.0	9.5	9.0	9.0
Roof/windscreen impact (6)	NO	MW	MW	NO
Tie wire (7)	10	10	10	10
Conductor failure	NO	NO	NO	NO
Upper fracture occurred (8)	-	-	-	-
Lower fracture occurred (9)	YES	YES	YES	NO
Rupture stress (MPa)	102.7	100.2	93.4	93.4

Test Parameter	Test Number 69	70	71	72
Pole material (1)	M	M	M	M
Test mode (2)	SLR15	SLR15	SLR15	SLR30
Lower modif. (3)	Slot	Slot	Slot	Slot
Lower hole dia. (cm)	0.52	0.52	0.36	1.43
Section modulus remaining-lower zone (cm^3)	3.60	3.60	3.60	1.35
Pole design strength (kN)	8.0	8.0	8.0	3.0
Impact vel. (m/s)	6.75	6.13	3.81	6.86
Velocity change (m/s) (5)	2.19 (21.4)	2.55 (24.9)	3.18 (37.2)	0.62 (6.1)
Peak decel. (g)	27.0	30.0	20.0	9.0
Average decel. (g)	12.6	11.0	8.8	3.5
Vehicle nose def. (cm)	10.0	10.0	9.0	5.8
Roof/windscreen impact (6)	LW	LW	NO	NO
Tie wire (7)	10	10	10	10
Conductor failure	NO	NO	NO	NO
Upper fracture occurred (8)	-	-	-	-
Lower fracture occurred (9)	YES	YES	NO	YES
Rupture stress (MPa)	105.3	87.7	100.2	87.7

Test Parameter	Test Number 73	74	75	76
Pole material (1)	M	M	M	M
Test mode (2)	SLR30	SLR30	SLR30	SLR30
Lower modif. (3)	Slot	Slot	Slot	Slot
Lower hole dia.(cm)	1.43	1.35	0.83	0.95
Section modulus remaining-lower zone (cm^3)	1.35	1.35	2.70	2.70
Pole design strength (kN)	3.0	3.0	6.0	6.0
Impact vel. (m/s)	6.33	4.23	7.24	6.36
Velocity change (m/s) (5)	0.39 (3.9)	0.79 (7.7)	1.39 (13.6)	2.20 (21.5)
Peak decel. (g)	10.0	13.0	20.0	22.5
Average decel. (g) *	N.A.	6.7	6.4	9.3
Vehicle nose def. (cm)	6.0	6.0	7.3	8.8
Roof/windscreen impact (6)	NO	SW	NO	MW
Tie wire (7)	10	10	10	10
Conductor failure	NO	NO	NO	NO
Upper fracture occurred (8)	-	-	-	-
Lower fracture occurred (9)	YES	YES	YES	YES
Rupture stress (MPa)	103.1	100.2	76.0	93.4

Test Parameter	Test Number 77	78	79	80
Pole material (1)	M	M	M	M
Test mode (2)	SLR30	SLR30	SLR30	SLR30
Lower modif. (3)	Slot	Slot	Slot	Slot
Lower hole dia. (cm)	0.91	0.52	0.56	0.52
Section modulus remaining-lower zone (cm^3)	2.7	3.6	3.6	3.6
Pole design strength (kN)	6	8	8	8
Impact vel. (m/s)	4.11	7.23	6.37	4.18
Velocity change (m/s) (5)	1.48 (14.5)	2.44 (23.8)	2.38 (23.3)	4.72 (46.2)
Peak decel. (g)	20.0	39.0	32.0	20.0
Average decel. (g)	6.7	13.2	11.4	11.2
Vehicle nose def. (cm)	7.0	10.0	10.0	9.3
Roof/windscreen impact (6)	SW	NO	SW	NO
Tie wire (7)	10	10	10	10
Conductor failure	NO	NO	NO	NO
Upper fracture occurred (8)	-	-	-	-
Lower fracture occurred (9)	YES	YES	YES	NO
Rupture stress (MPa)	104.6	102.7	104.6	88.0

Test Parameter	Test Number 81	82	83	84
Pole material (1)	M	M	M	M
Test mode (2)	SLR50	SLR50	SLR50	SLR50
Lower modif. (3)	Slot	Slot	Slot	Slot
Lower hole dia. (cm)	1.51	1.43	0.91	0.99
Section modulus remaining-lower zone (cm^3)	1.35	1.35	2.70	2.70
Pole design strength (kN)	3	3	6	6
Impact vel. (m/s)	7.17	3.95	3.94	6.97
Velocity change (m/s) (5)	1.20 (11.8)	0.95 (9.3)	0.90 (8.8)	1.11 (10.9)
Peak decel. (g)	11.0	16.0	18.0	20.0
Average decel. (g)	4.9	3.2	4.1	4.5
Vehicle nose def. (cm)	6.5	6.0	6.8	7.5
Roof/windscreen impact (6)	NO	SW	SW, MR	NO
Tie wire (7)	10	10	10	10
Conductor failure	NO	NO	NO	NO
Upper fracture occurred (8)	-	-	-	-
Lower fracture occurred (9)	YES	YES	YES	YES
Rupture stress (MPa)	88.0	103.1	105.3	88.0

Test Parameter	Test Number 85	86	87	88
Pole material (1)	M	M	M	I
Test mode (2)	SLR50	SLR50	SLR50	DLR50
Lower modif. (3)	Slot	Slot	Slot	Slot
Lower hole dia.(cm)	0.60	0.60	1.43	1.23
Section modulus remaining-lower zone (cm^3)	3.60	3.6	1.35	1.06
Pole design strength (kN)	8	8	3	3.1
Impact vel. (m/s)	4.01	7.00	6.95	7.03
Velocity change (m/s) (5)	4.01 (39.2)	2.13 (20.8)	1.16 (11.3)	N.A.
Peak decel. (g)	23.0	27.5	14.0	N.A.
Average decel. (g)	18.9	10.9	7.9	N.A.
Vehicle nose def. (cm)	8.6	10.0	7.0	6.5
Roof/windscreen impact (6)	NO	SW	LW	NO
Tie wire (7)	10	10	10	10
Conductor failure	NO	NO	NO	NO
Upper fracture occurred (8)	-	-	-	-
Lower fracture occurred (9)	NO	YES	YES	YES
Rupture stress (MPa)	88.0	104.6	100.2	213.1

Test Parameter	Test Number 89	90	91	92
Pole material (1)	M	M	M	M
Test mode (2)	SLR50	LP15	LP15	LP15
Lower modif. (3)	Slot	Slot	Slot	Slot
Lower hole dia.(cm)	0.56	1.59	1.59	1.59
Section modulus remaining-lower zone (cm^3)	3.6	0.90	0.90	0.90
Pole design strength (kN)	8	2	2	2
Impact vel. (m/s)	7.08	7.19	6.08	3.99
Velocity change (m/s) (5)	7.08 (69.3)	1.00 (9.8)	1.01 (9.9)	0.71 (6.9)
Peak decel. (g)	46.0	11.0	8.0	6.0
Average decel. (g)	17.2	7.8	5.5	3.3
Vehicle nose def. (cm)	12.0	6.0	6.0	6.0
Roof/windscreen impact (6)	NO	NO	LR	SW
Tie wire (7)	10	-	-	-
Conductor failure	NO	-	-	-
Upper fracture occurred (8)	-	-	-	-
Lower fracture occurred (9)	NO	YES	YES	YES
Rupture stress (MPa)	100.2	104.6	87.7	87.7

Test Parameter	Test Number 93	94	95
Pole material (1)	M	M	M
Test mode (2)	LPR15	LPR15	LPR15
Lower modif. (3)	Slot	Slot	Slot
Lower hole dia.(cm)	1.67	1.67	1.51
Section modulus remaining-lower zone (cm^3)	0.90	0.90	0.90
Pole design strength (kN)	2	2	2
Impact vel. (m/s)	3.98	6.10	7.16
Velocity change (m/s) (5)	0.59 (5.74)	0.90 (8.8)	1.03 (10.09)
Peak decel. (g)	6.0	10.0	9.0
Average decel. (g)	2.7	4.9	3.8
Vehicle nose def. (cm)	5.0	5.5	5.5
Roof/windscreen impact (6)	LW	NO	NO
Tie wire (7)	-	-	-
Conductor failure	-	-	-
Upper fracture occurred (8)	-	-	-
Lower fracture occurred (9)	YES	YES	YES
Rupture stress (MPa)	103.1	93.4	102.7

APPENDIX E

EXTRACTS RELATING TO POLE LOADING FROM THE OVERHEAD LINE MANUAL (SECV, 1978).

POLE TYPE		FOOTING			ALLOWABLE LOADS		WIND LOAD REFERRED TO HEAD (N)
LENGTH H (m)	STRENGTH (kN)	DEPTH D (m)	MIN. AUGER SIZE (mm)	RE-INFORCING	SHORT DURATION (N)	LONG DURATION (N)	
10	5	2·0	—	—	5 000	1 500	600
10	5	2·0	600	CONC.	6 000	1 500	600
10	8	2·0	600	CONC.	8 000	3 100	700
10	12	2·0	800	CONC.+LOG	12 000	5 800	900
11	3	2·1	—	—	3 000	1 400	800
11	5	2·1	—	—	5 000	1 450	700
11	5	2·1	600	CONC.	6 000	1 450	700
11	8	2·1	600	CONC.	8 000	2 950	900
11	12	2·1	600	CONC.+LOG	12 000	5 400	1 000
12	3	2·2	—	—	3 000	1 100	900
12	8	2·2	—	—	6 000	2 750	1 000
12	8	2·2	600	CONC.	8 000	2 750	1 000
12	12	2·2	760	CONC.+LOG	12 000	4 900	1 100
13	8	2·3	—	—	6 000	2 550	1 100
13	8	2·3	600	CONC.	8 000	2 550	1 100
13	12	2·3	760	CONC.+LOG	12 000	4 550	1 200
14	8	2·4	—	—	6 000	2 150	1 100
14	8	2·4	600	CONC.	8 000	2 150	1 100
14	12	2·4	760	CONC.+LOG	12 000	4 350	1 400
15	8	2·5	—	—	5 000	2 050	1 200
15	8	2·5	600	CONC.	8 000	2 050	1 200
15	12	2·5	760	CONC.+LOG	12 000	4 100	1 500
16	12	2·5	760	CONC.	8 000	3 500	1 600
16	12	2·5	760	CONC.+LOG	12 000	3 500	1 600
17	12	2·5	760	CONC.	8 000	3 300	1 800
17	12	2·5	760	CONC.+LOG	12 000	3 300	1 800
18	12	2·5	760	CONC.	8 000	3 950	1 900
18	12	2·5	760	CONC.+LOG	12 000	3 950	1 900
19	12	2·6	760	CONC.	8 000	3 800	2 000
19	12	2·6	760	CONC.+LOG	12 000	3 800	2 000
20	12	2·7	760	CONC.	8 000	3 400	2 100
20	12	2·7	760	CONC.+LOG	12 000	3 400	2 100
21	12	2·8	760	CONC.	12 000	3 350	2 300
22	12	2·9	900	CONC.	12 000		3 200
23	12	3·0	900	CONC.	12 000		3 400
24	12	3·1	900	CONC.	12 000		3 600
25	12	3·2	900	CONC.	12 000		3 700

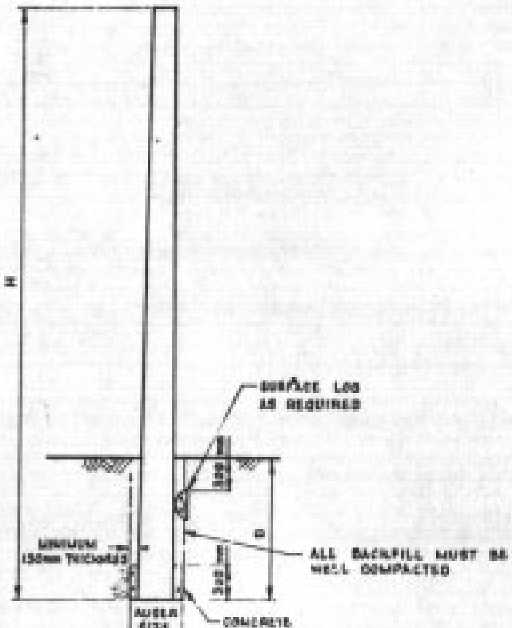

NOTE

THE FOOTINGS LISTED WILL ALLOW THE FULL RATED LOAD OF THE POLE TO BE UTILISED IN AVERAGE SOIL.
FOR POOR SOILS THE FOOTINGS SHOULD BE STRENGTHENED.
IN ROCKY GROUND WHERE BEARING CAPACITY IS HIGH, DEPTH 'D' MAY BE REDUCED BY AN AMOUNT NOT EXCEEDING 125 PER 1000 OF NORMAL SETTING.
LONG DURATION LOADS LISTED ARE ALL DEFLECTION LIMITS (1/[illegible] OF ABOVE GROUND HEIGHT FOR UP TO 17m POLES AND 1/[illegible] OF ABOVE GROUND HEIGHT FOR 18m AND LARGER POLES).
LONG DURATION STRENGTH LIMITS ARE ONE HALF OF SHORT DURATION LIMITS.

REVISION				
30-6-76	B	UNITS ALTERED.		
—	A	REDRAWN TO INCLUDE LONG DURATION LOADS.	—	—

DRAWN W.N.S.

STATE ELECTRICITY COMMISSION OF VICTORIA
DISTRIBUTION ENGINEERING DEPARTMENT

NOT TO SCALE | O/H LINE MANUAL VOL 1 SECT 1-2 | VX9/7020/105 B

POLE CONSTRUCTION
POLE AND FOOTING DETAILS
FOR WOOD POLES

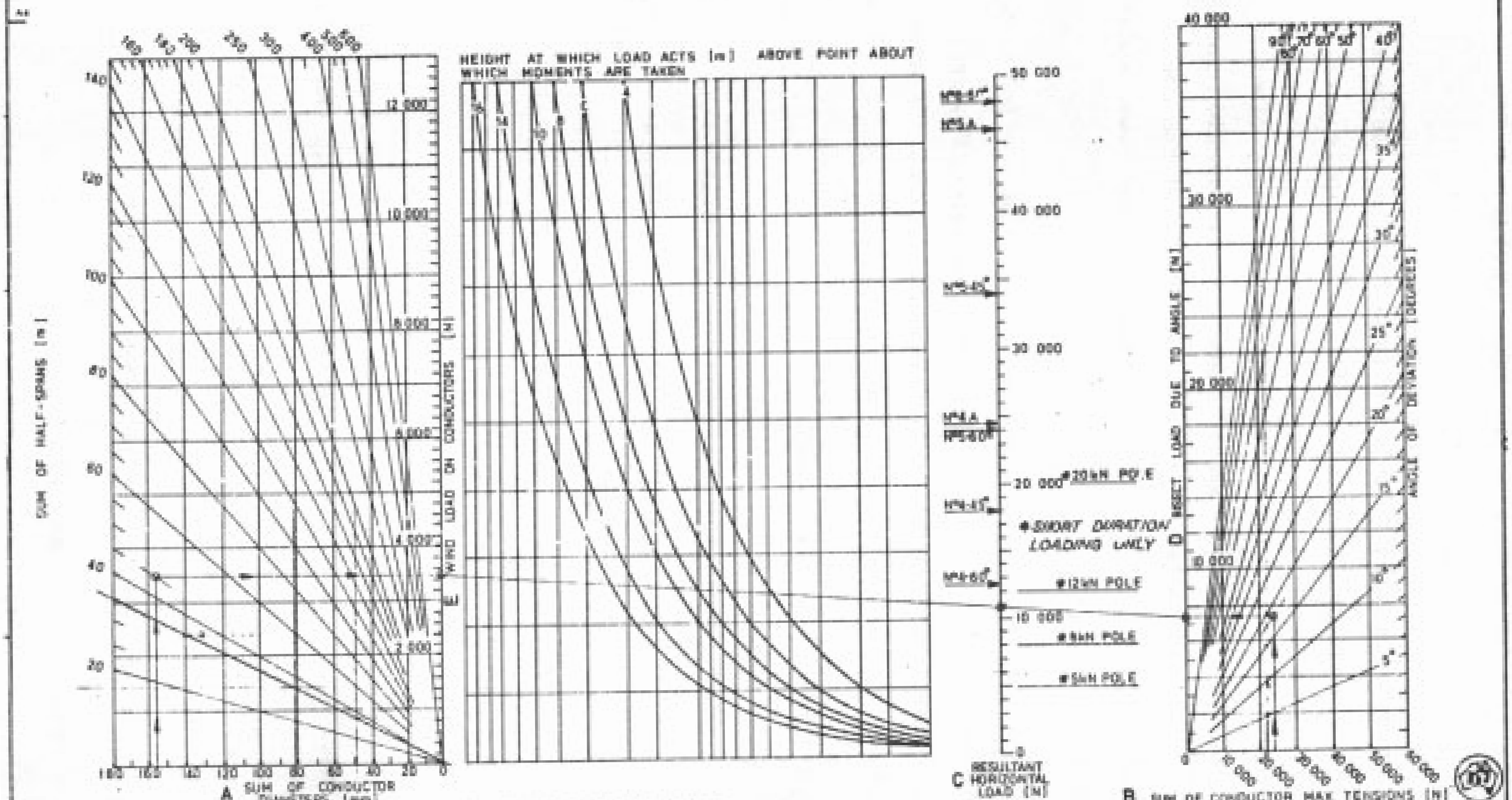

NOTES:
1. FOR UNGUYED ANGLE POLES LONG DURATION LOADING MUST BE CHECKED ALSO.
2. FOR MORE ACCURATE READING OF LOW LOADINGS, DIVIDE SCALES A,B,C,D AND E BY A CONVENIENT FACTOR (E.G. 10 OR 2)
3. FOR EXAMPLES ON THE USE OF THIS CHART REFER TO SHEET 2, VX9/M7020/8

3-4-75	A	SPANS & HEIGHTS WERE IN MILLIMETRES	

DRAWN J. G. T.

STATE ELECTRICITY COMMISSION OF VICTORIA
DISTRIBUTION ENGINEERING DEPARTMENT

SHEET 1 OF 2 | O/H LINE MANUAL VOL 1 SECT 13 | VX9 / M7020 / 7 A

POLE CONSTRUCTION
CHART FOR DETERMINING
POLE LOADING AND GUY SIZE

165.

APPENDIX F

MODEL FOR THE SHEAR STRENGTH OF THE SLOTTED-BASE POLE MODIFICATION

This Appendix details the derivation of an expression for the force F_S required to shear a slot-modified pole base.

Figure F.1 shows the model and the free body diagrams used in the derivation. It is assumed that the pole section above the load application point (car bumper height) and the conductors contribute little to the shear strength of the lower modified zone.

By considering the equilibrium of the pole section between the top of the slot and the load application point (Figure F.1b), an expression for the vertical forces in the four columns can be obtained :

$$V = \frac{F_S h}{d} + \frac{F_S \ell}{2d} \qquad \text{(F.1)}$$

where
- V = total vertical force on two columns
- h = distance between point of application of F_S and the top of the slot
- d = distance between centroids of adjacent column cross-sections
- ℓ = slot length.

For the column shown in Figure F.1c, the vertical forces are compressive and result in a compressive stress in the column of :

$$\sigma_c = \frac{V}{2A} \qquad \text{(F.2)}$$

where
- A = cross-sectional area of column.

From equations (F.1) and (F.2)

$$\sigma_c = \frac{F_S}{2Ad}\left(h + \frac{\ell}{2}\right)$$

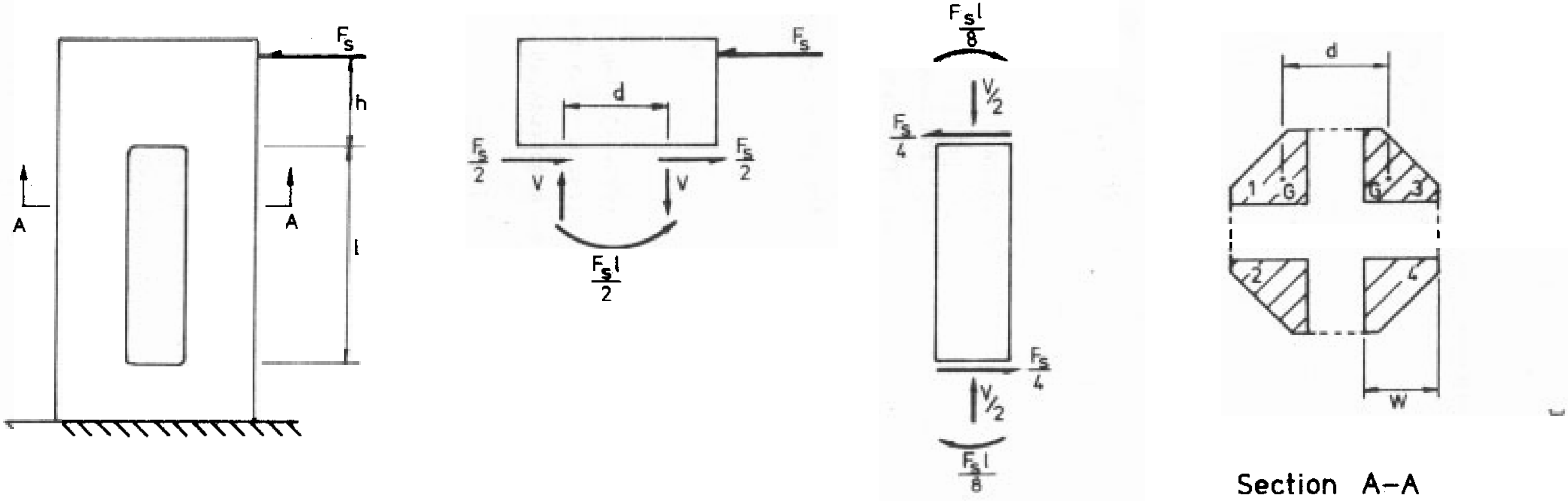

(a)
Slotted pole base

(b)
Free body diagram of section above the slots.

(c)
Free body diagram of one of the columns.

Figure F.1.

There are also bending stresses induced in the column by the applied moments and shear forces. **The maximum bending stress** occurs at the points of maximum bending moment **at each end of** the column.

The maximum bending moment M is given by :

$$M = \frac{F_S \ell}{8}$$

Therefore the maximum bending stress σ_b is :

$$\sigma_b = \frac{F_S \ell}{8Z}$$

where

Z = the section modulus of a single column.

The direct stress distribution across the top of the column shown in Figure F.1c is sketched in Figure F.2. This sketch applies to columns 1 and 2 in Figure F.1. It can be seen that the maximum stress is compressive and occurs at the inner face of the column :

$$\sigma = \frac{F_S \ell}{8Z} + \frac{F_S}{2Ad}\left(h + \frac{\ell}{Z}\right) \qquad \text{(F.3)}$$

At the lower end of the column, the maximum stress is also compressive and occurs at the outer face. For columns 3 and 4 in Figure F.1, the maximum stresses are of the same magnitude as for columns 1 and 2, but are tensile.

From Equation (F.3) the force F_S required to fail the modified base, given an ultimate stress σ_{ult}, is :

$$F_S = \frac{\sigma_{ult}}{\dfrac{h + \frac{\ell}{2}}{2Ad} + \dfrac{\ell}{8Z}} \qquad \text{(F.4)}$$

As well as direct stress failure, shear failure should also be considered. The shear stress τ in a column is given by :

$$\tau = \frac{F_S}{4A}$$

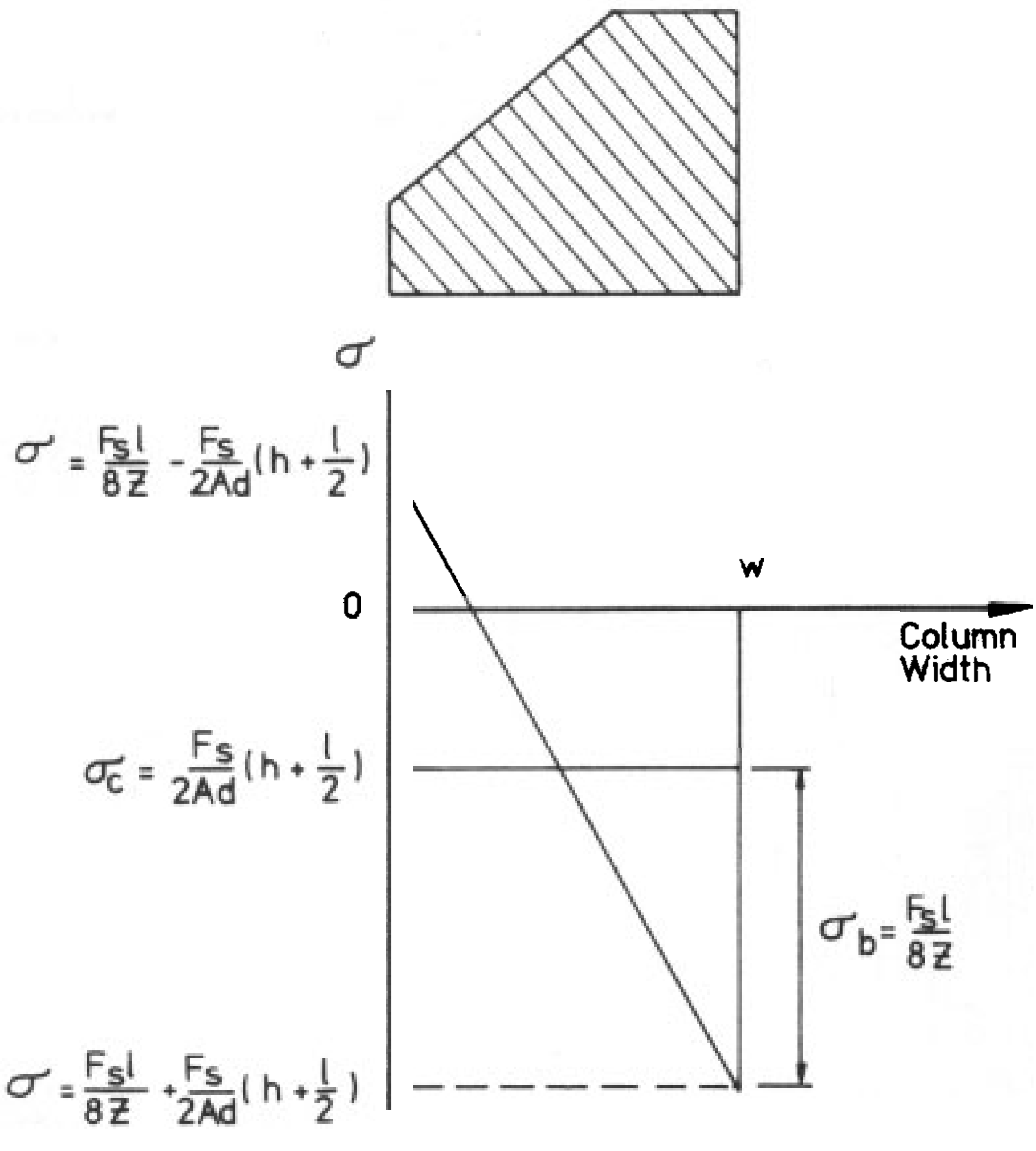

Figure F.2. Stress distribution across columns 1 and 2 in figure F.1.

For a column to fail in shear :

$$F_S = \frac{\tau_{ult}}{4A}$$

where τ_{ult} is the ultimate shear stress.

For the materials and dimensions used in the scale model tests, critical bending stresses were found to occur before critical shear stresses. Thus, for the same rated service load capacity, a pole modified with slots near its base will have a lower impact resistance than a pole modified according to the crossed-hole scheme, which fails in shear.